COOPERATIVE CATALYSIS AMONG ACTIVE SITES INTEGRATED IN POLYMER RANDOM COIL

ASHUTOSH THAKUR

Japan Advanced Institute of Science and Technology

Doctoral Dissertation

Referee-in-chief: Associate Professor Toshiaki Taniike

Japan Advanced Institute of Science and Technology

Referees: Professor Noriyoshi Matsumi

Japan Advanced Institute of Science and Technology

Professor Shinya Maenosono

Japan Advanced Institute of Science and Technology

Associate Professor Yuki Nagao

Japan Advanced Institute of Science and Technology

Professor Kotohiro Nomura

Tokyo Metropolitan University

Cooperative Catalysis Among Active Sites Integrated in Polymer Random coil

Ashutosh Thakur

s1440154

Transition metal-based olefin polymerization catalysts have tremendous industrial applications for the production of polyolefins which occupy half of the plastic industry. They are represented by two extreme classes: Molecular catalysts (metallocene and post-metallocene) and classical solid catalysts (Ziegler-Natta and Phillips). The former class exploits the advantage of precise design of active site structures by a variety of metal-ligand combinations for a superior activity and selectivity. In contrast, the latter class is advantageous for the accumulation of multiple functions over multi-length scales, while their inherent chemical and structural complexities lead to ill-defined characteristics and lower catalytic selectivity. Thus, the contrast of the characteristics has encouraged the development of a new class of catalysts, which would enable multifunctionality and high selectivity with well-defined features in a way to bridge the gap between molecular and solid catalysts. In this research, I attempt to develop a new catalyst system, with the aim to conceptually bridge the two extreme classes of catalysts. This involves, a bottom-up strategy based on the synthesis of well-defined polynorbornene (PNB) supports bearing different contents of aryloxide ligands at their side chain, and subsequent grafting of a half-titanocene precursor to confine a predefined number of metal centres in a nano-sized random coil of polymer chains (**Scheme 1**). A potential synergy or cooperation among multiple active sites integrated in a random coil is explored to accumulate functionality in a well-defined way.

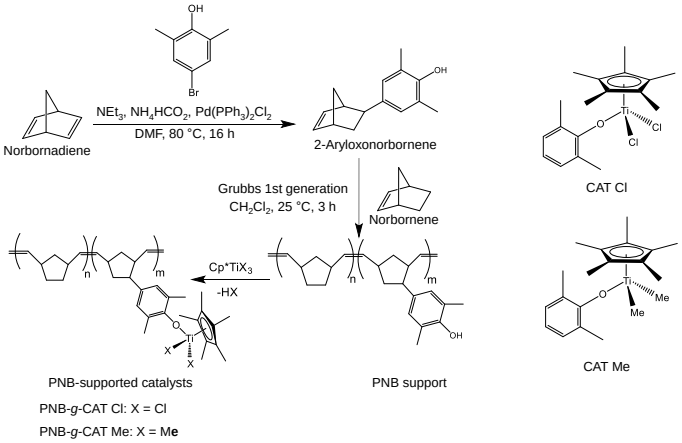

Scheme 1. Synthesis of PNB-supported catalysts.

The PNB supports were synthesized by Grubbs catalysed copolymerization between norbornene and 2-aryloxonorbornene, at a fixed norbornene/catalyst ratio of 200 mol/mol. Approximately 90% of the yield and nearly quantitative comonomer incorporation were observed over a wide range of feed composition. The PNB supports exhibited M_w/M_n values close to one. These facts assured the well-defined nature of the synthesized PNB supports. Dynamic light scattering (DLS) measurements revealed a random coil conformation of the chains of the PNB supports in a dilute toluene solution.

The PNB supports with different comonomer contents were used to graft two half-titanocene precursors Cp*$TiCl_3$ and Cp*$TiMe_3$. Successful synthesis was confirmed by comparing the ^1H, ^{13}C NMR and UV-Vis spectra of the PNB-supported catalysts with their molecular analogues (CAT Cl and CAT Me). The PNB-supported catalysts were employed in ethylene polymerization using modified methylaluminoxane (MMAO) or TIBA/$Ph_3CB(C_6F_5)_4$ as an activator. Ethylene polymerization was also conducted using the corresponding molecular analogues for comparison. It was found that the activation of the supported catalysts using MMAO was sterically hindered especially in terms of alkylation, which was circumvented by the utilization of a less bulky TIBA/$Ph_3CB(C_6F_5)_4$ activator system. When

TIBA/$Ph_3CB(C_6F_5)_4$ activator system was used, the activity of the supported catalysts was found to be greater than the corresponding molecular analogues. Furthermore, the activity improved by the increase of Ti centres per PNB chain, plausibly due to a synergy or cooperation among multiple active centres confined in a nano-sized random coil of PNB chains. Secondly, it was found that at a higher temperature, the highest activity in ethylene polymerization was achieved by employing a PNB-supported catalyst with the lowest active site density. In the absence of synergistic or cooperative effect, the enhanced activity of the PNB-supported catalyst with the lowest active site density indicated the stabilization of the active sites by site isolation. Also, the supported catalysts were superior to the molecular analogues in producing polyethylene with a higher molecular weight and narrower polydispersity when activated by TIBA/$Ph_3CB(C_6F_5)_4$ activator system.
Keywords: Bridging catalyst; soluble polymer support; half-titanocene catalyst; ethylene polymerization; active site density.

Preface

The present thesis is submitted for the Degree of Doctor of Philosophy at Japan Advanced Institute of Science and Technology, Japan. The thesis comprises of the results of the research work on the topic “Cooperative Catalysis Among Active Sites Integrated in Polymer Random Coil” under the supervision of Assoc. Prof. Toshiaki Taniike at the School of Materials Science, Japan Advanced Institute of Science and Technology during July 2014–March 2018.

First of all, Chapter 1 is a general introduction, which explains the detailed background and the objective of this research. Chapter 2 introduces a novel catalyst system in olefin polymerization, which is based on the synthesis of aryloxide-containing half-titanocene catalysts grafted to soluble polynorbornene chains and their application in ethylene polymerization. Chapter 3 reports the origin of cooperative catalysis embodied by aryloxide-containing half-titanocene catalysts confined in a single polynorbornene chain. Finally, Chapter 4 describes the general summary and conclusions of this thesis. To the best of my knowledge, the work is original, and no part of this thesis has been plagiarized.

School of Materials Science Ashutosh Thakur

Japan Advanced Institute of Science and Technology

March 2018

Acknowledgements

Firstly, I would like to express my sincere gratitude to my supervisor Assoc. Prof. Toshiaki Taniike, School of Materials Science, Japan Advanced Institute of Science and Technology, for his kind guidance, valuable suggestions and heartfelt encouragements throughout this work. I am thankful to him for his never ending patience, motivation and immense knowledge. His guidance helped me in all the time of research and writing of this thesis.

I am also heartily grateful to all members of Taniike laboratory for their valuable suggestions, cooperation and support.

I would also take an opportunity to express my sincere gratitude to Prof. Minoru Terano (JAIST) for his guidance and encouragement at a professional and personal level. I am also thankful to Assistant Prof. Patchanee Chammingkwan for her valuable inputs, cooperation and fruitful discussions and all the Terano laboratory members for their constant support and help.

I am grateful to Prof. Noriyoshi Matsumi (JAIST) for giving an opportunity to carry out GPC measurements in his laboratory and providing invaluable suggestions and guidance.

I would also like to sincerely thank the members of my review committee Prof. Noriyoshi Matsumi (JAIST), Prof. Shinya Maensono (JAIST), Assoc. Prof. Yuki Nagao (JAIST), and Prof. Kotohiro Nomura (Tokyo Metropolitan University), who have spent their valuable time to read the thesis, for their insightful comments and remarks to enhance the quality of this thesis from various perspectives.

I would like to express deep regards to my parents and my brother for supporting my ambitions. Without their blessings and moral support, this research would have not been accomplished.

I extend my special thanks to my friends Bulbul Maira, Neha Sharma, Rohit Gagan, Angana Goswami, and Akanksha Matta for their utmost care and moral support. Also, without taking the names, I would like to sincerely thank all my friends and close

associates for their strong and positive influences in my life.

Finally, I thank God for giving me the strength and wisdom to complete this research and sending all these people in my life.

School of Materials Science Ashutosh Thakur

Japan Advanced Institute of Science and Technology

March 2018

Table of Contents

Chapter 1

General Introduction

1.1 Catalysts

Definition

Catalysts are chemical entities, that are responsible for the kinetic acceleration of a reaction without participating in the overall reaction scheme [1]. A catalyst lowers the free energy of activation ($\Delta G^{\ddagger}$) of a reaction by providing new pathways for its progress. As a result, lower energy input is required for a catalyzed reaction as compared to an uncatalyzed reaction [1,2]. Fig. 1 is an example of the influence of a catalyst in the progress of a reaction (A + B → C) in solution.

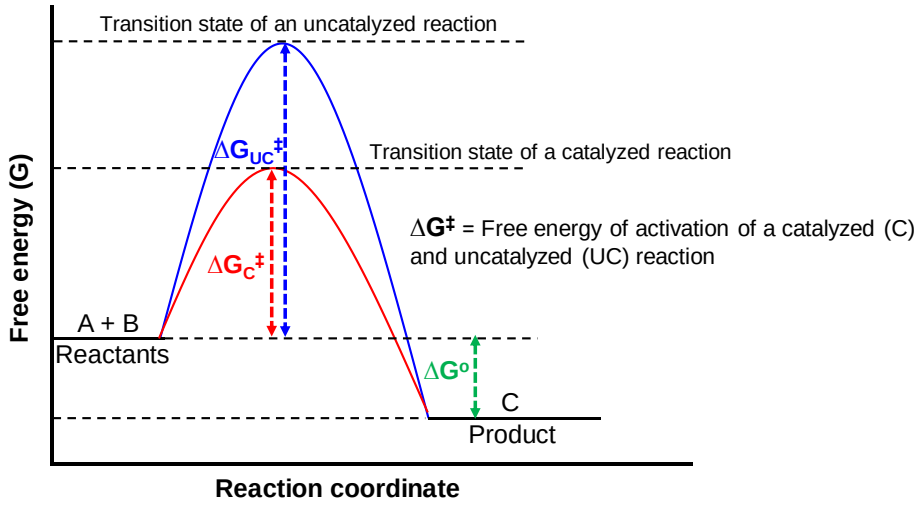

Fig. 1. Energy profile of a reaction in progress (A + B → C).

The rate of formation of product (C) is given by Eq. (1),

$$R_C = d[C]/dt = k[A][B] \qquad \text{Eq. (1).}$$

k is the rate constant of the reaction, which can be correlated to the free energy of activation by Eq. (2) based on the transition state theory [3],

$k = \kappa k_B T/h \exp(-\Delta G^{\ddagger}/RT)$ Eq. (2).

Where, κ is a proportionality constant known as a transmission coefficient [3], k_B is the Boltzmann constant, h is the Planck constant and R is the molar gas constant.

Since $\Delta G = \Delta H - T\Delta S$, Eq. (2) can be expressed in terms of the enthalpy of activation ($\Delta H^{\ddagger}$) and the entropy of activation ($\Delta S^{\ddagger}$) by Eq. (3),

$k = \kappa k_B T/h \exp(\Delta S^{\ddagger}/R)\exp(-\Delta H^{\ddagger}/RT)$ Eq. (3).

Eq. (3) is known as Eyring equation, from which the $\Delta H^{\ddagger}$ and $\Delta S^{\ddagger}$ of a chemical reaction can be calculated by plotting ln(k/T) vs. 1/T, which would give a straight line with the slope as $-\Delta H^{\ddagger}/R$ and the intercept as $\ln(\kappa k_B/h)+\Delta S^{\ddagger}/R$. A catalyst influences both the $\Delta H^{\ddagger}$ and $\Delta S^{\ddagger}$ of a chemical reaction so as to minimize the $\Delta G^{\ddagger}$ as compared to an uncatalyzed reaction.

In Fig.1, the initial and final states of the reactants and the product are same, both for a catalyzed and uncatalyzed reactions. Thus, the overall free energy change (ΔG^o) is same for both the reactions. This implies that the thermodynamically unfavourable reactions ($\Delta G^o > 0$) cannot be made feasible by a catalyst. Thus, the main role of a catalyst in a thermodynamically feasible reaction is to improve the reaction rate as well as the product selectivity (concentration of the desired product with respect to all the products). Catalysts can improve the product selectivity because they can accelerate competitive reactions by different extents.

Importance of catalysts in life and lifestyle

Catalysts are integral components of most of the modern chemical processes, as

they are indispensable to improve the reaction efficiency in terms of energy consumption and atom economy. Catalysts have found direct applications in fuel and energy sectors, automobile industries to control the emission of harmful exhaust gases, polymer industries, pharmaceutical industries, food processing, and etc. By and large, catalysts contribute to the 30% of the world economy, which is a remarkable number to understand their direct influences on human lifestyle [4]. Catalysts are also important for life, for example, enzymes are the biocatalysts essential for many important biochemical reactions.

1.2 Classification of Catalysts

Based on design concepts and functions, catalysts can be broadly classified into three categories: i) Enzyme catalysts, ii) molecular catalysts and iii) solid catalysts.

Enzyme catalysts

Enzymes are homogenous catalysts, which work in the biological systems [2,5]. Enzymes are proteins or nucleic acids, bearing a precisely designed active site, which can transform a substrate to a specific product with almost 100% selectivity [6]. Many enzymes require additional organic or inorganic compounds for their activity, which are known as cofactors [5]. The key features, which make enzyme catalyzed reactions to be extremely selective with high catalytic turnovers are [6-8]:

(i) The active site structure is specific to a reaction in terms of its shape and charge distribution. For instance, functional groups in the substrate can interact with

functional groups in the active site by hydrogen bonding, electrostatic or Van der Waals interactions, which in turn increases high local substrate concentrations around an active site. Also, the binding of the substrate induces a favourable conformational change in the active site, which restores its original conformation after releasing the product. These result into high enzyme-substrate binding affinity.

(ii) High enzyme-substrate binding affinity also results from the favorable binding of a hydrophobic substrate in the hydrophobic pocket of an enzyme in an aqueous environment.

(iii) The affinity of an enzyme for a specific reaction transition state is higher than that for the reactants or products. This lowers the free energy of activation of the entire reaction by stabilization of the transition state.

(iv) Many metalloenzymes activate substrates by multimetallic cooperative catalysis, in which two or more metal centers are fixed in close proximity to activate both electrophilic and nucleophilic reactants by a concerted mechanism, leading to improved activity and selectivity as compared to nonproximate catalytic centers. Scheme 1, represents the proposed mechanism of metal centres mediated cooperative catalysis of urease enzyme in the reaction of hydrolysis of urea into carbon dioxide and ammonia [8].

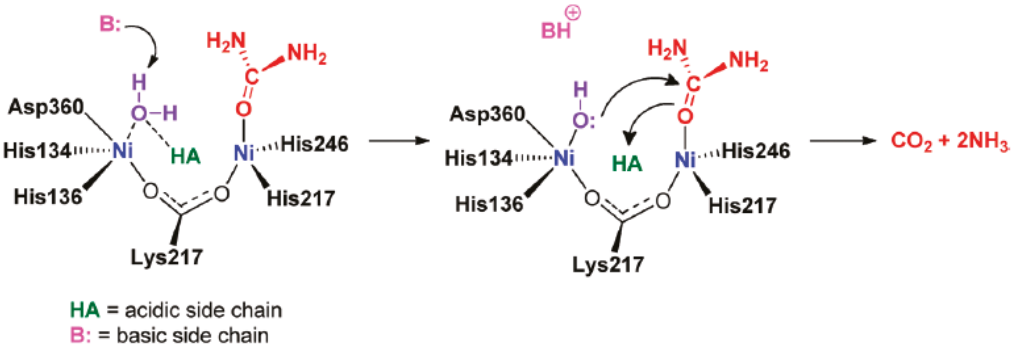

Scheme 1. Proposed mechanism of metal centres mediated cooperative catalysis of urease enzyme [8].

The two Ni centres of the urease urease enzyme (Scheme 1) are present at a distance of 3.5 Å from each other and they interact with the reactants (H_2O and urea) by non covalent bonds, which in turn helps to bring the reactants closer to each other. With the help of the acidic and the basic side chains of the enzyme, the nucleophilic addition to the carbonyl group takes place by a concerted pathway to form the hydrolyzed products in a single step. Thus, the cooperation between the two Ni centres improves local reagent concentrations and provide conformationally favourable active site -substrate interactions for improved activity and selectivity.

The kinetics of enzyme catalyzed reactions are described by Michaelis Menten mechanism [5]. According to this mechanism, an enzyme-substrate complex is formed in the first step. The rate-limiting step is the transformation of the bound substrate to product.

A number of bio-transformations are carried out using enzymes on an industrial scale, such as high fructose corn syrup production using glucose isomerase enzyme,

lactose free milk production using lactase enzyme, enantioselective synthesis of L-aspartate using aspartase enzyme and etc [9]. The advantages of using enzyme as catalyst in industries are:

(i) Supreme selectivity of enzyme catalyzed reactions for a specific product. Many products are isolated as a single enantiomer, which makes the process extremely efficient and cost effective.

(ii) Enzymes are highly active under mild conditions of temperature, pressure and pH. Moreover, enzyme catayzed reactions can be performed in aqueous environment. These make enzyme catalyzed reactions environmentally friendly.

(iii) Enzymes can catalyze a diverse range of the reactions, which make them promising for a number of applications on an industrial scale.

In spite of the advantages, the usage of enzymes for many reactions is limited by the lack of stability under harsh operational conditions and high cost of synthesis [9].

Molecular catalysts

Molecular catalysts are small molecules, including transition metal complexes, which are soluble in the reaction medium [10,11]. Transition metal complexes, which contain less than 18 electrons in their valence shells are coordinatively unsaturated and can function as catalysts [12]. Molecular catalysts work in homogeneous catalysis, in which, all the reactants, activator/cocatalyst, and the catalyst are present in a single phase of a dispersant (organic solvent). Molecular catalysts contribute to all industrial

catalytic processes by 10-15%. The advantages and disadvantages associated with molecular catalysts are [10-12]:

Advantages:

(i) Molecular catalysts enable the precise bottom-up design of active site structures for a superior activity and selectivity.

(ii) Molecular catalysts are well-defined. This is because the structure as well as its relationship with the performance of a catalyst can be studied at a molecular level, using diffraction and spectroscopic techniques. Based on these understanding, the performance of a molecular catalyst can be tuned by proper selection of the metal ion, ligand environment and operational conditions.

(iii) In reaction medium, molecular catalysts are dissolved within the fluid. Hence, there is negligible diffusion limitations of reagents to reach the active sites, which results into high catalytic turnover frequency.

Disadvantages:

(iv) Molecular catalysts possess lower thermal stability and they can perform only under relatively mild operational conditions, which limit their industrial applicability. Molecular catalysts generally work in a liquid phase, thus the boiling point of the solvent decides the highest temperature at which the catalysis can be performed.

(v) Molecular catalysts are dissolved in the same phase as the reactants, and hence, the separation of the product from the catalysts at end of the reaction is difficult

and expensive.

(vi) In the homogeneous catalytic processes, the recovery of molecular catalysts is a serious problem, which makes the processes very costly, especially when expensive metals like rhodium, palladium, gold and platinum are used.

Due to the disadvantages, molecular catalysts get little applications in many industrial processes such as cracking, reformation, steam reforming and ammonia synthesis, which routinely require harsh operational conditions (high temperature and pressure). However, due to their advantages, molecular catalysts are very useful for the synthesis of tailor-made plastics, fine chemicals, pharmaceutical compounds and etc. The major applications of molecular catalysts were triggered by the great success of C–C cross coupling reactions, olefin metathesis/polymerization reactions, asymmetric synthesis and so on [13-19]. These reactions are extremely useful from the prospect of organic chemistry and its related industries. A few examples of industrially useful molecular catalysts are listed in Scheme 2. A Rh-based complex is used for asymmetric hydrogenation reaction. It is used for the manufacture of L-DOPA, which is a drug for Parkinson's disease [12]. A Ni-based complex is used in the oligomerization of ethylene to higher molecular weight α-olefins, popularly known as shell higher olefin process (SHOP) [12]. Ru- and Mo-based complexes are used in olefin metathesis reactions and popularly known as Grubbs, Hoveyda-Grubbs and Schrock catalysts, respectively [13,14]. A Pd-based complex is used in C–C cross coupling reactions, especially Suzuki reaction [15].

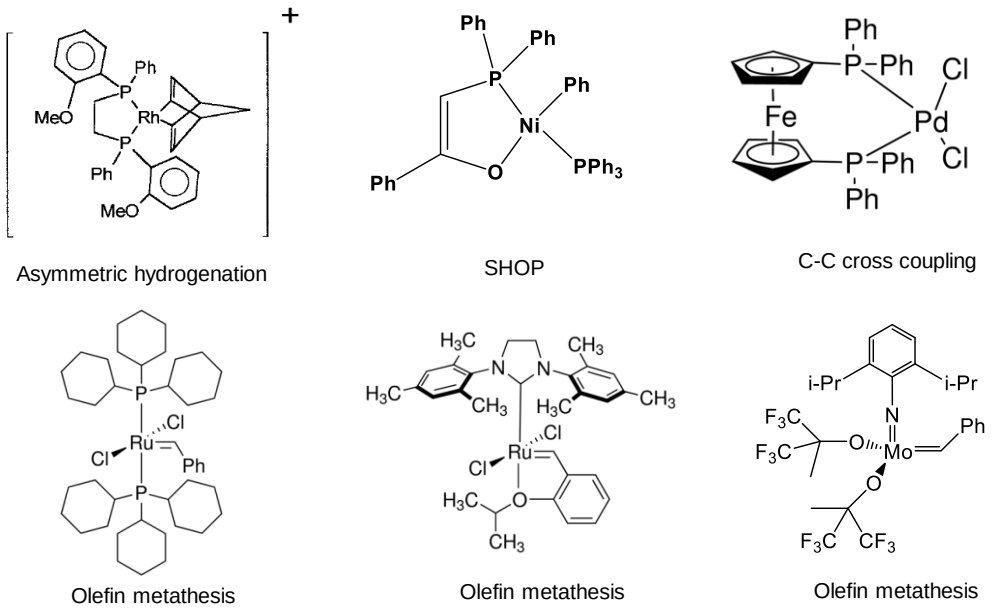

Scheme 2. Examples of industrially useful molecular catalysts.

There are several types of olefin metathesis reactions, such as ring closing metathesis (RCM), acyclic diene metathesis (ADMET), ring opening metathesis polymerization (ROMP), ring opening metathesis (ROM) and cross metathesis (CM), which are efficiently catalyzed by several generations of Ru-based (Grubbs type) and Mo-based (Schrock type) catalysts [13,14,20,21]. Since ROMP by the Grubbs catalyst has been extensively used in this dissertation, the polymerization mechanism, and the catalysis are discussed below.

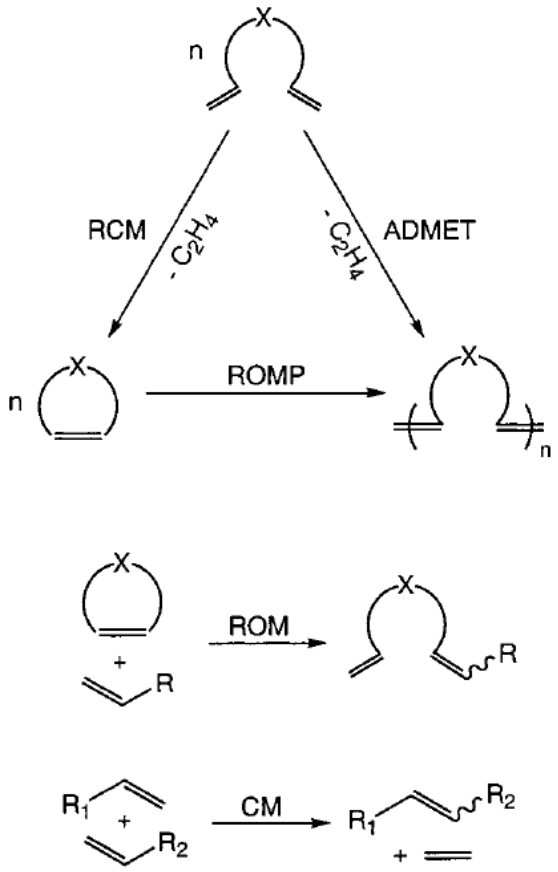

Scheme 3. Types of olefin metathesis reactions [14].

Ring opening metathesis polymerization:

Ring opening metathesis polymerization (ROMP) is a useful process for controlled synthesis of functional organic polymers [22-24]. Due to the functional group tolerance of Ru [20,25], Grubbs catalyzed ROMP has been recognized as a suitable methodology to synthesize well-defined and functional polynorbornene [23,24]. In terms of polymer chemistry, ROMP is a chain growth polymerization of cyclic olefins into linear polymers known as cycloolefin polymers (COC). The cyclic olefins, which contain a high degree of ring strain (> 5 kcalmol^{-1}) are the active monomers in

ROMP [20]. Through polymerization, the ring strain in the cyclic olefin monomer is released, which becomes the driving enthalpic force of the polymerization, balanced by the entropic loss. The most commonly used monomers are cyclobutene, cyclopentene, cis-cyclooctene, norbornene and its derivatives such as tetracyclododecene and etc.

Scheme 4, illustrates the mechanism of ROMP [20]. The initiation step begins with π-coordination of monomer to a transition metal alkylidene complex followed by [2+2] cycloaddition reaction to make a four-membered metallacyclobutane intermediate. This intermediate undergoes a cycloreversion reaction to form a new metal alkylidene, which is the propagating site of the polymerization. During propagation, the analogous steps are repeated until the polymerization stops by the consumption of all monomer, reaction equilibrium or chain termination. Grubbs catalyzed ROMP is commonly terminated by the addition of ethyl vinyl ether. In addition to the mechanism illustrated in Scheme 4, the equilibrium in the reaction medium can be established via other pathways, such as intermolecular chain-transfer and intramolecular chain-transfer (backbiting) reactions. The chain transfer reactions would lead to the formation of polydisperse polymers.

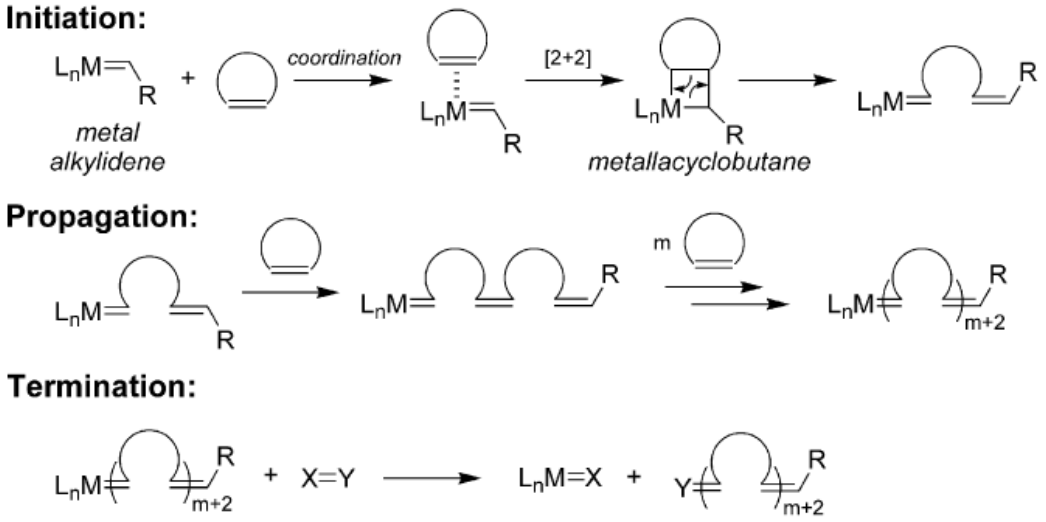

Scheme 4. A general mechanism of ROMP [20].

Considering the equilibrium nature of ROMP reactions, in order to perform efficient living ROMP, the catalyst is needed to satisfy the following requirements [20]: (1) High activity, (2) rapid initiation kinetics compared to the propagation kinetics, (4) negligible chain transfer reactions or undesired termination during the polymerization, (5) facile reaction with terminating agents, and (6) tolerance toward moisture, air, and organic functional groups.

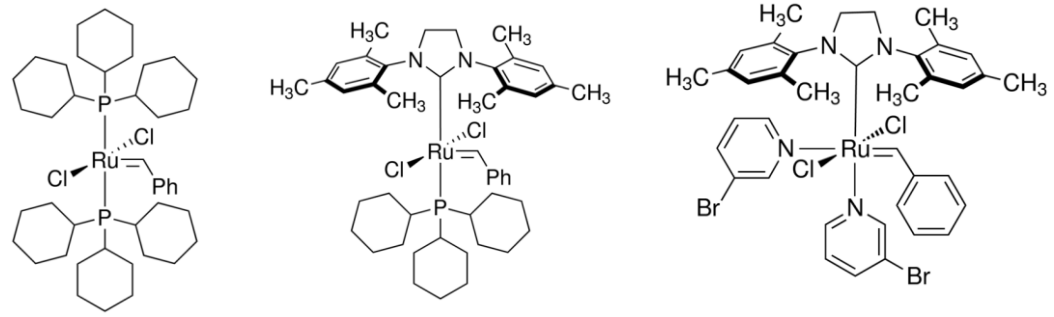

Grubbs 1st generation | Grubbs 2nd generation | Grubbs 3rd generation

Scheme 5. Three generations of Grubbs catalysts.

The molecular structures of three consecutive generations of Grubbs catalysts are shown in Scheme 5. All of the three catalysts show high activity in ROMP of a variety of monomers, especially norbornene derivatives. However, the much higher rate of propagation as compared to the rate of initiation in ROMP by the Grubbs 1st and 2nd generation catalysts leads to the formation of polymers with polydispersity index (PDI) around 1.2 [26]. This fact also lowers the ability of these catalysts to control the molecular weight of product polymers. Combination of N-heterocyclic carbene and pyridine ligands led to the Grubbs 3rd generation catalyst, by which the rate of initiation in ROMP can be significantly enhanced [27]. With this advantage, the Grubbs 3rd generation catalyst makes it possible to synthesize nearly monodisperse polymers with completely controlled molecular weight. This development in Grubbs catalysts is a good example to demonstrate the fact that by proper choice of the ligand, the performance of a molecular catalyst can be tailored.

Solid catalysts

Solid catalysts are heterogeneous catalysts [28]. They use coordinative unsaturation created on solid surfaces for catalysis [29]. In heterogeneous catalysis, the reactants are either in gas or in liquid phase, while the catalysts remain in the solid phase [30]. Mostly, solid catalysts are multicomponent, typically composed of catalytically active components, support or carrier and promoters [30]. Many industrial solid catalysts utilize a variety of transition metals as the active components. Supports are solid materials, which provide a large surface area for the accommodation of

the catalytically active components by chemisorption. Some commonly employed materials as solid supports are alumina (Al_2O_3), silica (SiO_2), titania (TiO_2), zeolites, clay minerals, activated carbon, cross-linked polymers, graphene and etc. The promoters are the substances that are not catalytically active but can enhance the performance of a catalyst [30]. The advantages and disadvantages associated with solid catalysts are:

Advantages:

(i) Solid catalysts are thermally robust and possess much higher stability as compared to molecular catalysts.

(ii) Solid catalysts make use of support materials to anchor transition metals instead of expensive ligands. Supports make solid catalysts cheap, easily separable from reaction medium and reusable when expensive metals are used.

(iii) Solid catalysts are multifunctional as they offer the advantage of the integration of multi-components over multi-length scales for the accumulation of multiple functions. For instance, the catalytically active components of solid catalysts decide the intrinsic activity, selectivity and stability of a catalyst. Whereas, supports control the morphology and provide mechanical strength to the catalysts. Furthermore, supports act as macro ligands, which improve stability of the active sites by protecting from external impurities and dissipating the heat released during chemical events. The chemical reactions with solid catalysts are diffusion controlled [31] and therefore, porous solid supports can also dictate the selectivity (*e.g.* shape selectivity in zeolites) of a catalyst [30]. Further, promoters can electronically influence the catalyst surfaces, control the growth of catalyst

particles in a way to influence activity and selectivity of solid catalysts [30].

Disadvantages:

(iv) Solid catalysts possess multiple active sites, each of them with its own activity and selectivity. This make overall activity and selectivity of a catalyst low. Due to their ill-defined characteristics, it is very difficult to study structure-performance relationship (SPR) of solid catalysts. Moreover, most of the solid catalysts are empirically developed in terms of performance optimization by conventional top-down design. Thus, the lack of SPR makes it very demanding to tune the performance of solid catalysts.

(v) In reactions with solid catalysts, the reagents which are in another phase (gas or liquid) must diffuse into the pores and subsequently get adsorbed on the catalytically active surfaces. After reaction, the products are also required to diffuse out of the pores. These pore diffusion causes mass transport problem [31]. Moreover, for any exothermic or endothermic reaction with solid catalysts, a considerable temperature gradient may exist along the particle diameter, which causes heat transfer problem [31]. These heat and mass transfer limitations can strongly affect the kinetics solid catalysts, even though these are useful for the stability and selectivity of a catalyst.

The advantages of solid catalysts make them most suitable for many industrial applications. Solid catalysts contribute to 80-85% of all industrial catalytic processes [30]. The most notable applications include: ammonia synthesis, oil refineries, production of hydrocarbons from CO and H_2 (Fischer Tropsch process),

production of fine chemicals, automotive catalytic converters (three-way catalyst), industrial polyolefin productions (Ziegler-Natta and Phillips catalysts), conversion of biomass into fuels and chemicals, green and sustainable chemical transformations and so on [30-36].

1.3 Olefin Polymerization Catalysts

Brief overview

Polyolefins are regarded as the most successful thermoplastic materials due to their broad range of applications, highly developed manufacturing technology and huge market share. With a global production of approximately 152 million metric tons in the year of 2016 and forecasted growth of 6% per year for the next 5 years [37], it is easy to imagine their scientific, social, and economic impact in the modern world. The remarkable consumption of polyolefins is the consequence of their excellent thermomechanical properties and easy processability in combination with exceptionally low production cost. With the aid of composite technology, polyolefins are getting attentions for new applications so as to replace expensive and environmentally risky materials [38-45]. Because of the continuous efforts devoted over the last 60 years in both industry and academy to various disciplines that include catalysis, reaction engineering, characterization, processing and polymer properties, the field of polyolefins has become not only multi-disciplinary but also scientifically and technologically matured.

The journey of catalytic olefin polymerization started in 1951 with the discovery of a Cr-based catalyst by Hogan and Banks at Phillips Petroleum followed by the discovery of a Ti-based catalyst ($TiCl_4/AlEt_3$) in 1953 by Ziegler [46,47]. These discoveries led to the successful production of high density polyethylene (HDPE). In the next years, pioneering work of Natta on the isoselective polymerization of propylene with another Ziegler-type catalyst ($TiCl_3/AlEt_2Cl$) opened the new field of stereoregular polypropylene (PP) [48]. Due to their great contributions, Karl Ziegler and Giulio Natta were awarded the Nobel Prize in Chemistry in the year 1963. The next 50 years of research and development brought several new generations of $MgCl_2$-supported Ziegler-Natta (ZN) catalysts, which are highly active as well as highly stereospecific with multi-grained catalyst particles having uniform size and spherical morphology [49]. These advancements helped the industries for the commercial production of thermoplastic polymers (HDPE, isotactic polypropylene (iPP), linear low-density polyethylene (LLDPE)) and elastomers (polybutadiene, polyisoprene, ethene-propene rubber, ethylene-propylene-butadiene terpolymer) with ZN catalysts. During the same period, the great development of Phillips catalyst, which is composed of hexavalent Cr species supported on multi-grained SiO_2, transformed it to an extremely versatile industrial catalyst, which now produces almost 40% of the world's total HDPE in hundreds of specialized grades [50]. The great commercial success of ZN and Phillips catalysts can be attributed to the following reasons: (1) ZN and Phillips catalysts are multisite catalysts [49-52]. As a result, the polymers produced by them possess broad molecular weight distribution (MWD). Broad MWD improves flowability of

polymers in the molten state at high shear rates and imparts higher zero-shear viscosities, which are important in extrusion processes and blow molding applications [52,53]. Moreover, due to the multisite nature, Phillips catalyst produces HDPE bearing short and long chain branches with excellent mechanical and rheological properties [52], (2) the multi-grained particles of ZN and Phillips catalysts enable to achieve long standing polymerization kinetics as well as the morphology control of final polymer particles by "replication" phenomenon [49,50], (3) high polymerization activity of ZN and Phillips catalysts versus very cheap cost of catalyst synthesis makes them highly cost effective for industrial polyolefin production. While the commercial success of Ziegler-Natta and Phillips catalysts brought revolution in polyolefin industries, their complicated structural and chemical characteristics were the bottlenecks to understand many fundamental aspects regarding the olefin polymerization mechanism. The scarce concentration of the catalytically active species formed on solid supports with large porosity and high surface area makes it extremely challenging to investigate them using advanced surface science techniques. Moreover, the polymers produced by these solid catalysts have broad distribution in microstructures and are heterogeneous in chemical compositions, mainly due to the presence of multiple active sites [49-52]. Thus, microstructural characterization of the product polymers is not suitable as a fingerprint technique to understand the active site structure and mechanism of polymerization. Nevertheless, classical solid catalysts have played the major catalytic role in industries for the large-scale production of low-cost polyolefins over the last decades and even till now [53].

Although, the development of single-site molecular catalysts and their use in olefin polymerization were started way back in 1957 based on a Cp_2TiCl_2/alkyl aluminum system by Natta, the results were not satisfactory due to the inefficient activation of the catalyst [54]. The revolution in the explorations and design of high performance and single-site metallocene-based molecular catalysts for olefin polymerizations began after the serendipitous discovery of a methylaluminoxane (MAO) activator [55]. With the combination of early transition metal-based metallocene catalysts and MAO, it became possible to synthesize polymers with high stereoregularity, uniform chemical compositions and narrow molecular weight distribution, being ideal for studying the olefin polymerization mechanism as well as structure performance relationship (SPR) [18]. The knowledges of SPR have further enabled the fine tuning of polymer microstructures by a variety of metal-ligand combinations. The search for new generations of non-metallocene molecular catalysts with tailored ancillary ligands led to the development of post-metallocene single-site catalysts, represented by early transition metal-based constrained geometry and phenoxyimine (FI) catalysts, as well as late transition metal based α-diimines and bis(imino)-pyridine catalysts [56-59]. The new functions explored by these catalysts have expanded the scope for the synthesis of next-generation specialty polyolefins having high stereo and regioregularity, controlled branched density and polar functional groups. These new polyolefins afforded completely different chemical, physical and rheological properties, thus opening a possibility of new applications for polyolefin-based materials. Furthermore, the mechanistic study of olefin enchainment

and chain-transfer processes by molecular catalysts became clearer with the development structurally well-defined cocatalysts [60].

The above discussions have made it very clear that although both the classical solid catalysts and tailored molecular catalysts produce polyolefins by transition-metal catalyzed coordination insertion polymerization, the obtained polymers are largely different in microstructures. This is because both the classes of catalysts differ in their catalytic functions. Thus, it is necessary to understand the functions of classical solid catalysts (*e.g.*, ZN) and tailored molecular catalysts (metallocene and post-metallocene) in order to conceptually bridge these two extreme classes of catalysts in olefin polymerization.

Ziegler-Natta catalysts

Heterogeneous ZN catalysts are the major catalysts for the industrial polyolefin production, especially for more than 99% of iPP [49]. These industrial catalysts are primarily composed of $TiCl_4$ cosupported on activated $MgCl_2$ together with a Lewis base compound known as an internal donor (ID) [34,49,61]. The role of the ID is to activate $MgCl_2$ during catalyst preparation and drastically improve the stereospecificity of a catalyst. The $TiCl_4$/ID/$MgCl_2$ pro-catalysts are used in combination with alkylaluminum compounds (AlR_3) and a second Lewis base compound known as an external donor (ED) [34,49,61]. The main role of the ED is to augment the stereospecifying the role of the ID [34,61]. During polymerization, a contact between the pro-catalyst with the Lewis acidic cocatalyst results into a loss of a large quantity of

the ID by complexation. An ED effectively substitutes the lost ID to maintain the stereospecificity of a catalyst. Apart from improving stereospecificity of a catalyst, donors significantly influence other catalytic properties such as activity, hydrogen response, comonomer incorporation efficiency and molecular weight distribution of product polymers [62]. It has been established that the performance of a ZN catalyst system depends more on the combination of donors rather than on the individual ID or ED. However, the choice of the combination of donors is greatly empirical, similar to the highly empirical developments of the ZN catalysts themselves over the last 60 years [62].

The reasons of $MgCl_2$ as the solely successful support is attributed to the similarity of its crystal structure to that of $TiCl_3$ in terms of interatomic distances and crystal forms [49,63]. Mechanically or chemically activated $MgCl_2$ usually exists in the δ-form, of which the catalytically useful surfaces are coordinatively unsaturated (110) and (104) lateral planes [62-65]. $TiCl_4$ is epitaxially adsorbed (Scheme 6) on these $MgCl_2$ surfaces due to similar ionic radii between Ti^{4+} and Mg^{2+} [62]. The mononuclear Ti species are formed on the (110) surface and dinuclear (Ti_2Cl_8) Ti species are formed on the (104) surface [62]. Active sites for propylene polymerization are considered as monoalkylated Ti(III) species, which are formed after the extraction and alkyl substitution of terminal Cl atoms with alkylaluminum cocatalyst [62]. The mononuclear and dinuclear Ti species on the (110) and (104) surfaces were respectively assigned by Busico et al. as aspecific and isospecific active sites [63]. Later on, an active site model of ZN catalysts was postulated by Busico et al., based on

statistical analyses of polymer stereosequences and is known as the three-site model [64], which was further modified by Terano et al [51]. According to the three-site model, stereospecificity of Ti species supported on $MgCl_2$ is decided by the absence or presence of bulky ligands, $L_{1,2}$ (Cl or donor) at the neighboring coordinatively unsaturated metal sites (Mg, Ti or Al), irrespective of their location ((110) or (104)) and nuclearity. Since the Ti dinuclear species on the (104) surface does not have any coordinative unsaturation at the neighboring metal sites, therefore it is considered that donors coadsorb with the Ti mononuclear species on the (110) surface, interact with neighbouring Ti species in a non-bonded fashion to convert it into an isospecific active site [62].

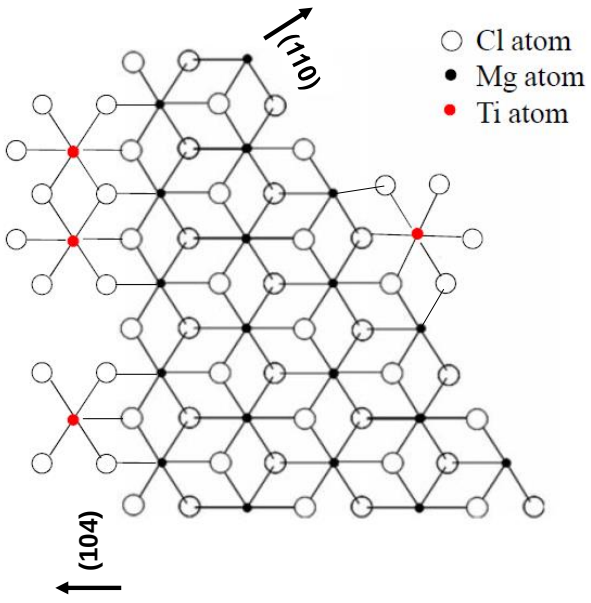

Scheme 6. Model of mononuclear and dinuclear Ti species on $MgCl_2$ (110) and (104) surfaces.

Active ZN catalysts can be prepared by prolonged milling of crystalline $MgCl_2$ with an intern ID. This mechanically activated $MgCl_2$ powders are then treated with $TiCl_4$ to synthesize a $TiCl_4$/ID/$MgCl_2$ pro-catalyst [49]. This mechanochemical route of catalyst preparation is no longer used for the preparation of industrial ZN catalysts since it cannot control the morphology of catalyst particles, while spherical particle morphology with uniform size distribution are essential for plant operation. The state-of-the-art ZN catalysts are thus prepared by chemical routes, in which support precursors with spherical morphologies such as $MgCl_2$-alcohol adducts and magnesium alkoxides ($Mg(OR)_2$) are treated with excess of $TiCl_4$ and an internal donor to chemically convert them to $TiCl_4$/ID/$MgCl_2$ pro-catalysts [49,66,67].

The modifications of ZN catalysts have been continued for the last 60 years in order to control morphology and improve the activity, stereospecificity and hydrogen response of the catalysts or in other words to integrate functions in one catalytic system. Along these modifications, the five generations of ZN catalysts that have been industrialized are partly listed in Table 1.

Table 1

Generations of ZN catalysts and their propylene polymerization performance[a] [49]

Generation	Chemical composition	Productivity (kg-PP/g-Cat)	Isotactic index (wt.%)	Morphology control	Post-process requirements
First	δ-$TiCl_3$0.33$AlCl_3$ + $AlEt_2Cl$	0.8-1.2	90-94	Not possible	Deashing and atactic removal
Second	δ-$TiCl_3$ + $AlEt_2Cl$	3-5	94-97	Possible	Deashing
Third	$TiCl_4$/Ester/$MgCl_2$ + AlR_3/Ester	5-10	90-95	possible	Atactic removal
Fourth	$TiCl_4$/Diester/$MgCl_2$ + TEA/Alkoxysilane	10-25	95-99	Possible	Not required
Fifth	$TiCl_4$/Diether/$MgCl_2$ + $AlEt_3$/Alkoxysilane	25-35	95-99	Possible	Not required

[a]Polymerization conditions: Pressure = 0.7 MPa, t = 4 h, T = 70 °C, solvent = hexane, H_2 for molecular weight control.

In the first-generation catalysts, the process suffered from low productivity of the catalysts and required the removal of catalyst residues (deashing) from obtained polymers. The low activity of the first-generation catalysts was due to their small surface area. The preparation methodology of the second-generation catalysts allowed morphology control and greatly improved the surface area of the catalysts. As a result,

the activity improved by five times as compared to the first-generation catalysts. The introduction of activated $MgCl_2$ support and organic esters (*e.g.* ethylbenzoate and methyl-*p*-tolulate) as ID and ED further improved the activity of the third-generation catalysts. The morphology of these catalysts can also be controlled by the proper choice of a preparation method (*e.g.* chemical method). The fourth- and fifth-generation catalysts have different donor systems. The fourth-generation catalysts were developed using an alkylphthalate as ID and an alkoxysilane as ED. The stereospecificity of the fourth-generation catalysts was significantly higher as compared to the third-generation catalysts. The use of 1,3-diethers as ID in the fifth-generation ZN catalysts led to high stereospecificity and exceptionally high catalytic activity as compared to the previous generations. Moreover, the use of 1,3-diethers as ID remove the necessity of ED in the fifth-generation catalysts due to the persistent adsorption of diethers on $MgCl_2$ surfaces [61]. Moreover, the iPP produced by the fifth-generation catalysts have a narrow molecular weight distribution, suitable for film grades. Thus, the integration of functions in ZN catalysts progressed with the development of the catalysts interms of productivity, stereospecificity, morphology, and molecular weight distribution of product polymers.

ZN catalysts are multi-site catalysts. ZN catalysts equip great multifunctionality as they integrate multi-components over multilength scales [68]. The performance of a ZN catalyst depends on two factors: 1) Type and nature of the active sites, which can dictate the activity of a catalyst as well as primary structure and polydispersity of produced polymer [68], and 2) hierarchical but irregular agglomeration of primary

building units, which results into a range of porosity from micro to macropores within a catalyst macroparticle [68]. The structural hierarchy influences the polymerization kinetics, comnomer (linear α-olefin) incorporation efficiency of a catalyst as well as the resultant morphology of the polymer particles through fragmentation and replication phenomena during polymerization [68,69]. While the former factor largely depends on surface chemistry, *i.e.*, an interplay among $MgCl_2$ surface, $TiCl_4$, internal and external donors, the latter factor is mainly determined through preparation methods and conditions.

Metallocene and post-metallocene catalysts

Metallocene catalysts are soluble organometallic coordination compounds [18]. The general structure of a metallocene of the Cp_2MCl_2 (IV) type is shown in Scheme 7. Metallocenes are called sandwich compounds, in which the central metal atom is placed between two cyclopentadienyl or substituted cyclopentadienyl (Cp) rings. The central metal is bonded through the π electron donation from the cyclopentadienyl rings. When activated with methylaluminoxane (MAO), metallocene catalysts of the Cp_2MCl_2 (IV) type shows high activity in ethylene polymerization. In contrast to ill-defined ZN or Phillips catalysts, metallocene catalysts show only one type of active sites. Because of the single site nature, metallocene catalysts produce high molecular weight polymers with a narrow molecular weight distribution (M_w/M_n = 2) and uniform chemical compositions [18]. Under appropriate conditions, the activity of a metallocene catalyst could be 10 to 100-fold greater than that of classical ZN catalysts. Scheme 8

represents the mechanism for olefin polymerization using metallocene catalyst in the presence of methylaluminoxane (MAO) or tri-*iso*-butylaluminum (TIBA)/$Ph_3CB(C_6F_5)_4$ activator system [18]. The first step is the alkylation of the metallocene complex in the presence of an excess of alkylaluminum compounds (MAO or TIBA). Abstraction of an alkyl group by Lewis acidic MAO or Ph_3C^+ cation generates a metal alkyl cationic species, stabilized by a weakly coordinating anion. This coordinatively unsaturated metal cation is the actual active site for the polymerization. Coordination insertion of a monomer to the active site generates a propagating site, in which continuous monomer insertion takes place and thus a growing polymer chain with an active end is formed. In all the propagation steps, the cationic site is believed to be stabilized by a counter anion [18]. The growing polymer chain may terminate by a chain-transfer reaction. There are several possible pathways of chain-transfer reaction, such as, β-H elimination to the metal centre, β-H transfer to monomer, chain transfer to hydrogen and chain transfer to alkylaluminum [70].

Since the ligands 'L' are coordinated to the cationic site, they can strongly influence the catalytic performance by sterically and electronically modifying the active site. Thus, the electron transfer ability of a ligand as well as its steric environment around the metal centre would influence the rate, orientation and mode of monomer insertion as well as the chain transfer rate of a growing polymer chain and the stability of the active site. These in turn influences the productivity and comonomer incorporation efficiency of the catalyst as well as the molecular weight, stereo- and regioregularity of the product polymers.

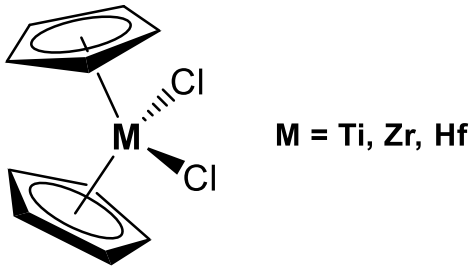

Scheme 7. Structure of metallocene catalysts of the type Cp_2MCl_2.

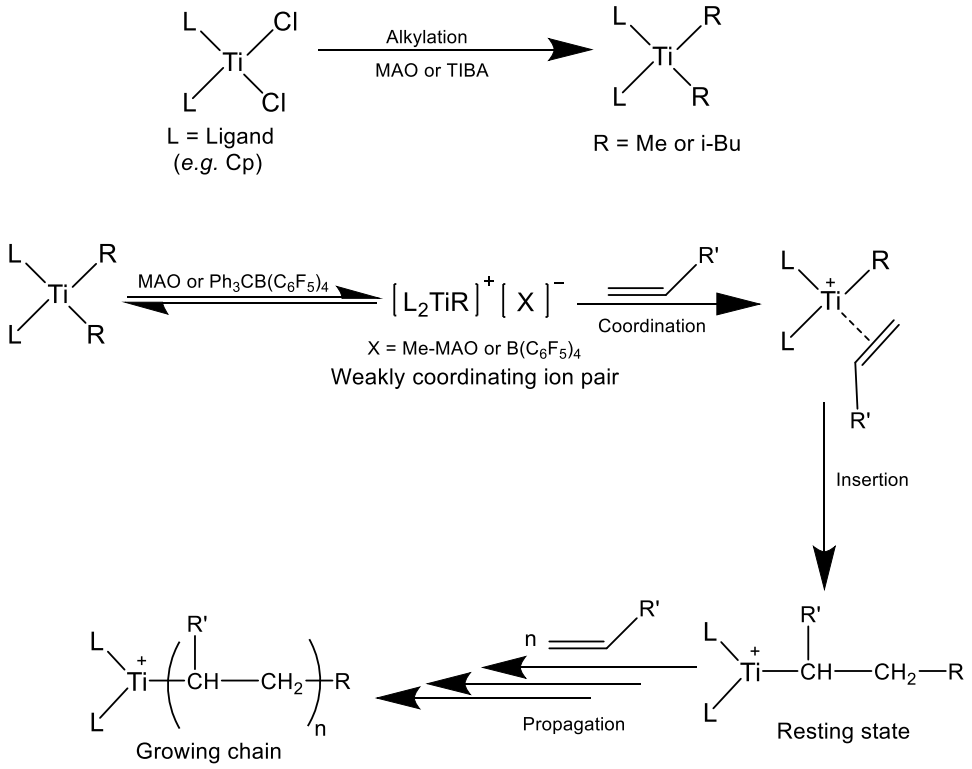

Scheme 8. Mechanism of olefin polymerization using metallocene catalysts in the presence of MAO or (TIBA)/$Ph_3CB(C_6F_5)_4$ activator system.

Metallocene catalysts are advantageous for fine tuning of catalytic performance by ligand modifications [71]. The catalysts presented in Scheme 7 are achiral because of the free rotation of the Cp rings and therefore cannot afford stereoregular

polypropylene. The stereoregularity of polymer produced by metallocene catalysts is related to the molecular symmetry of the metallocene complex [71,72]. Kaminsky et al. obtained highly isotactic PP at a good yield using C_2 symmetric chiral ansa-metallocene (*rac*-Et(Ind)$_2$ZrCl$_2$) [72,73] as shown in Scheme 9. When one of the indenyl groups was replaced with a Cp group, the steric environment around the Zr centre was affected, which in turn influenced the orientation of monomer insertion in one side and resulted into the production of hemi isotactic PP. On the other hand, Ewen et al., synthesized syndiotactic PP by using C_s symmetric ansa-metallocene (i-Pr(Flu)(Cp)ZrCI$_2$) [72,74] as shown in Scheme 9.

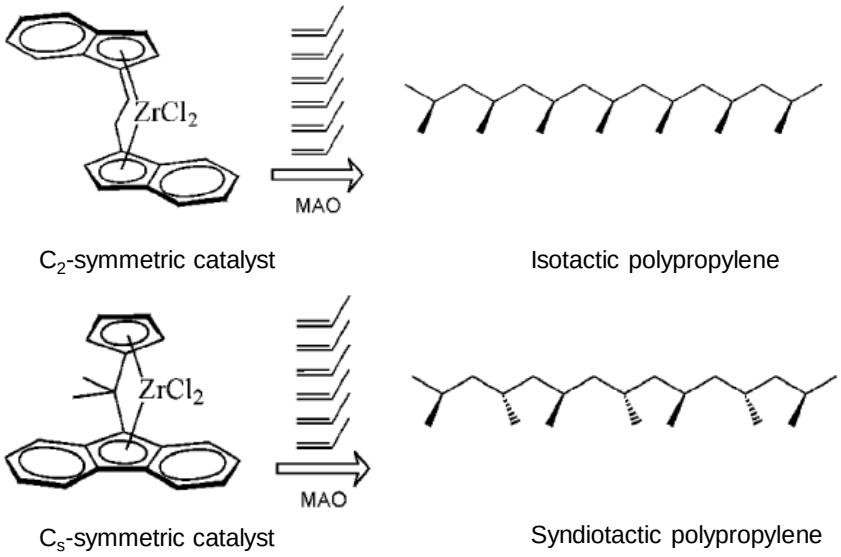

Scheme 9. Effect of molecular symmetry of metallocene catalysts on stereoregularity of polypropylene [72].

The molecular structure of a metallocene complex can be accurately determined by X-ray crystallography coupled with NMR spectroscopy. The molecular structure in combination with the microstructural information of resulting polymers (*e.g.* stereoregularity) make it possible to understand the exact correspondence between the active-site structure and its performance. These knowledges further enable the researchers to tune the polymer structure with the aid of ligand modification around a central metal atom.

The search for new metal-ligand combinations in order to incorporate new functionalities in single-site catalysts, led to the development of post-metallocene catalysts [56-59,75-77]. Scheme 10 represents a few examples of post-metalocene catalysts. One commercially successful catalyst is a constrained geometry catalyst (CGC) developed by Dow and Exxon [56]. The most unique feature of this catalyst is the sterically open nature of the active site, which allows it to incorporate a variety of other monomers (*e.g.* 1-hexene, styrene, norbornene) into polyethylene. Additionally, this catalyst can produce adequate amounts of short and long chain branches in the absence of comonomer. When compared to ordinary metallocenes, the CGC catalyst exhibits increased stability toward MAO and high thermal stability as they can produce higher molecular-weight polymers with narrow dispersity at high polymerization temperatures. Further progress in the post-metallocene catalytic polymerization of olefins was brought by the pioneering work of Brookhart on late transition metal based α-diimine complexes. The α-diimine complexes with late transition metals such as Ni and Pd have offered a unique ability of producing branched PEs without using

comonomers via a “chain-walking” mechanism [75,76]. The extent of branching can be controlled via modification of the α-diimine ligand, the metal type, or polymerization conditions. Moreover, these late transition-metal complexes are capable of synthesizing functionalized polyolefins by polymerization of polar monomers due to their high tolerance to polar functional groups [75-77]. Another important class of post-metallocene catalysts are bis-phenoxyimine (FI) catalysts, which are C_2 symmetric organometallic complexes. FI catalysts exhibit many unique characteristics based on the concept of ligand oriented catalyst design [57]. With the aid of ligand modifications (R_1 and R_2), FI catalysts can perform highly controlled living ethylene polymerizations and produce ultrahigh molecular weight polyethylene (UHMWPE) with narrow dispersity. With FI catalyst, the activity of level of 6552 kg-PE/mmol-Zr h was achieved in ethylene polymerization, which is one of the highest activity ever reported for any catalytic reaction [57]. Moreover, FI catalysts can incorporate higher α-olefins and norbornene, as well as can perform highly syndiospecific and isospecific polymerizations of both propylene and styrene with very high catalyst efficiency.

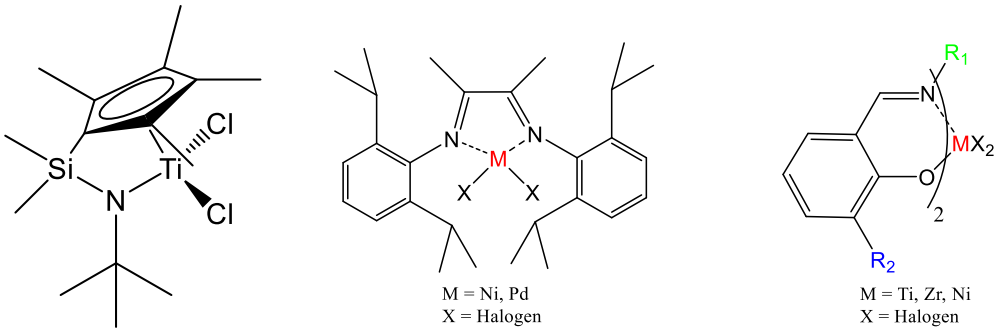

CGC catalyst α-diimine catalyst FI catalyst

Scheme 10. Selected examples of post-metallocene catalysts.

The effect of ligand modifications on catalytic performance is well demonstrated by a series of non-bridged half-metallocene complexes [78], represented in Scheme 11. In these catalysts, the performance can be tailored by changing the electronic and/or steric environment around the metal centre (*e.g.* Ti) through ligand modifications (Cp' and L) [78]. In the elegant research by Nomura et al., a variety of non-bridge half-metallocene catalysts containing ancillary (*e.g.* aryloxide, ketimide) ligands were synthesized and successfully employed in ethylene (co)polymerization [78-84]. The catalysts exhibited notable activity and remarkable incorporation of a variety of comonomers (1-butene, 1-hexene, styrene, norbornene, cyclohexene, cyclopentene, vinylcyclohexene and etc.) to form a variety of polymers such as LLDPE, cycloolefin copolymer (COC) and etc. with unique microstructures, which are otherwise not possible to synthesize via ordinary metallocenes (*e.g.* Cp_2TiCl_2). Furthermore, the polymers obtained with these catalysts usually possess high molecular weights and narrow molecular weight distributions.

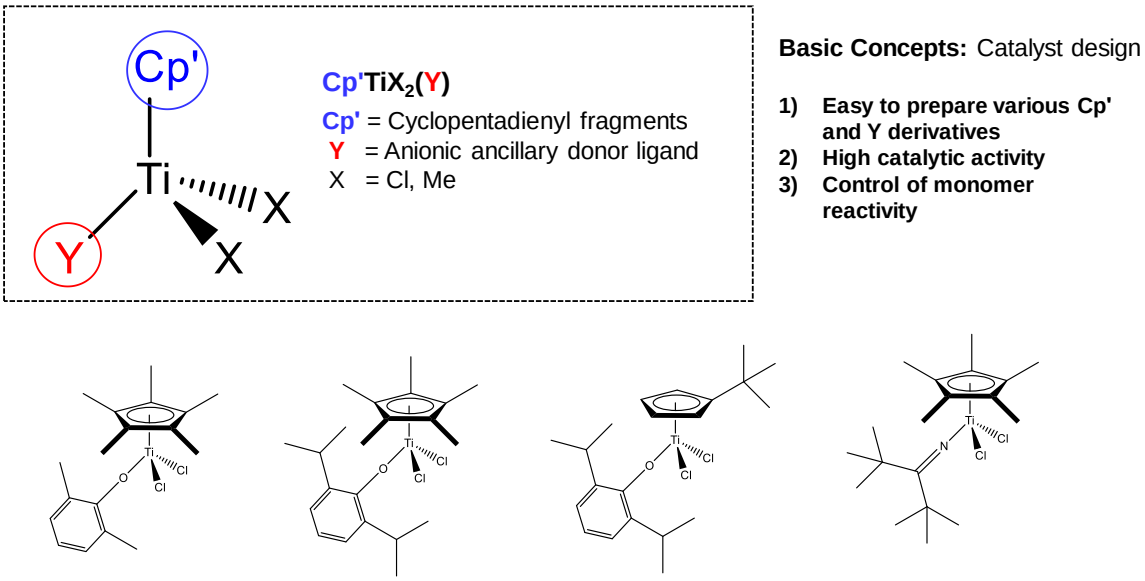

Scheme 11. Design concept and selected examples of non-bridge half-metallocene catalysts [78].

From the above discussions, it can be concluded that molecular catalysts in olefin polymerization are advantageous in terms of tailor-made performance by a variety of metal-ligand combinations. These catalysts can synthesize olefin based materials with new microstructures, which are inaccessible with classical solid catalysts. Each structure of molecular catalysts can make each polyolefin structure special. Moreover, their well-defined structures enable the understanding of many mechanistic aspects of olefin polymerization catalysis. However, to incorporate a new, molecular catalysts require ligand modification. Therefore, despite the advantages, molecular catalysts are inferior to solid catalysts interms of number of functions that can be accumulated per catalyst structure, which makes the molecular catalysts less functional in catalysis.

1.4. Bridging Catalysts in Olefin Polymerization

A bridging catalyst is a catalyst which can conceptually bridge the two extreme ends of catalysts, i.e., molecular catalysts with well-defined but less functional features and solid catalysts with multifunctional but ill-defined features. In the field of olefin polymerization, the concept of bridging catalysts has been long regarded as an important subject in both academy and industry, as accounted by the industrial relevance of both the classical solid catalysts and the tailored molecular catalysts in the production of distinct grades of polyolefins. In this regard, different approaches have been developed for the establishment of a "bridging" catalyst.

Surface organometallic chemistry approach

Surface organometallic chemistry (SOMC) approach is from the side of solid catalysts. In the case of solid catalysts, proper understanding of catalytic processes at a molecular level is obscured by the surface inhomogeneity and the co-presence of different kinds of active sites and their very low concentrations [85]. Thus, the absence of a rational structure-performance relationship (SPR) of solid catalysts has made their development highly empirical. The objective of SOMC is to construct a well-defined active site on solid surfaces, and thereby to clarify SPR [29,85-87]. For example, Basset et al used nonporous partially dehydroxylated silica (SiO_2) aerosils, partially dehydroxylated γ-alumina (Al_2O_3) and a mixture of partially dehydroxylated SiO_2 aerosils and γ-Al_2O_3, which contained surface hydroxyl groups at known concentrations. The hydroxyl groups were reacted with an organometallic complex

$Cp^*Zr(CH_3)_3$ through precise control of each elementary reaction occurring between the organometallic complex and surface hydroxyls [86]. The supported complex was characterized by various spectroscopic techniques (solid state NMR, EXAFS, XANES, in situ IR etc.), which gave molecular insight of the identity of model catalytic species. For instance, when partially dehydroxylated SiO_2 was used, only one type of neutral Zr species (**A**) was formed as represented in Scheme 12. When the mixture of partially dehydroxylated SiO_2 and γ-Al_2O_3 was used, the complex ($Cp^*Zr(CH_3)_3$) can also react with the Lewis acidic sites of γ-Al_2O_3 to form partially or fully cationic Zr species (**B** and **C**) as minor products in addition to neutral Zr species (**A**) as the major product. Since γ-Al_2O_3 contains both surface hydroxyl groups and Lewis acidic sites and their reaction with $Cp^*Zr(CH_3)_3$ resulted into the formation of several neutral and cationic Zr species (**D** to **F**) as represented in Scheme 12. Ethylene polymerization was conducted using the supported catalysts in the absence and presence of MAO to understand the behavior of the model catalytic species, so as to clarify SPR of the solid catalysts. Thus, SOMC is considered as the transfer of the concepts of molecular catalysts to surface science and heterogeneous catalysts in a way to eliminate the blackbox of classical solid catalysts [85].

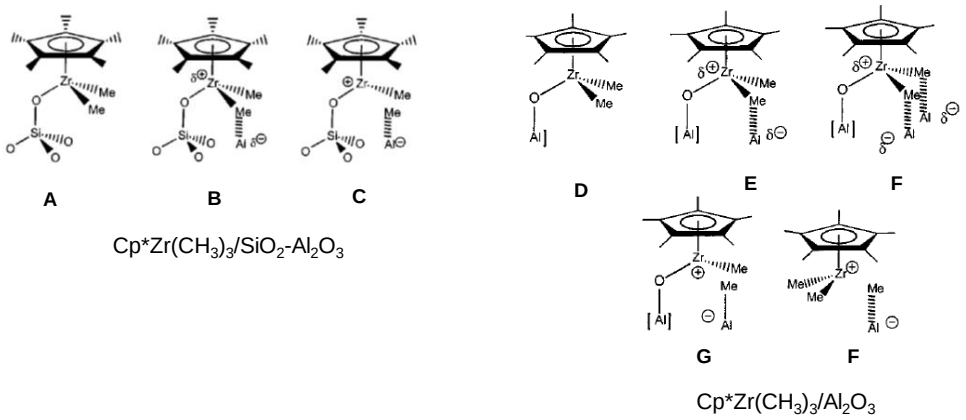

Scheme 12. Surface species created on silica and alumina surfaces [86].

Supported molecular catalysts approach

Inspite of the distinguished features provided by molecular catalysts, they are difficult to be used in the existing operational plants. This is because, the molecular catalysts do not possess a specific morphology as a solid. Homogeneous polymerization processes where a polymer is soluble in an organic solvent are limited to the production of lower crystallinity polymers (*e.g.* elastomers). Most of the polyolefin plants are operated in slurry- or gas-phase processes to produce polymers of higher density or crystallinity (*e.g.* HDPE, iPP), which are insoluble in the reactor diluent or fluidizing gas stream [88]. For continuous operation, these processes require the use of morphologically uniform catalyst particles to prevent reactor fouling [53,88]. Thus, to transfer the novel and distinguished features of the molecular catalysts to existing plants, they are required to be supported on an insoluble carrier. For this purpose, a molecular catalyst is grafted to a solid support such as silica or cross-linked polystyrene by replacing one of its ligands with a similar ligand that is

covalently bonded to the support *via* a linker [53,88-91]. Also, in some cases, a molecular catalyst is supported by the complexation with ion-exchanged clay minerals as support-activators [53]. In the supported molecular catalysts approach, the solid support mitigates reactor fouling during polymerization and the use of a linker helps to retain the single-site nature of the molecular catalyst on solid surfaces. This supported molecular catalysts approach is different from SOMC in a sense that here most of the synthetic effort is to preserve the molecular character of the supported complex. An example is shown in Scheme 13 for the syntheses of a supported FI molecular catalyst. In this method, a FI molecular catalyst was grafted to surface modified silica nanoparticles (*ca*. 50 nm diameter) via a long spacer [91]. The supported catalyst afforded UMMWPE particles with uniform spherical morphology.

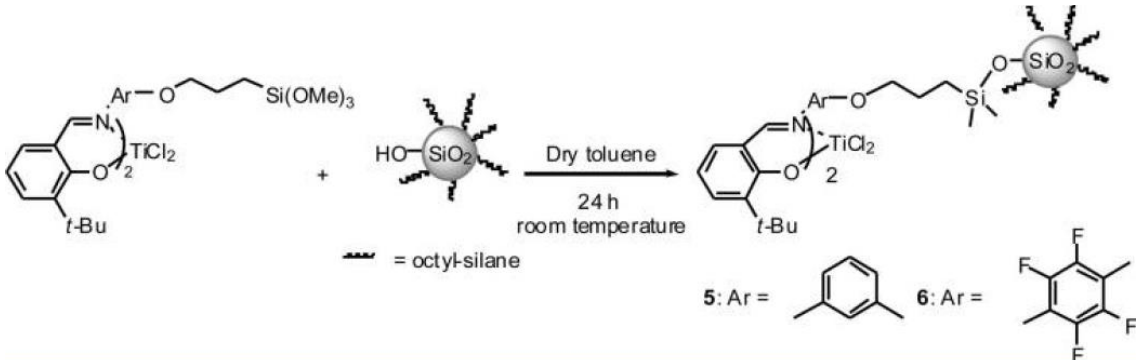

Scheme 13. Synthesis of a supported FI catalyst [91].

Mitsubishi Chemical Corporation and Japan Polychem Corporation have extensively studied "support-activators" to develop industrially applicable supported metallocene catalysts for olefin polymerization [92-95]. For this purpose, acid-treated

montmorillonite (MMT) clay was used to support a zirconocene catalyst as shown in Scheme 14 [93]. After acid treatment, MMT was treated with an alkylaluminum reagent to scavenge the intercalated H_2O molecules. The acid treated MMT possessing strong-acid sites was exploited as support-activator for the zirconocene catalyst (Scheme 14) and it resulted into highly active supported catalyst. In propylene polymerization, the activity level of 68400 kg-PP/mol-Zr·h was achieved using the supported catalyst [94]. The molecular weight distribution of the resultant PP was fairly narrow (M_w/M_n = 2.7). Moreover, spherical morphology of the catalyst particles can be obtained by spray-dry granulation of clay minerals [92-94].

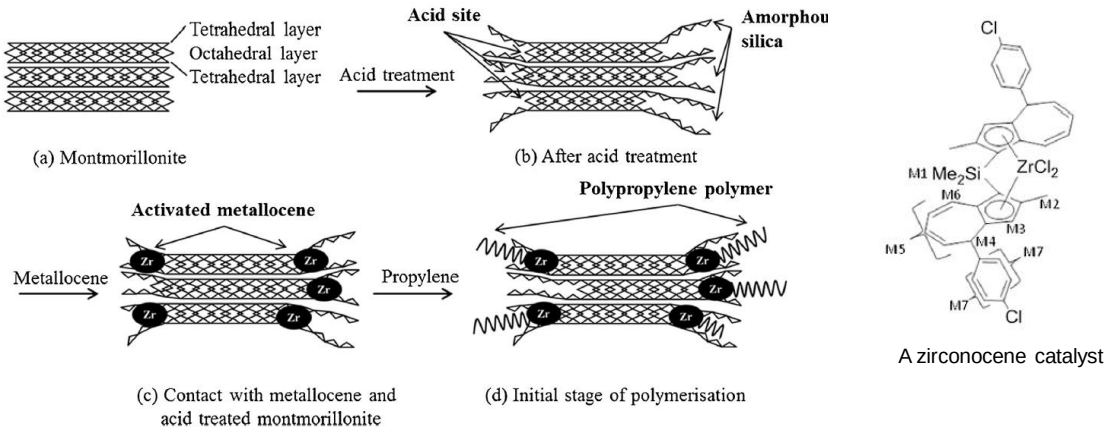

Scheme 14. Synthesis of a clay mineral-supported zirconocene catalyst [93].

Great successes in the field of olefin polymerization was achieved by the work in Japan Polypropylene Corporation, in which two different types of molecular catalysts were immobilized on a single support for tandem catalysis [95]. In this process, a molecular catalyst which can form macromonomers by β-H elimination was

co-supported with a molecular catalyst which can perform stereoselective polymerization on a solid support (*e.g.* clay) for the *in-situ* production of long-chain branched polypropylene, which had been hardly achieved by conventional catalysts.

Binuclear catalysts approach

The concept of multimetallic cooperative catalysis of enzymes in biological systems transferred to single site olefin polymerization catalysts led to the development of a family of binuclear molecular catalysts [8,100]. In this class of catalysts, function integrations have been achieved by the cooperation between two proximate metal centres present in a binuclear complex. In the pioneering research of Marks *et al.*, a series of constrained geometry-based homo and hetero binuclear molecular catalysts were synthesized, and their synergistic combination with a binuclear cocatalyst was explored [8,96-100]. Scheme 15 represents homo and hetero binuclear catalysts and a binuclear cocatalyst synthesized by Marks et al. [96,97]. This combination maximizes the catalyst-cocatlyst nuclearity (Scheme 15) and brings the two metal centres to a closest possible distance for cooperative catalysis. The said cooperation between two sterically open proximate metal centres *via* secondary agostic interaction significantly influences the monomer enchainment and the chain transfer kinetics, which in turn leads to unique catalytic consequences such as higher activity, enhanced branching, higher α-olefin incorporation, and molecular weight increment as compared to their mononuclear analogues [96-100].

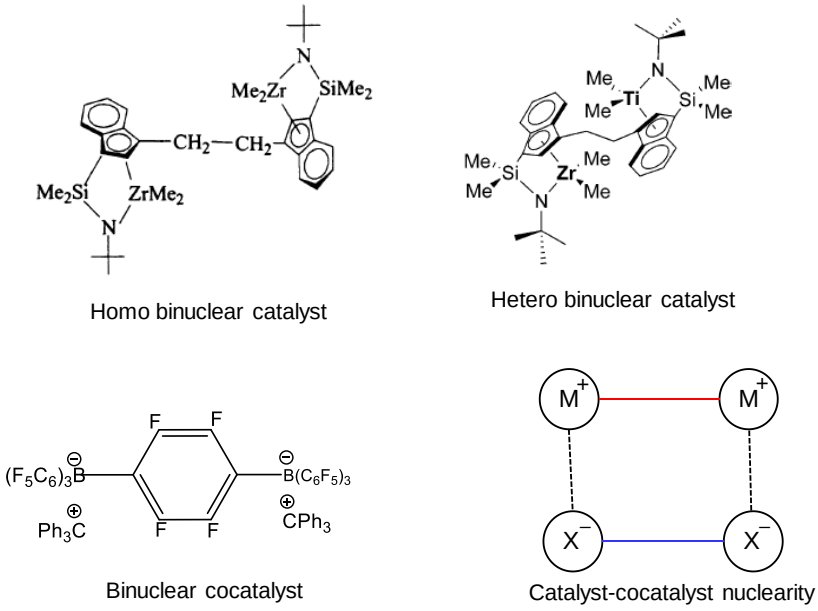

Scheme 15. Examples of binuclear catalysts and their synergistic combination with a binuclear cocatalyst [96,97].

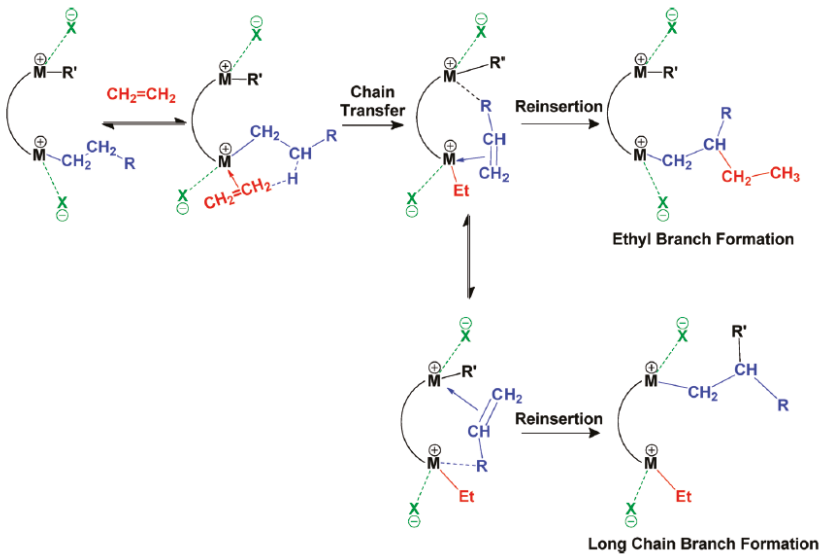

Scheme 16. Representation of short and long chain branch formation in ethylene polymerization with a binuclear catalyst (M^+ is a cationic metal centre and X^- is a counter anion) [8].

Scheme 16 represents the proposed mechanism of short and long chain branch formation in a growing PE chain by the cooperation between two proximate metal centres (M) in a binuclear complex. The cooperation via secondary agostic interaction improves the affinity to α-olefins as compared to ethylene so as to promote their incorporation and subsequently branching.

The concept of binuclear catalyst was successfully extended to tandem catalysis [97,98]. In tandem catalysis, two molecular catalysts having different functions cooperate in a single process. For example, the hetero binuclear catalyst represented in Scheme 15 was used in tandem catalysis for the production of long chain branched polyethylene (LCB PE) [97]. The Zr-based CGC catalyst could produce macromonomers *via* β-H elimination, which were reinserted into the proximate Ti centres to form LCB PE as shown in Scheme 17. It was found that the branching density of PEs produced by the hetero binuclear catalyst was much higher than those produced by the equimolar mixture of the individual mononuclear catalysts.

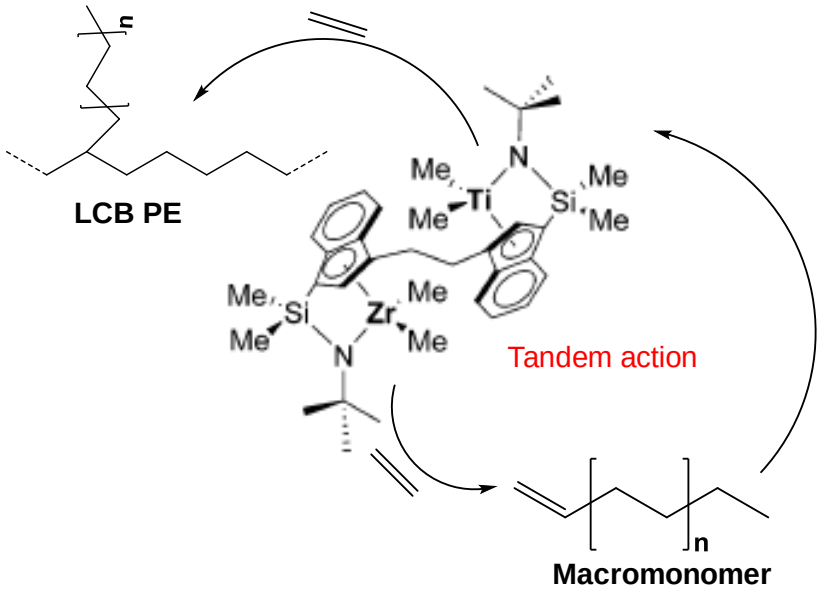

Scheme 17. Tandem catalysis by hetero binuclear catalyst for the production of long chain branched polyethylene [97].

1.5 Purpose of the Present Research

In the field of catalytic olefin polymerization, the great contrast of the characteristics between classical solid catalysts and tailored molecular catalysts have long been motivating the scientists to find a way to bridge the gap between the two extreme classes of catalysts. For this purpose, from the side of solid catalysts, a surface organometallic chemistry (SOMC) approach was developed to establish structure-performance relationship (SPR) using model catalyst systems. On the other hand, from the side of molecular catalysts, a supported molecular catalysts approach was developed to exploit the distinguished features of molecular catalysts in existing operational plants. Furthermore, the concept of tandem catalysis enabled to integrate two molecular catalysts with two different functions on a single support. Finally,

successful function integrations in a single molecule was demonstrated by cooperative catalysis with binuclear complexes. All of these approaches contributed greatly to bridge the gap between molecular and solid catalysts. However, each one of them has their limitations: Although, SOMC has been successful to clarify SPR of solid catalysts, the catalysts suffer from low activity and the formation of multiple surface species. Hence, the molecular character of the supported complex is significantly lost in this approach. On the other hand, in supported molecular catalysts approach, the prime concern is to maintain the molecular character of the supported complex on solid surfaces. For this, the molecular catalyst is tethered to a solid support using a long spacer, in the cost of lesser active site stability as compared to classical solid catalysts. This is because, in the case of classical solid catalysts the active sites are formed directly on solid surfaces, where surface acts as a rigid ligand to protect the active sites by site isolation, mass transport and heat transfer phenomena. Moreover, in most of the cases for supported molecular catalysts, lower activity was reported as compared to their molecular analogues as is usual for using solid supports [53,88,89]. In the case of binuclear molecular catalysts, surely the advantage is the design precession at the molecular level *i.e.*, a proper placement of two metal centres at an optimum distance for maximum cooperation to embody catalytic multifunctionality in a single complex [100]. But the synthetic limitation restricts the number of nuclei, *i.e.* the number of functions, integrable in a single molecule. The integration on solid surfaces would not have such limitation, but combination over two molecular catalysts have not been realized to the best of our knowledge. Based on above discussions, I have come to the conclusion

that a concept to embody catalytic multifunctionality on the basis of well-defined structural features is an important direction to design a bridging catalyst. In this research I aimed to introduce a new option of bridging catalyst for olefin polymerization. For this purpose, I successfully applied a bottom-up strategy for the synthesis of well-defined and multifunctional catalyst. This started from the synthesis of polynorbornene (PNB) with uniform chain length and bearing different contents of ancillary donor ligands at side chain by Grubbs ring-opening metathesis polymerization (ROMP). These PNB were used as soluble support to graft a molecular catalyst and thus to confine multiple active centres in a nano-sized random coil of PNB chains. Such a supported catalyst equips well-defined characteristics in terms of active site design analogous to the molecular catalyst as well as controlled active site density in a random coil of a single polymer chain, whose size is defined by the Flory radius. The basic aim of this research is to explore the cooperative catalysis among neighbouring active sites confined in a nano-sized random coil in order to accumulate functionality in olefin polymerization by a single catalyst system.

References

[1] J. Hagen, Industrial Catalysis: A Practical Approach, Wiley–VCH, Weinheim, 2006, Chapter 1, pp. 1–8

[2] P. Atkins, J.D. Paula, Atkin's Physical Chemistry, Oxford-University Press, Oxford, 2008, Chapter 23, pp. 839–845.

[3] P. Atkins, J.D. Paula, Atkin's Physical Chemistry, Oxford-University Press, Oxford, 2008, Chapter 24, pp. 869–885.

[4] http://www.langmuir-research.org/Mission.html, 11/10/2017.

[5] V. Leskovac, Comprehensive Enzyme Kinetics, Kluwer Academic Publishers, New York, 2004, Chapter 1, pp. 1-6.

[6] L. Marchetti, M. Levine, ACS Catal. 1 (2011) 1090–1118.

[7] R.M. Haak, S.J. Wezenberg, A.W. Kleij, Chem. Commun. 46 (2010) 2713–2723.

[8] M. Delferro, T.J. Marks, Chem. Rev. 111 (2011) 2450–2485.

[9] D.J. Xuereb, R. Raja, Catal. Sci. Technol. 1 (2011) 517–534.

[10] B. Cornils, W.A. Herrmann, in: B. Cornils (Ed.), W.A. Herrmann (Ed.), Applied Homogeneous Catalysis with Organometallic Compounds, Vol. 1, Wiley–VCH, Weinheim, 2002, Chapter 1, pp. 1–16.

[11] W.A. Herrmann, B. Cornils, Angew. Chem. Int. Ed. 36 (1997) 1048–1067.

[12] S. Bhaduri, D. Mukesh, Homogeneous Catalysis: Mechanisms and Industrial Applications, Wiley-Interscience, New York, 2000.

[13] A.M. Echavarren, D.J. Cárdenas, in: A. de Meijere (Ed.), F. Diederich (Ed.), Metal-Catalyzed Cross-Coupling Reactions, Wiley–VCH, Weinheim, 2004, Chapter 1,

pp. 1–40.

[14] T.M. Trnka, R.H. Grubbs, Acc. Chem. Res. 34 (2001) 18–29.

[15] N. Miyaura, A. Suzuki, Chem. Rev. 95 (1995) 2457–2483.

[16] G.J. Britovsek, V.C. Gibson, D.F. Wass, Angew. Chem. Int. Ed. 38 (1999) 428–447.

[17] T. Hayashi, Acc. Chem. Res. 33 (2000) 354–362.

[18] W. Kaminsky, A. Laban, Appl. Catal. A: Gen. 222 (2001) 47–61.

[19] L.C. Wilkins, R.L. Melen, Coord. Chem. Rev. 324 (2016) 123–139.

[20] C.W. Bielawski, R.H. Grubbs, Prog. Polym. Sci. 32 (2007) 1–29.

[21] R.R. Schrock, Acc. Chem. Res. 23 (1990) 158–165.

[22] K. Nomura, M.M. Abdellatif, Polymer 51 (2010) 1861–1881.

[23] A. Leitgeb, J. Wappel, C. Slugovc, Polymer 51 (2010) 2927–2946.

[24] B. Xue, K. Ogata, A. Toyota, Polym. Degrad. Stab. 93 (2008) 347–352.

[25] P. Schwab, R.H. Grubbs, J.W. Ziller, J. Am. Chem. Soc. 118 (1996) 100–110.

[26] M.S. Sanford, J.A. Love, R.H. Grubbs, J. Am. Chem. Soc. 123 (2001) 6543–6544.

[27] T.L. Choi, R.H. Grubbs, Angew. Chem. 115 (2003) 1785–1788.

[28] J.M. Thomas, W.J. Thomas, Principle and Practice of Heterogeneous Catalysis, Wiley–VCH, Weinheim, 2014, Chapter 8, pp. 629–645.

[29] M.M. Stalzer, M. Delferro, T.J. Marks, Catal. Lett. 145 (2015) 3–14.

[30] J. Hagen, Industrial Catalysis: A Practical Approach, Wiley–VCH, Weinheim, 2006, Chapter 5–7, pp. 99–292.

[31] L. Forni, Catal. Today 52 (1999) 147–152

[32] J. Weitkamp, ChemCatChem 4 (2012) 292–306.

[33] S. Matsumoto, Catal. Today 90 (2004) 183–190.

[34] K. Soga, T. Shiono, Prog. Polym. Sci. 22 (1997) 1503–1546.

[35] G.W. Huber, S. Iborra, A. Corma, Chem. Rev. 106 (2006) 4044–4098.

[36] B.K. Min, C.M. Friend, Chem. Rev. 107 (2007) 2709–2724.

[37] https://www.inkwoodresearch.com/reports/global-polyolefin-market-2017-2025, 10/11/2017

[38] H. Kim, S. Kobayashi, M.A.A. Rahim, M.J. Zhang, A. Khusainova, M.A. Hillymer, A.A. Abdala, C.W. Macoskv, Polymer 52 (2011) 1837–1846.

[39] B. Maira, P. Chammingkwan, M. Terano, T. Taniike, Macromol. Mater. Eng. 300 (2015) 679–83.

[40] Q. Airong, B. Maira, R. Strauss, Y. Zhao, P. Chammingkwan, G. Mizutani, T. Taniike, Polymer 127 (2017) 251–258.

[41] B. Maira, P. Chammingkwan, M. Terano, T. Taniike, Compos. Sci. Technol. 144 (2017) 151–59.

[42] S. Ehlert, C. Stegelmeier, D. Pirner, S. Forster, Macromolecules 48 (2015) 5323–5327.

[43] M. Bieligmeyer, S.M. Taheri, I. German, J. Breu, F.D. Agosto, S. Forster, J. Am. Chem. Soc. 134 (2012) 18157–18160.

[44] I. Plesa, P.V. Notingher, S. Schlog, C. Sumereder, M. Muhr, Polymers 8 (2016) 173–239.

[45] T. Kashiwagi, R.H. Harris, R.M. Briber, S.R. Raghavan, W.H. Awad, J.R. Shields,

Polymer 45 (2004) 881–891.

[46] J.P. Hogan, R.L. Banks, US. Patent 530617, 1953 to Phillips Petroleum.

[47] K. Ziegler, G.H. Gellert, K. Zosel W. Lehmkuhl, W. Pfohl, Angew. Chem. 67 (1955) 424.

[48] G. Natta, J. Polym. Sci. 16 (1955) 143–154.

[49] E. Albizzati, U. Giannini, G. Collina, L. Noristi, L. Resconi, in: E.P. Moore Jr. (Ed.), Polypropylene Handbook, Hanser, New York, 1996, Chapter 2, pp. 11–98.

[50] M.P. McDaniel, ACS Catal. 1 (2011) 1394–1407.

[51] B. Liu, T. Nitta, H. Nakatani, M. Terano, Macromol. Chem. Phys. 204 (2003) 395–402.

[52] K. Tonosaki, T. Taniike, M. Terano, J. Mol. Catal. A: Chem. 340 (2011) 33–38.

[53] J.R. Severn, J.C. Chadwick, R. Duchateau, N. Friederichs, Chem. Rev. 105 (2005) 4073–4147.

[54] G. Natta, P. Pino, G. Mazzanti, U. Giannini, J. Am. Chem. Soc. 79 (1957) 2975–2976.

[55] W. Kaminsky, Macromolecules 45 (2012) 3289–3297.

[56] A.L. McKnight, R.M. Waymouth, Chem. Rev. 98 (1998) 2587–2598.

[57] H. Makio, T. Fujita, Acc. Chem. Res. 42 (2009) 1532–1544.

[58] L.K. Johnson, C.M. Killian, M. Brookhart, J. Am. Chem. Soc. 117 (1995) 6414–6415.

[59] B.L. Small, M. Brookhart, A.M. Bennett, J. Am. Chem. Soc. 120 (1998) 4049–4050.

[60] E.Y. Chen, T.J. Marks, Chem. Rev. 100 (2000) 1391–1434.

[61] T. Taniike, M. Terano, in: W. Kaminsky (Ed.), Polyolefins: 50 Years after Ziegler and Natta I, Springer-Verlag, Berlin Heidelberg, 2013, Chapter 4, pp. 81–97.

[62] T. Taniike, M. Terano, J. Catal. 293 (2012) 39–50.

[63] V. Busico, P. Corradini, L. De Martino, A. Proto, V. Savino, E. Albizzati, Makromol. Chem. 186 (1985) 1279–1288.

[64] V. Busico, R. Cipullo, G. Monaco, G. Talarico, M. Vacatello, J.C. Chadwick, A.L. Segre, O. Sudmeijer, Macromolecules 32 (1999) 4173–4182.

[65] V. Busico, M. Causa, R. Cipullo, R. Credendino, F. Cutillo, N. Friederichs, R. Lamanna, A. Segre, V.V.A. Castelli, J. Phys. Chem. C. 112 (2008) 1081–1089.

[66] M. Terano, A. Murai, M. Inoue, K. Miyoshi, JP Patent 1987-158704 (1987), to Toho Catalyst Co., Ltd..

[67] M. Ferraris, F. Rosati, US Patent 4469648 (1984), to Montedison S.P.A.

[68] T. Taniike, T. Funako, M. Terano, J. Catal. 311 (2014) 33–40.

[69] T. Funako, P. Chammingkwan, T. Taniike, M. Terano, Macromol. React. Eng. 9 (2015) 325–332.

[70] P.D. Hustad, R.L. Kuhlman, E.M. Carnahan, T.T. Wenzel, D.J. Arriola, Macromolecules 41 (2008), 408–4089.

[71] G.W. Coates, Chem. Rev. 100 (2000) 1223–1252.

[72] P. Corradini, G. Guerra, L. Cavallo, Acc. Chem. Res. 37 (2004) 231–241.

[73] W. Kaminsky, K. Kulper, H.H. Brintzinger, F.R.W.P. Wild, Angew. Chem. Int. Ed. 24 (1985) 507–508.

[74] J.A. Ewen, R.L. Jones, A. Razavi, J.D. Ferrara, J. Am. Chem. Soc. 110 (1988) 6255–6256.

[75] S.D. Ittel, L.K. Johnson, M. Brookhart, M. Chem. Rev. 100 (2000) 1169–1203.

[76] G.J.P. Britovsek, V.C. Gibson, D.F. Wass, Angew. Chem. Int. Ed. 38 (1999) 428–447.

[77] M.C. Baier, M.A. Zuideveld, S. Mecking, Angew. Chem. Int. Ed. 53 (2014) 9722–9744.

[78] K. Nomura, J. Liu, S. Padmanabhan, B. Kitiyanan, J. Mol. Catal. A: Chem. 267 (2007) 1–29.

[79] K. Nomura, N. Naga, M. Miki, K. Yanagi, Macromolecules 31 (1998) 7588–7597.

[80] K. Nomura, T. Komatsu, Y. Imanishi, Macromolecules 33 (2000) 8122–8124.

[81] H. Zhang, K. Nomura, Macromolecules 39 (2006) 5266–5274.

[82] K. Nomura, M. Tsubota, M. Fujiki, Macromolecules 36 (2003) 3797–3799.

[83] J. Liu, K. Nomura, Adv. Synth. Catal. 349 (2007) 2235–2240

[84] W. Wang, M. Fujiki, K. Nomura, J. Am. Chem. Soc. 127 (2005) 4582–4583.

[85] C. Copéret, M. Chabanas, R.P.S. Arroman, J.M Basset, Angew. Chem. Int. Ed. 42 (2003) 156–181.

[86] M. Jezequel, V. Dufaud, M.J. Ruiz-Garcia, F. Carrillo-Hermosilla, U. Neugebauer, G.P. Niccolai, F. Lefebvre, F. Bayard, J. Corker, S. Fiddy, J. Evans, J.P. Broyer, J. Malinge, J.M. Basset, J. Am. Chem. Soc. 123 (2001) 3520–3540.

[87] C. Copéret, J.M. Basset, Adv. Synth. Catal. 349 (2007) 78–92.

[88] G.G. Hlatky, Chem. Rev. 100 (2000) 1347–1376.

[89] B. Heurtefeu, C. Bouilhac, É. Cloutet, D. Taton, A. Deffieux, H. Cramail, Prog. Polym. Sci. 36 (2011) 89–126.

[90] M. Klapper, D.J. Nietzel, J.W. Krumpfer, K. Mullen, Chem. Mater. 26 (2014),802−819.

[91] A. Amgoune, M. Krumova, S. Mecking, Macromolecules 41 (2008) 8388–8396.

[92] T. Tayano, T. Sagae, T. Atsumi, H. Uchino, M. Murata, T. Sato, Polyolefins Journal 3 (2016) 79-92.

[93] T. Tayano, H. Uchino, T. Sagae, S. Ohta, S. Kitade, H. Satake, M. Murata, J. Mol. Catal. A: Chem. 420 (2016) 228–236.

[94] T. Tayano, H. Uchino, T. Sagae, K. Yokomizo, K. Nakayama, S. Ohta, H. Nakano, M. Murata, Macromol. React. Eng. (2017) 1600017.

[95] S. Hotta, K. Asuka, S. Kitade, K. Takahashi, I. Kouzai, T. Tayano, US Patent 20150010747A1 (2015), to Japan Polypropylene Corporation.

[96] L. Li, M.V. Metz, H. Li, M.-C. Chen, T.J. Marks, L. Liable-Sands, A.L. Rheingold, J. Am. Chem. Soc. 124 (2002) 12725–12741.

[97] J. Wang, H. Li, N. Guo, L. Li, C.L. Stern, T.J. Marks, Organometallics 23 (2004) 5112−5114.

[98] S. Liu, A. Motta, A.R. Mouat, M. Delferro, T.J. Marks, J. Am. Chem. Soc. 136 (2014) 10460–10469.

[99] M.R. Salata, T.J. Marks, Macromolecules 42 (2009) 1920−1933.

[100] J.P. McInnis, M. Delferro, T.J. Marks, Acc. Chem. Res. 47 (2014) 2545−2557.

Chapter 2

Synthesis of Aryloxide-Containing Half-Titanocene Catalysts Grafted to Soluble Polynorbornene Chains and Their Application in Ethylene Polymerization: Integration of Multiple Active Centres in a Random Coil

ABSTRACT:

A series of monodisperse polynorbornene (PNB) chains bearing different contents of aryloxide ligands at their side chain were synthesized by Grubbs ring-opening metathesis copolymerization between norbornene and 2-aryloxonorbornene. These PNB chains were employed as a soluble support for grafting half-titanocene complexes to afford structurally well-defined supported catalysts, where a pre-defined number of Ti centres was confined in a nano-sized random coil of PNB chains. Extensive investigation in ethylene polymerization revealed unique catalytic features of these soluble polymer-supported catalysts, represented by a synergistic activity enhancement among multiple active centres confined in a random coil. The well-defined nature of these novel polymer-supported catalysts is powerful in studying interactions between active centres and supports as well as among active centres themselves in catalysis.

2.1. Introduction

Catalysts, which are the integral component of most of the modern chemical processes, can be categorized into two primary classes: Molecular catalysts and solid catalysts. The former class corresponds to small molecules, including transition metal complexes. They are soluble and featured with the advantage of tailor-made performance by a variety of metal-ligand combinations [1,2]. Moreover, integrated knowledge of organic and organometallic chemistry enables the precise bottom-up design of active site structures for a superior activity and selectivity. This is exemplified by the success story of C–C cross coupling reactions, olefin metathesis/polymerization reactions, asymmetric synthesis and so on [3-9]. To the other extreme, solid catalysts utilize coordinative unsaturation created on solid surfaces [10]. In general, they are cheap, separable, reusable and thermally robust, which make them suitable for industrial applications. The most notable applications include oil refineries, production of fine chemicals, automotive catalytic converters, industrial polyolefin productions, conversion of biomass into fuels and chemicals, green and sustainable chemical transformations and so on [11-17]. Solid catalysts offer the advantage of the integration of multi-components over multi-length scales for the accumulation of multiple functions [18]. Whereas, their inherent chemical and structural complexities lead to ill-defined characteristics, which are hardly controlled based on conventional top-down design, resulting in inferior catalytic selectivity. Thus, the contrast of the characteristics encourages the catalyst community to focus on new concepts so as to bridge the gap between molecular and solid catalysts. An

illustration is the "International Symposium on Relations between Homogeneous and Heterogeneous Catalysis", which already has accomplished seventeen successful meetings [19].

In the field of olefin polymerization, the above-mentioned bridging concept has been long regarded as an important subject in both academy and industry, as accounted by the industrial relevance of both the classical solid catalysts and the tailored molecular catalysts in the production of distinct grades of polyolefins [20-23]. In this regard, different approaches have been developed for the establishment of a “bridging” catalyst. One of these approaches is from the side of solid catalysts, especially based on surface organometallic chemistry [24,25]. A uniform active site structure is constructed on solid surfaces through precise control of each reaction occurring between an organometallic complex and support (*e.g.* silica) surfaces. Characterization of the supported complex gives molecular insight of the identity and behaviour of model catalytic species, thus being powerful to study structure-performance relationships of solid catalysts. Another approach is based on supported molecular catalysts [26-28], which aims to transfer the distinguished features of the molecular catalysts to existing plants. For this purpose, a molecular catalyst is grafted to a solid support such as silica or cross-linked polystyrene by replacing one of its ligands with a similar ligand that is covalently bonded to the support *via* a linker. Here, the solid support mitigates reactor fouling during polymerization and the use of a linker helps to retain the single-site nature of the molecular catalyst on solid surfaces. Further successes have been brought by immobilizing two types of molecular catalysts (tandem catalysis) on a single

support. Representatively, a macromonomer forming site and a stereoselective polymerization site are co-supported on a solid surface for the *in-situ* production of long-chain branched polypropylene, which had been hardly achieved by conventional catalysts [29]. Function integrations have also been achieved in a class of binuclear molecular catalysts by the cooperation between two proximate metal centres present in a binuclear complex [30]. In the pioneering research of Marks *et al.*, a series of constrained geometry based homo and hetero binuclear molecular catalysts were synthesized, and their synergistic combination with a binuclear cocatalyst was explored [30-32]. In these binuclear catalysts, cooperation between two metal centres *via* secondary agostic interaction significantly influenced the monomer enchainment and the chain transfer kinetics, which in turn led to unique catalytic consequences such as higher activity, enhanced branching, higher α-olefin incorporation, and molecular weight increment as compared to their mononuclear analogues. Most notably, the binuclear catalysts have embodied catalytic multifunctionality at a molecular precision, even though the synthetic limitation restricts the number of nuclei, *i.e.* the number of functions, integrable in a single molecule. The integration on solid surfaces would not have such limitation, but combination over two molecular catalysts have not been realized to the best of my knowledge. Thus, a concept to embody catalytic multifunctionality on the basis of well-defined structural features is an important direction to design a bridging catalyst in the field of olefin polymerization.

Based on the above discussions, this chapter provides another option of bridging catalysts for olefin polymerization: Polynorbornene (PNB) with uniform chain length

and bearing ancillary donor ligands at side chain was synthesized by Grubbs ring-opening metathesis polymerization (ROMP) [33,34], and used as a soluble support for a molecular catalyst. Such a supported catalyst equips well-defined characteristics in terms of active site design analogous to the molecular catalyst as well as controlled active site density in a random coil of a single polymer chain, whose size is defined by the Flory radius. Moreover, potential synergy among neighbouring active sites confined in a random coil would help to accumulate functionality in an unrestricted way.

There have been a few examples in literature, in which chain-end or side-chain functionalized linear/star shaped PNB was used as a support for molecular catalysts and employed in organic transformations, where performance similar to the molecular catalyst was obtained [35-39]. In addition, the solubility of PNB can be exploited to perform catalysis under homogeneous conditions in a good solvent and recycle the catalyst by recovering it through reprecipitaion in a poor solvent. Nomura and co-workers immobilized half-titanocene complexes at the chain end of PNB through aryloxide ligands and employed the resultant catalysts in ethylene (co)polymerization [40]. These catalysts showed similar performance to the molecular analogues in terms of the molecular weight, molecular weight distribution and comonomer incorporation. These previous studies established PNB as a promising support for molecular catalysts, but exploration of support-mediated catalytic multifunctionality by confining multiple active centres in the random coil of soluble and well-defined PNB has been scarcely studied, especially in olefin polymerization.

In the present chapter, I have synthesized a norbornene derivative containing an aryloxo pendant group by a Pd-catalysed reductive Heck-coupling reaction, followed by its copolymerization with norbornene. A series of well-defined PNB supports were synthesized with different comonomer contents and utilized to graft half-titanocene complexes [41]. The synthetic methodologies and the potential synergy among multiple active centres confined in a random coil were discussed.

2.2 Experimental

2.2.1. Materials

All commercially available reagents were of a research grade and used without further purification unless specified. Bicyclo[2.2.1]hepta-2,5-diene (norbornadiene), 4-bromo-2,6-dimethyphenol, bis(triphenylphosphine)palladium(II) dichloride ($Pd(PPh_3)_2Cl_2$), bicyclo[2.2.1]hept-2-ene (norbornene), 2,6-dimethylphenol, pentamethylcyclopentadienyltitanium (IV) trichloride (Cp^*TiCl_3), and trityl tetrakis(pentafluorophenyl)borate ($Ph_3CB(C_6F_5)_4$) were purchased from Tokyo Chemical Industry. Ammonium formate (NH_4HCO_2), the Grubbs 1st generation catalyst, and ethyl vinyl ether, 1-octene and1,1,2,2-tetrachloroethane-d_2 were purchased from Sigma-Aldrich. 1,2,4-trichlorobenzene and triethylamine were purchased from Kanto Chemical. Triethylamine was purified by distillation under reduced pressure. *N*,*N*-dimethylformamide (DMF, Wako Pure Chemical Industries) was dried over molecular sieves 4A and N_2 bubbling. Trimethyl pentamethylcyclopentadienyltitanium (IV) (Cp^*TiMe_3) was purchased from Strem

Chemicals. Modified methylaluminoxane (MMAO) and tri-*iso*-butylaluminum (TIBA) were donated by Tosoh Finechem. Ethylene of a research grade was donated by Sumitomo Chemical and used as delivered. Dichloromethane (CH_2Cl_2) and toluene of an anhydrous grade (Sigma-Aldrich and Wako Pure Chemical Industries) were used for the synthesis of PNB supports and catalysts. They were further dehydrated over molecular sieves 3A and 4A, respectively, in teflon sealed flasks and bubbled with N_2 prior to use. Diethyl ether of an anhydrous grade was purchased from Tokyo Chemical Industry and degassed before use. Toluene (Kanto Chemical) for polymerization was stored in a pressurized tank after being passed through a column of molecular sieves 4A and bubbled with N_2. Deuterated chloroform ($CDCl_3$, Kanto Chemical) was stored over molecular sieves 3A in a teflon sealed schlenk tube and degassed before use.

2.2.2. Measurements

All ^1H and ^{13}C $\{^1H\}$ NMR spectra were recorded on a 400 MHz Bruker Advance spectrometer in $CDCl_3$ at 25 °C and all chemical shifts were given in ppm. The residual peak of $CHCl_3$ at 7.26 ppm and the peak of $CDCl_3$ at 77.16 ppm were used as references in ^1H and ^{13}C NMR, respectively. The number-average molecular weight (M_n), weight-average molecular weight (M_w) and the polydispersity index (M_w/M_n) of PNB supports were determined by gel permeation chromatography (GPC, Shimadzu SCL-10A) equipped with a RID-10A detector and calibrated with polystyrene standards. Tetrahydrofuran (THF) of a GPC grade (Wako Pure Chemical Industries, stabilizer-free) was used as the eluent with an isocratic flow rate of 1.0 mL/min at 35 °C. To analyse

functional groups of PNB supports, attenuated total reflectance infrared spectroscopy (ATR-IR, Perkin Elmer Spectrum 100 FT-IR) was used in the range of 500-4000 cm^{-1} using a diamond crystal. The size of a PNB chain, defined as a hydrodynamic diameter, was determined by dynamic light scattering (DLS, Zetasizer 3000) at a scattering angle of 173° in toluene (1.0 mg/mL). The molecular weight distribution of polyethylene (PE) was determined by high-temperature GPC (Waters 150C) equipped with polystyrene gel columns (Showa Denko AD806M/S) and an IR detector (MIRAN 1A) at 140 °C using 1,2,4-trichlorobenzene as the eluent and calibrated with polystyrene standards. The melting temperature (T_m) and crystallinity (X_c) of PE were acquired on a differential scanning calorimeter (DSC, Mettler Toledo DSC-822) based on the first heating cycle at 10 °C/min up to 180 °C under 200 mL/min of N_2. The 1-octene incorporation amount in ethylene/1-octene copolymers was determined based on $^{13}C\{^1H\}$ NMR on a 400 MHz Bruker Advance spectrometer at 120 °C using 1,2,4-trichlorobenzene as a solvent and 1,1,2,2-tetrachloroethane-d_2 (4/1, v/v) as an internal lock and reference.

2.2.3. Synthesis of 4-bicyclo[2.2.1]hept-5-en-2-yl-2,6-dimethylphenol

A schlenk tube was exchanged with N_2 and charged with norbornadiene (46 mmol), 4-bromo-2,6-dimethylphenol (9.0 mmol), triethylamine (28 mmol) and NH_4HCO_2 (37 mmol). The mixture was dissolved in DMF (15 mL), to which $Pd(PPh_3)_2Cl_2$ (0.40 mmol) was added. The solution was heated at 80 °C for 16 h under N_2 with constant stirring, and subsequently poured into a beaker containing acidic

water. The product was extracted with CH_2Cl_2, washed with deionized water, dehydrated over anhydrous Na_2SO_4, and finally isolated by silica column chromatography (1/9 v/v ethylacetate/hexane) in 80% yield. Figs. 1a,b represent the ^1H and ^{13}C NMR spectra of the synthesized 2-aryloxonorbornene. The exo-isomer was obtained as the major product (> 95.0%).

^1H NMR (400 MHz, $CDCl_3$, δ): 1.37-1.46 (m, 1H, H_3), 1.52-1.64 (m, 2H, H_7), 1.65-1.74 (m, 1H, H_3), 2.25 (s, 6H, H_e), 2.60 (dd, J = 9.6 Hz, 1H, H_2), 2.83 (bs, 1H, H_4), 2.95 (bs, 1H, H_1), 4.49 (s, 1H, OH), 6.15 (dd, J = 7.4 Hz, 1H, H_6), 6.24 (dd, J = 7.4 Hz, 1H, H_5), 6.90 (s, 2H, H_b).

^{13}C NMR (100 MHz, $CDCl_3$, δ): 16.2 (C_e), 33.6 (C_7), 42.3 (C_4), 43.0 (C_1), 45.9 (C_3), 48.7 (C_2), 122.8 (C_c), 127.9 (C_b), 137.3 (C_5), 137.5 (C_6), 137.8 (C_a), 150.1 (C_d).

HRMS(ESI) m/z: $[M–H]^+$ calculated for $C_{15}H_{18}O$, 213.290; found, 213.128.

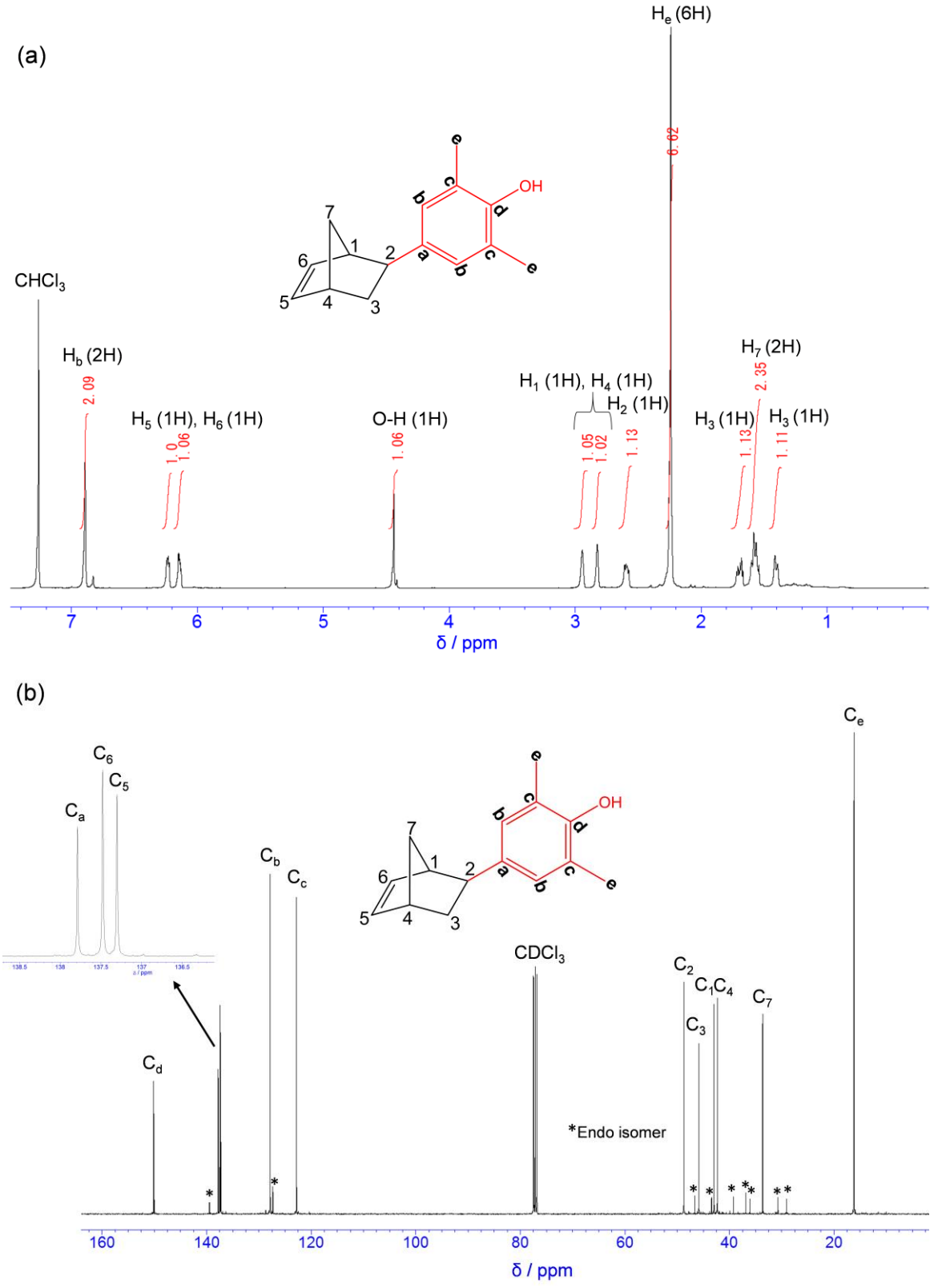

Fig. 1. a) ^{1}H and b) ^{13}C NMR spectra of 2-aryloxonorbornene.

2.2.4. Synthesis of PNB supports

In a typical experiment, *e.g.* run 4 in Table 1, the synthesized 2-aryloxonorbornene (0.68 mmol) and norbornene (12.8 mmol) were dissolved in CH_2Cl_2 (12 mL) in a schlenk tube under N_2. To this, a solution of the Grubbs 1st generation catalyst (8.0 mmol/L) in CH_2Cl_2 (8.0 mL) was added at room temperature. After 3 h, the polymerization was quenched by adding an excess of ethyl vinyl ether. The polymer was precipitated from methanol, washed with methanol on a filter, again reprecipitated from CH_2Cl_2/diethyl ether, and finally collected as a white solid. The peaks in the ^1H and ^{13}C NMR (Figs. 2,3) spectra were consistently assigned based on literature [42,43] as follows.

^1H NMR (400 MHz, $CDCl_3$, δ): 0.90-1.13 (m, 1H, H_7), 1.20-1.46 (m, 2H, $H_{5,6}$), 1.65-2.01 (m, 3H, $H_{5,6,7}$), 2.20 (s, 6H, H_e), 2.42 (bs, 2H, $H_{1,4}$, *trans*), 2.78 (bs, 2H, $H_{1,4}$, *cis*), 4.42 (s, 1H, OH), 5.12-5.25 (m, 2H, ,$H_{2,3}$, *cis*), 5.26-5.42 (m, 2H, $H_{2,3}$, *trans*), 6.78 (s, 2H, H_b).

^{13}C NMR (100 MHz, $CDCl_3$, δ): 16.2 (C_e); 32.3, 32.5, 33.0, 33.2, 38.6, 38.8, 41.5, 42.2, 43.3, 43.6, 50.5, 50.8, 52.0 (saturated carbons of PNB backbone); 122.6 (C_c), 127.7 (C_b); 130.9, 133.0, 133.2, 133.3, 133.9, 134.1, 134.7 (olefinic carbons of PNB backbone); 137.2 (C_a), 150.2 (C_d).

*2.2.5. Synthesis of PNB-g-CAT Cl (**1a**)*

A flame-dried schlenk tube was exchanged with N_2 and charged with a solution of Cp*$TiCl_3$ (1.8 mmol) in CH_2Cl_2 (20 mL). To this, a solution of a PNB support (1/6

equivalent of the aryloxide ligand with respect to Cp^*TiCl_3) in CH_2Cl_2 (30 mL) was added dropwise under N_2 with continuous stirring at room temperature. The reaction was slowly warmed to the boiling temperature of the solvent and then refluxed for 36 h. Thereafter, the product was precipitated out by adding diethyl ether, and unreacted Cp^*TiCl_3 was washed out. PNB-*g*-CAT Cl (**1a**) was obtained in 75-80% yield as a red solid after repetitive washing with diethyl ether and vacuum drying for several hours.

*2.2.6. Synthesis of PNB-g-CAT Me (**1b**)*

To a solution of $C_p^*TiMe_3$ (0.16 mmol) in toluene (0.4 mL), a solution of a PNB support (1 equivalent of the aryloxide ligand with respect to Cp^*TiMe_3) in toluene (6.0 mL) was added dropwise under N_2 with continuous stirring at room temperature. The reaction mixture was stirred for 90 min, and then the solvent was removed by vacuum drying to directly afford PNB-*g*-CAT Me (**1b**) as a yellow solid.

*2.2.7. Synthesis of $Cp^*Ti(O\text{-}2,6\text{-}Me_2C_6H_3)Cl_2$ (**CAT Cl, 2a**)*

The complex was synthesized according to the reference [44]. The structure was confirmed by ^1H and ^{13}C NMR spectroscopy (Figs. 9,11).

^1H NMR (400 MHz, $CDCl_3$, δ): 2.22 (s, 15H, Cp–C$\underline{H}_3$), 2.28 (s, 6H, H_e), 6.83 (t, J = 7.6 Hz, 1H, H_a), 6.95 (d, J = 7.6 Hz, 2H, H_b).

^{13}C NMR (100 MHz, $CDCl_3$, δ): 13.2 (Cp–$\underline{C}H_3$), 17.4 (C_e), 123.0 (C_c), 128.5 (C_b), 128.9 (C_a), 132.7 (Cp), 162.2 (C_d).

*2.2.8. Synthesis of Cp*Ti(O-2,6-$Me_2C_6H_3$)Me_2 (**CAT Me**, **2b**)*

The complex was synthesized according to the reference [44] with slight modifications. A flame-dried schlenk tube was exchanged with N_2 and charged with a solution of Cp*$TiMe_3$ (1.0 mmol) in toluene (5.0 mL). To this, a solution of 2,6-dimethylphenol (1.0 mmol) in toluene (2.0 mL) was added dropwise at room temperature. The reaction was stirred for 90 min and then dried under vacuum to afford a yellow coloured solid. Quantitative conversion was confirmed by ^{1}H and ^{13}C NMR spectroscopy (Figs. 13,15).

^{1}H NMR (400 MHz, $CDCl_3$, δ): 0.48 (s, 6H, Ti–C$\underline{H}_3$), 1.95 (s, 15H, Cp–C$\underline{H}_3$), 2.19 (s, 6H, H_e), 6.80 (t, J = 7.6 Hz, 1H, H_a), 7.0 (d, J = 7.8 Hz, 2H, H_b).

^{13}C NMR (100 MHz, $CDCl_3$, δ): 11.8 (Cp–$\underline{C}H_3$), 17.4 (C_e), 54.2 (Ti–$\underline{C}H_3$), 120.5 (C_c), 122.4 (Cp), 127.9 (C_a), 128.2 (C_b), 161.5 (C_d).

2.2.9. Ethylene homopolymerization

Ethylene homopolymerization was performed in a 1 L autoclave equipped with a mechanical stirrer rotating at 350 rpm, where two types of activator systems, MMAO and TIBA/$Ph_3CB(C_6F_5)_4$ were employed. In a typical experiment, *e.g.* run 12 in Table 4, toluene (300 mL) and MMAO (Al = 30 mmol) were introduced into the reactor and the solution was saturated with ethylene (0.6 MPa, absolute pressure) at 30 °C for 30 min. Thereafter, a toluene solution (1.0 mL) of PNB-*g*-CAT Cl (Ti = 5.0 μmol) was injected into the reactor to initiate the polymerization. The polymerization was conducted for 10 min with a continuous supply of ethylene at 0.6 MPa. The resultant

polymer was repeatedly washed with acidic ethanol/deionized water, collected by filtration and dried under vacuum for several hours at 60 °C. The same procedure was applied in the case of the other activator system. For example, in run 24 of Table 4, TIBA (2.5 mmol) was added instead of MMAO, and the polymerization was initiated by the addition of PNB-*g*-CAT Cl (Ti = 5.0 μmol) and $Ph_3CB(C_6F_5)_4$ (5.0 μmol) in this order.

2.2.10. Ethylene/1-octene copolymerization

Ethylene copolymerization was conducted in a 1 L autoclave equipped with a mechanical stirrer rotating at 350 rpm. In a typical experiment, *e.g.* run 41 in Table 7, toluene (300 mL), TIBA (Al = 2.5 mmol), and 1-octene (96 mmol) were introduced into the reactor and the solution was saturated with ethylene (0.4 MPa, absolute pressure) at 30 °C for 30 min. Thereafter, a toluene solution (1.0 mL) of PNB-*g*-CAT Cl (**1c)** (Ti = 5.0 μmol) was injected into the reactor, followed by the injection of a toluene solution (1.0 mL) of $Ph_3CB(C_6F_5)_4$ (5.0 μmol) to initiate the polymerization. The polymerization was conducted for 10 min with a continuous supply of ethylene at 0.4 MPa. The resultant polymer solution was poured into acidic ethanol, collected by filtration, washed with ethanol and dried under vacuum for several hours at 60 °C.

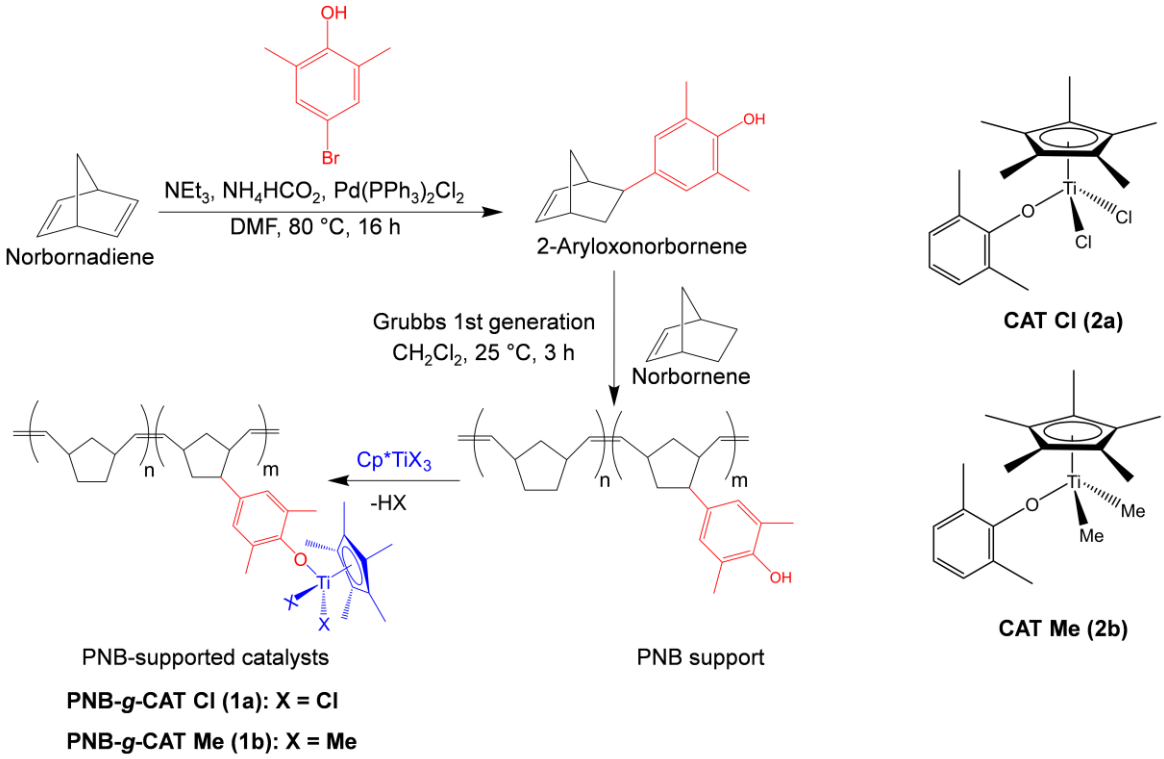

Scheme 1. Synthesis of soluble PNB-supported catalysts.

2.3. Results and discussion

2.3.1. Synthesis and characterization of PNB supports

In order to synthesize PNB supports, copolymerization was performed between norbornene and 2-aryloxonorbornene containing 2,6-dimethylphenol, a less hindered phenol as a pendant group (Scheme 1). For this, the Grubbs 1st generation catalyst was chosen, primarily due to its high efficiency to polymerize a variety of norbornene derivatives at room temperature and tolerance toward protic functional groups [34,45]. In literature, the ROMP of norbornene derivatives containing 2,6-di-*t*-butylphenol as a pendant group using the Grubbs 1st generation catalyst was reported, which yielded PNB bearing hindered phenol with a narrow molecular weight distribution [46]. The

polymerization results are summarized in Table 1. At a fixed norbornene/catalyst ratio of 200 mol/mol, random copolymerization was conducted at room temperature with increasing the 2-aryloxonorbornene fraction in the feed (runs 1 to 8). The successful PNB support synthesis was confirmed by both ^{1}H and ^{13}C NMR spectra (Figs. 2 and 3). Fig. 2 represents a typical ^{1}H NMR spectrum of a PNB support (run 4, Table 1), in which the peaks due to the protons of PNB backbone as well as those of the pendant group were quantitatively observed. The obtained PNB supports consisted of a mixture of *trans* and *cis* conformations, where the *trans* conformation dominated over 73% as is usual for the Grubbs 1st generation catalyst [45]. The comonomer content in different PNB supports was calculated based on Eq. (1),

$$Comonomer\ content\ (mol\%) = \frac{\frac{1}{6} I_{H_e}}{\frac{1}{2} I_{H_{1,4}}} \times 100 \qquad \text{Eq. (1).}$$

Fig. 4 shows the ATR-IR spectra of three PNB supports. The IR spectrum of a homo PNB sample is also shown for comparison. The spectra were consistently assigned based on literatures [47,48]. Significant peaks which appeared in the spectrum are: i) Strong absorption at 965 cm^{-1}, originated from hydrogen deformation at olefinic carbons in a trans conformation; ii) Absorption at 1446 cm^{-1} due to the CH_2 group of the cyclopentane ring; iii) Absorptions at 1664 and 1740 cm^{-1}, due to the C=C stretching vibrations of the olefinic double bonds (*cis* and *trans*) of the PNB backbone. Their weak intensities suggested that the *trans* conformation dominated in all the polymers; iv) Strong absorption around 2850-3000 cm^{-1} due to C─H stretching vibrations. Apart from the above common peaks for the PNB structure, the peaks which appeared due to

the aryloxide pendant groups are: v) A sharp and intense peak at 1190 cm^{-1} due to the C─O stretching vibrations; vi) Absorptions at 1490 and 1620 cm^{-1}, both due to the C=C stretching vibrations of the benzene ring; vii) A sharp but minor peak at 3615-3630 cm^{-1} due to the O─H stretching vibrations of the phenolic group. In Fig. 4, the intensities of the peaks due to the aryloxide pendant group increases with the increase in the 2-aryloxonorbornene content in the resultant copolymers.

Table 1

Results of PNB support synthesis[a]

Run	Comonomer in feed[b] (mol%)	Norbornene /catalyst (mol/mol)	Isolated yield (%)	*trans*[c] (%)	Comonomer content[c] (mol%)	M_n[d] × 10^{-4}	M_w/M_n[d]	Pendant group/chain[e]
1	0.7	200	97	84	0.5	5.5	1.17	3
2	2.2	200	94	84	2.0	5.3	1.20	11
3	3.0	200	94	84	2.7	5.7	1.24	16
4	5.0	200	95	84	4.8	7.0	1.18	36
4'[f]	5.0	200	92	84	4.7	6.9	1.19	35
5	11	200	92	82	10	7.7	1.16	82
6	17	200	93	79	15	6.5	1.14	103
6'[f]	17	200	90	79	14	6.9	1.14	103
7	23	200	92	76	21	8.2	1.20	183
8	33	200	85	73	32	n.d.[g]	n.d.[g]	n.d.[g]
9	5.0	100	96	84	5.0	4.5	1.15	24

[a] Polymerization conditions: Norbornene = 12.8 mmol, catalyst = 64.0 μmol (runs 1-8) or 128 μmol (run 9), CH_2Cl_2 = 20 mL, T = 25 °C, t = 3.0 h.

[b] [2-aryloxonorbornene/(norbornene + 2-aryloxonorbornene)] × 100.

[c] Calculated from ^{1}H NMR.

[d] Determined by GPC.

[e] Calculated from the M_n value and the comonomer content.

[f] Reproduction tests.

[g] Not determined.

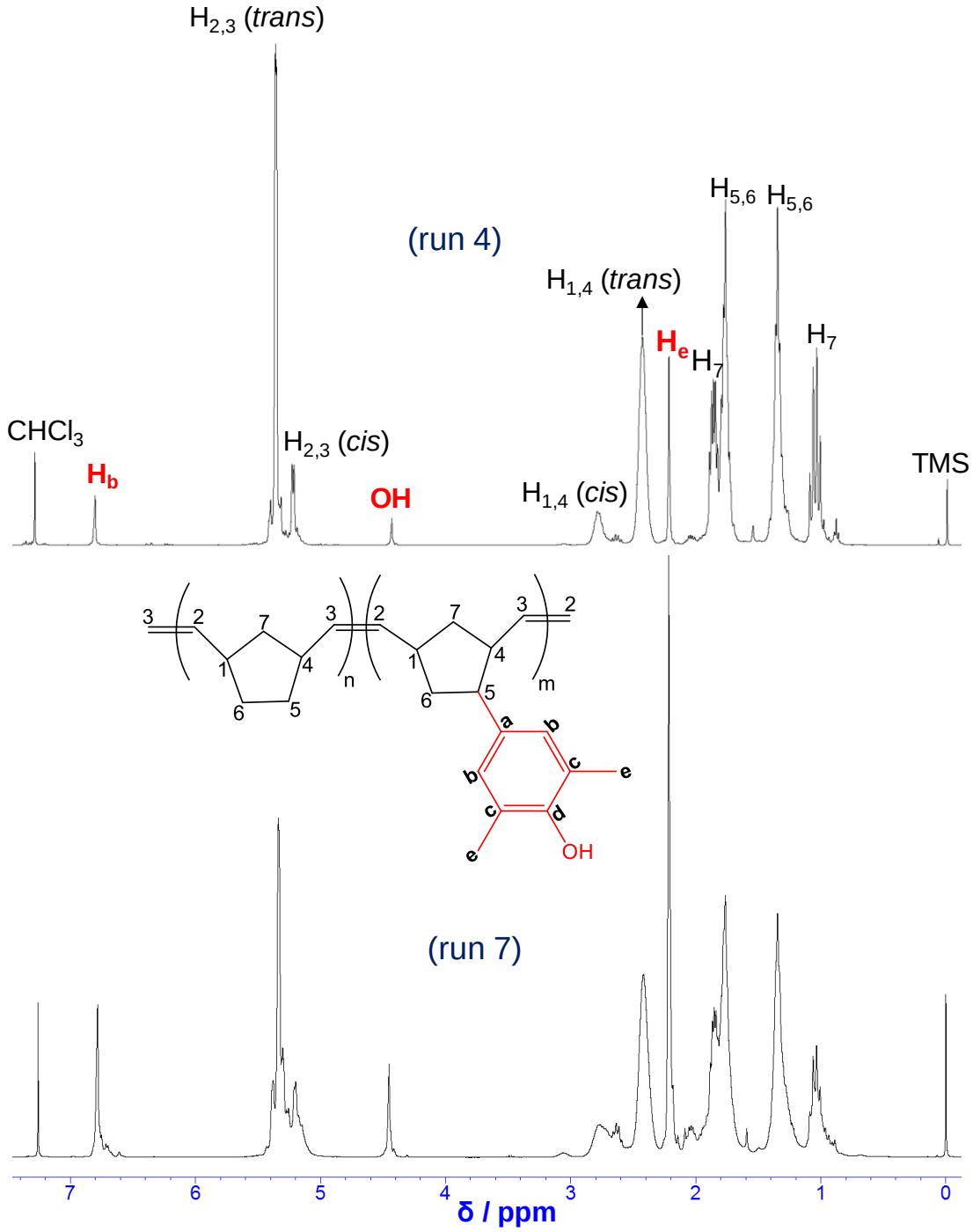

Fig. 2. ^{1}H NMR spectra of two PNB supports (Table 1) with different 2-aryloxonorbornene contents.

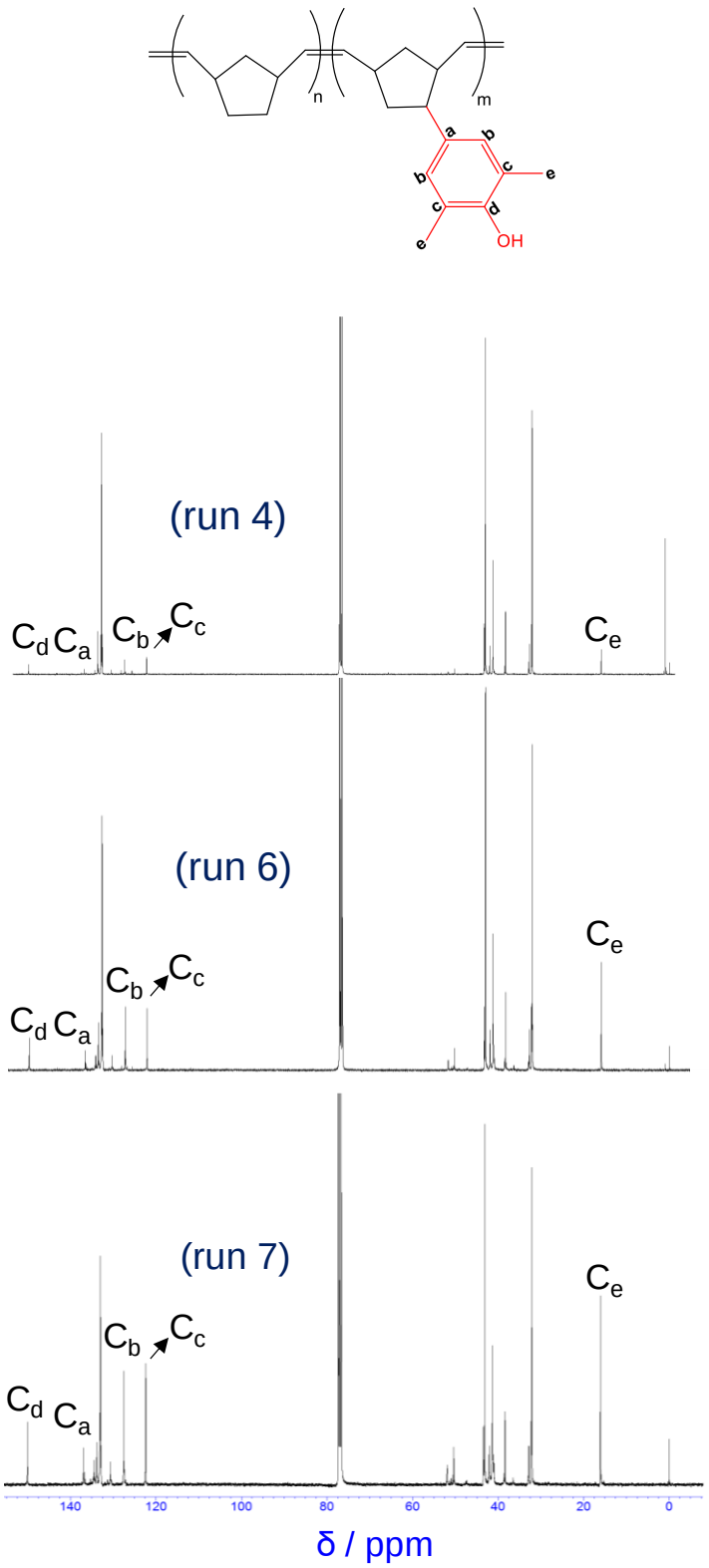

Fig. 3. ^{13}C NMR spectra of three PNB supports (Table 1) with different 2-aryloxonorbornene contents.

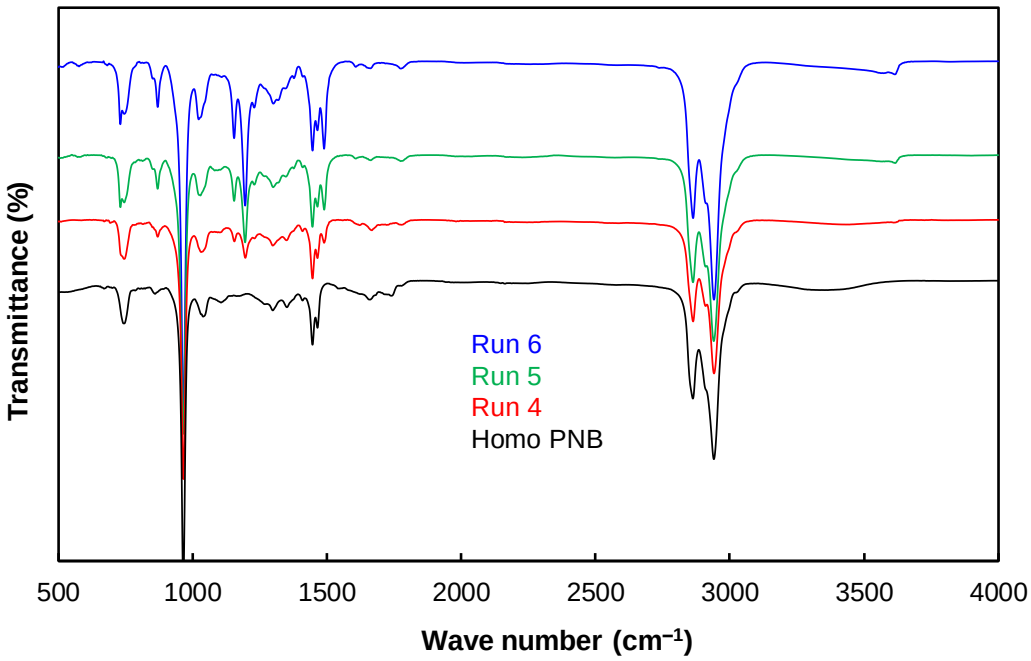

Fig. 4. ATR-IR spectra of three PNB supports with different 2-aryloxonorbornene contents and a homo PNB as a reference.

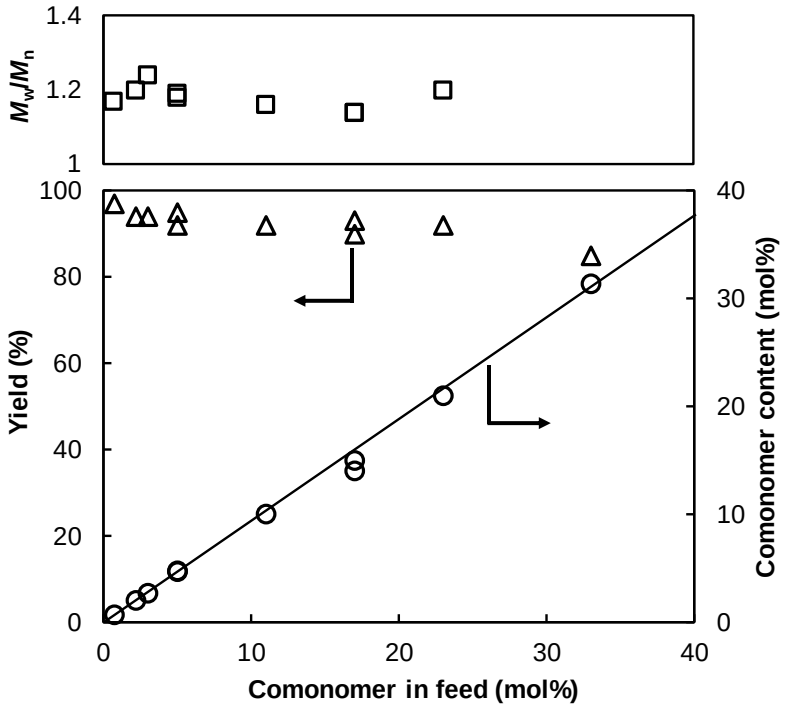

Fig. 5. Summary of PNB support synthesis (runs 1 to 8 in Table 1).

In Table 1, runs 4,4' and 6,6' represent the reproducibility of support synthesis. In all the entries of Table 1, approximately 90% of the yield and nearly quantitative comonomer incorporation were observed over a wide range of feed composition (Fig. 5), which in turn suggests that the bulky aryloxo substituent hardly altered the reactivity of the internal double bond of the 2-aryloxonorbornene.

The PNB supports exhibited M_w/M_n values close to one as represented in Figs. 5 and 6. These facts assured the well-defined nature of the synthesized PNB supports. However, it should be noted that the observed M_n values were higher than those estimated from the initial monomer/catalyst ratio. This deviation could be attributed to the much higher rate of propagation as compared to the rate of initiation in ROMP using the Grubbs 1st generation catalyst [49]. Nonetheless, neither M_n nor M_w/M_n was affected by the 2-aryloxonorbornene content, which suggested the feasibility of a rational investigation of the effect of the active site density on catalysis by employing the synthesized PNB supports. This is a clear advantage over non-cross-linked polystyrene supports synthesized by a radical polymerization method, in which both M_n and M_w/M_n were affected by the comonomer incorporation [50]. Owing to the narrowest molecular weight distribution, the number of pendant groups per chain was reasonably calculated for each PNB support from their respective M_n and comonomer content, which was found to vary in the range of 3–183 for runs 1 to 8. Thus, the series of the PNB supports provided the identical chain length while bearing different amounts of pendant groups per chain. As shown in run 9 (Fig. 6), the molecular weight of the support was easily adjusted by changing the norbornene/catalyst ratio without affecting the molecular weight distribution and the comonomer content.

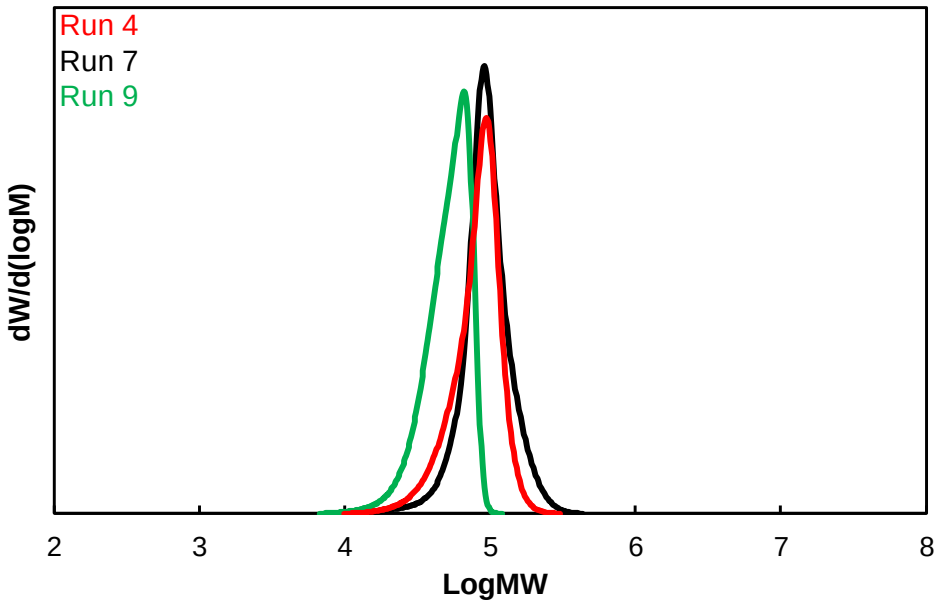

Fig. 6. Molecular weight distribution of PNB supports.

In order to confirm the status of PNB chains, DLS measurements were performed. Fig. 7 represents the size distribution of three PNB supports (runs 1,4,6 in Table 1) in a dilute toluene solution.

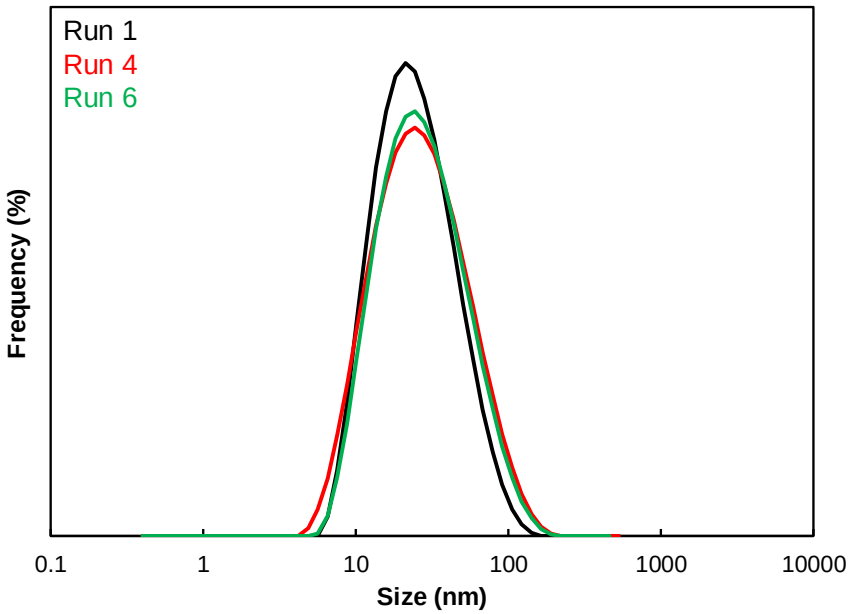

Fig. 7. Size distribution of three PNB supports (runs 1,4,6 in Table 1) in toluene at 1.0 mg/mL, measured by DLS.

Table 2

Representative dimensions of PNB chains in a random coil state

PNB support	$(< R_F^2 >^{1/2})^a$ (nm)	$(< R_G^2 >^{1/2})^b$ (nm)	$(< R_D^2 >^{1/2})^c$ (nm)	$(< R_H^2 >^{1/2})^c$ (nm)	PDI[d]
Run 1	33	13	29	14	0.27
Run 4	37	15	34	17	0.29
Run 6	34	13	33	16	0.28

[a] Calculated based on Eq. (2).

[b] Calculated based on Eq. (3).

[c] Measured by DLS

[d] Polydispersity index that represents the width of the size distribution.

The hydrodynamic diameter ($< R_D^2 >^{1/2}$) of a PNB chain can be measured directly using the DLS technique and the obtained values for three different PNB supports are shown in Table 2. For a PNB support (*e.g.*, run 4 in Table 1), the hydrodynamic diameter ($< R_D^2 >^{1/2}$) was found to be 34 nm with a polydispersity index of 0.29. In general, a polymer chain dissolved in a good solvent at a sufficiently dilute concentration prefers a random coil state, which is the entropically most favorable conformation for a macromolecule. Its end-to-end distance ($< R_F^2 >^{1/2}$) can be calculated based on Eq. (2) [51],

$$< R_F^2 >^{1/2} = a_F N^{3/5} \qquad \text{Eq. (2).}$$

where N and a_F correspond to the number of rigid segments and the segmental length,

respectively. Based on molecular mechanics calculations as well as in literature [52], the a_F value of PNB is reasonably estimated as 1.4 nm, which corresponds to 3 repeating units. In the case of run 4, the theoretical end-to-end distance was derived as 37 nm. Assuming a relationship of Eq. (3) [51],

$$< R_G^2 >^{1/2} = \frac{< R_F^2 >^{1/2}}{(6.66)^{1/2}} \qquad \text{Eq. (3).}$$

the theoretical radius of gyration ($< R_G^2 >^{1/2}$) was derived as 15 nm, in close agreement with the measured hydrodynamic radius ($< R_H^2 >^{1/2}$, a half of $< R_D^2 >^{1/2}$) of 17 nm. These results indicated that the synthesized PNB supports possessed a well-defined random coil conformation in toluene. The obtained results are consistent with the computer simulations carried out on the chain conformations and dynamics of PNB by Haselwander et al [53]. They found that isolated PNB chains exhibit a random coil conformation but are rigid over a wide range of temperature owing to the high rotational energy barriers [53]. As the result, unlike flexible chains, PNB chains do not collapse at a lower temperature or even in the presence of a significantly poorer solvent. It must be noted that the concentration of PNB chains in polymerization medium is much smaller than 1.0 mg/mL, and thus it is reasonable to presume that each chain of the PNB-supported catalysts can adopt a random coil conformation in the polymerization medium.

2.3.2. Synthesis and characterization of PNB-supported catalysts

For the synthesis of PNB-supported catalysts, two half-titanocene precursors, Cp*$TiCl_3$ and Cp*$TiMe_3$ were chosen as depicted in Scheme 1, and their grafting was explored mainly based on a PNB support with approximately 5 mol% of the

comonomer content (run 4 in Table 1). Fig. 8 represents a typical ^{1}H NMR spectrum of PNB-*g*-CAT Cl (**1a**), in which the grafting of Cp*$TiCl_3$ to the PNB support was confirmed with a shift in the peak position of methyl protons of the Cp ring from 2.39 to 2.20 ppm. A similar peak shift was also observed in the case of the molecular analogue (Fig. 9).

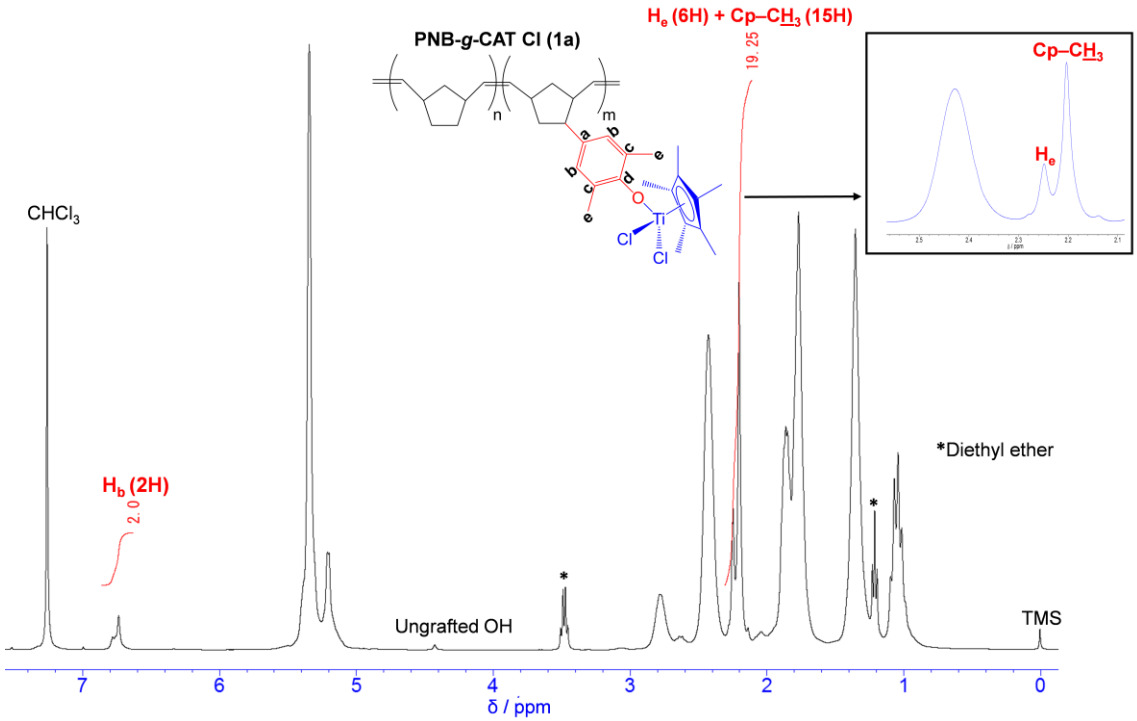

Fig. 8. ^{1}H NMR spectrum of PNB-*g*-CAT Cl (**1a**).

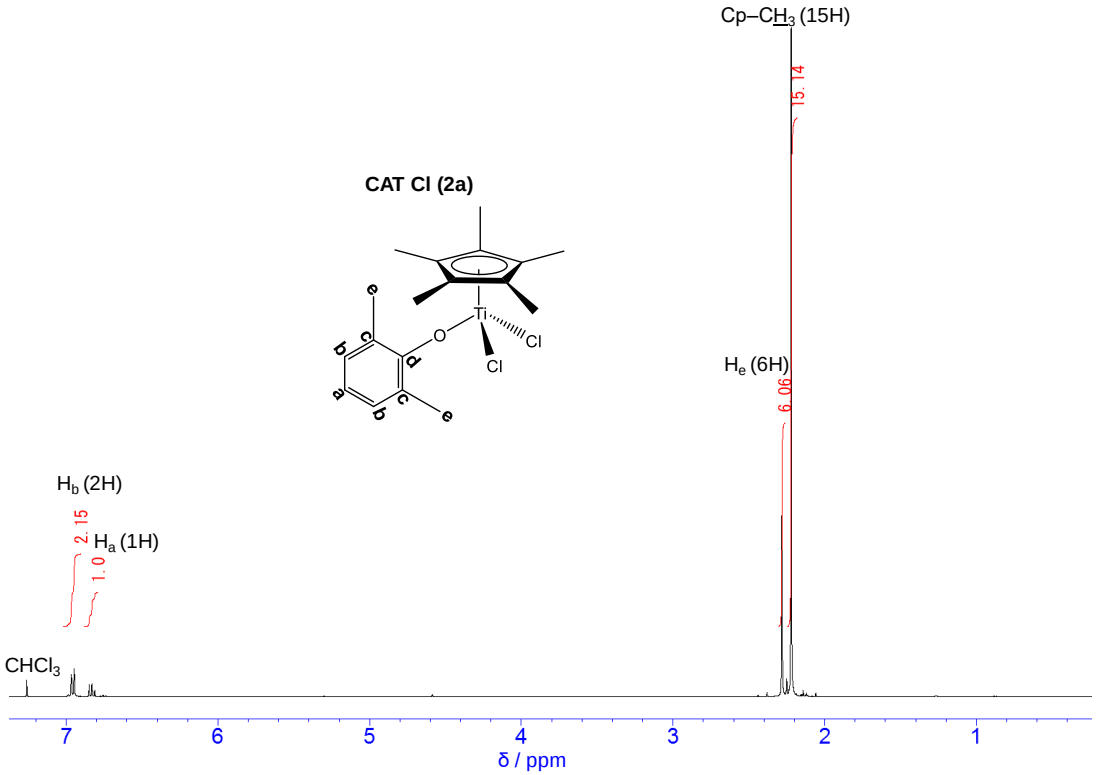

Fig. 9. ^{1}H NMR spectrum of CAT Cl (**2a**).

Successful catalyst synthesis was further confirmed by ^{13}C NMR (Table 3 and Fig. 10). For instance, the peak position of the carbon (C_d) that is bonded to the oxygen of the aryloxo group was found to be shifted from 150.2 to 160.7 ppm. The other important peaks were also shifted (Table 3) by the grafting, and these shifts were consistent with those observed for the molecular analogue (Fig. 11).

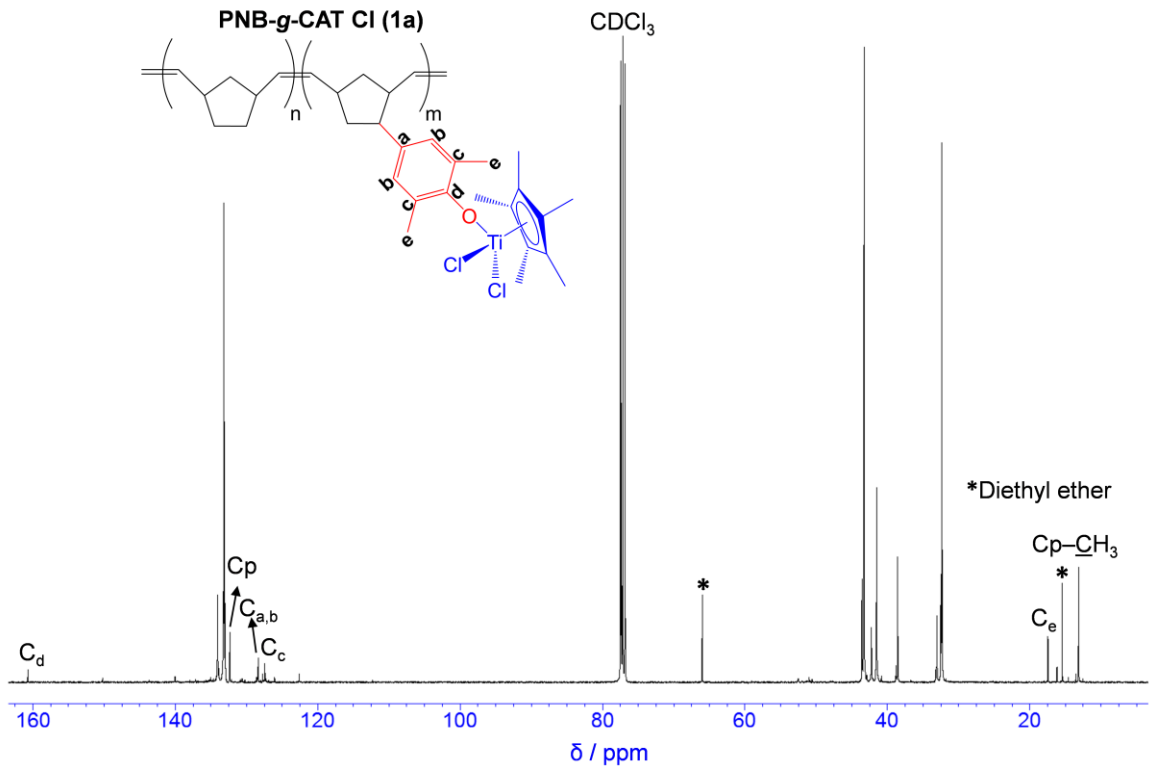

Fig. 10. ^{13}C NMR spectrum of PNB-*g*-CAT Cl (**1a**).

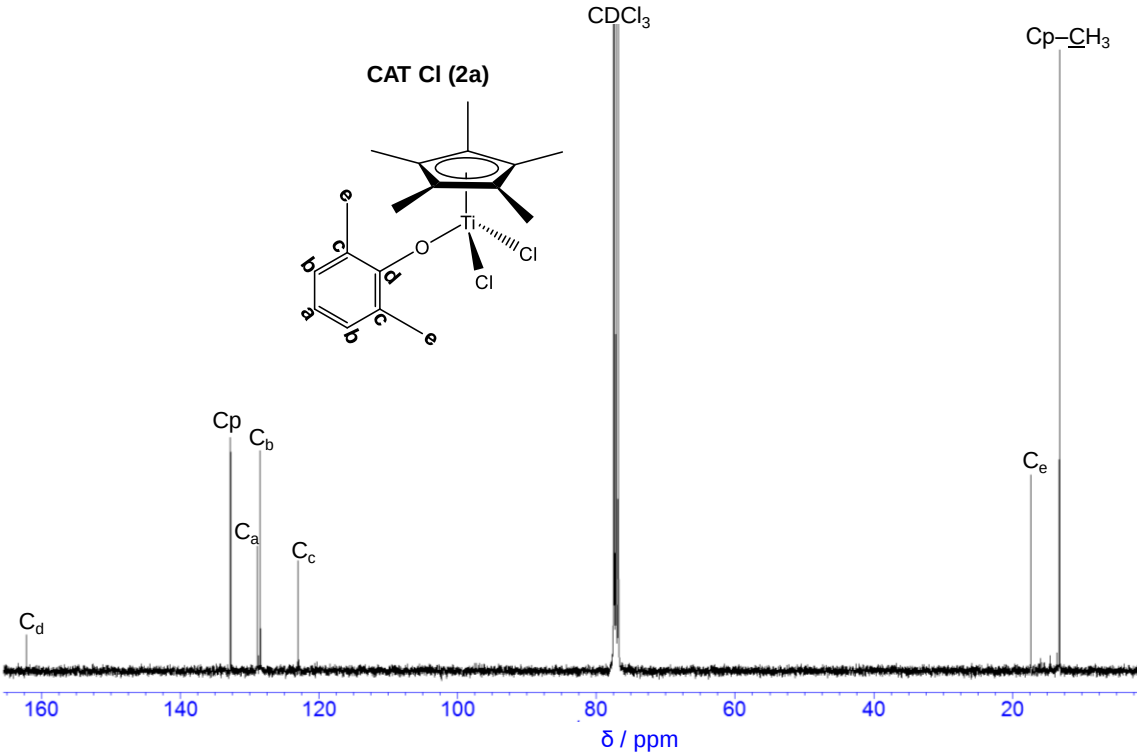

Fig. 11. ^{13}C NMR spectrum of CAT Cl (**2a**).

Moreover, a sharp peak corresponding to Cp–C<u>H</u>$_3$ was observed without any splitting, which suggested the absences of the unreacted precursor and undesired side products (*e.g.* bis(aryloxy)cyclopentadienyltitanium (IV) chloride). The grafting reaction of Cp*TiCl$_3$ was rather sluggish owing to the difficulty in the replacement of chloride by the aryloxide ligand. It was presumed that accumulation of released HCl (as a side product) in the reaction might cause an incomplete grafting of the precursor. In order to remove HCl, the reaction was refluxed in the presence of CH_2Cl_2 as a low boiling-point solvent. The refluxing never reduced the solubility of PNB-*g*-CAT Cl, assuring the absence of any unwanted oxidative cross-linkage. Contrary, an attempt to treat a PNB support with routinely used *n*-BuLi as a base caused the formation of an insoluble yellowish gel. *Ca.* 88% of grafting was derived from ^{1}H NMR (Fig. 8) based on Eq. (4), which corresponded to the grafting of roughly 32 Ti centres per chain.

$$Graft\ yield\ (\%) = \frac{\frac{1}{15} I_{Cp-CH_3}}{\frac{1}{2} I_{H_b}} \times 100 \qquad \text{Eq. (4).}$$

Table 3

Representative chemical shifts (ppm) in ^{13}C NMR

Sample	Cp–<u>C</u>H$_3$	C$_e$	Ti–<u>C</u>H$_3$	Cp	C$_d$
PNB-*g*-CAT Cl (**1a**)	13.1	17.4	n.a.[a]	132.3	160.7
CAT Cl (**2a**)	13.2	17.4	n.a.[a]	132.7	162.2
PNB-*g*-CAT Me (**1b**)	11.7	17.6	53.6	122.2	159.7
CAT Me (**2b**)	11.8	17.4	54.2	122.4	161.5
PNB support (run 3)	n.a.[a]	16.2	n.a.[a]	n.a.[a]	150.2
Cp*TiCl$_3$	14.6	n.a.[a]	n.a.[a]	138.0	n.a.[a]
Cp*TiMe$_3$	12.2	n.a.[a]	61.0	122.4	n.a.[a]

[a] Not applicable.

The reaction between the PNB support and Cp^*TiMe_3 was carried out in toluene at room temperature, as it was found to be facile owing to easier replacement of methyl by the aryloxide ligand. The successful grafting was confirmed by ^1H and ^{13}C NMR in a similar fashion to PNB-*g*-CAT Cl (**1a**). Representatively, the peak position of the protons of Ti–C$\underline{H}_3$ was found to be shifted from 0.75 to 0.44 ppm for the PNB-*g*-CAT Me (**1b**, Fig. 12) with respect to 0.48 ppm for the molecular analogue (Fig. 13). The peak positions of the carbons of C_d and Ti–$\underline{C}H_3$ were shifted from 150.2 and 61.0 ppm to 159.7 and 53.6 ppm, respectively (Fig. 14), which were very similar to the shifts observed for the molecular analogue (Table 3 and Fig. 15). The total absence of undesired grafted Ti species was ascertained by the sharp peak of the 15 protons of the Cp–C$\underline{H}_3$ without any splitting. Moreover, the quantitative appearance of the Ti–C$\underline{H}_3$ protons was observed with respect to the phenyl protons (H_b) of the aryloxide ligand. This fact together with the complete disappearance of the phenolic proton validated 100% grafting, corresponding to 36 Ti centres per chain. It is important to note that the synthesized catalyst was highly sensitive to moisture as compared to its chloride counterpart. The reaction with moisture reduced the relative amount of the Ti–C$\underline{H}_3$ protons in ^1H NMR, and eventually formed a gel plausibly due to the oxygen-mediated cross-linkage among polymer chains. To circumvent this problem, all the manipulations were performed in a rigorously dehydrated environment.

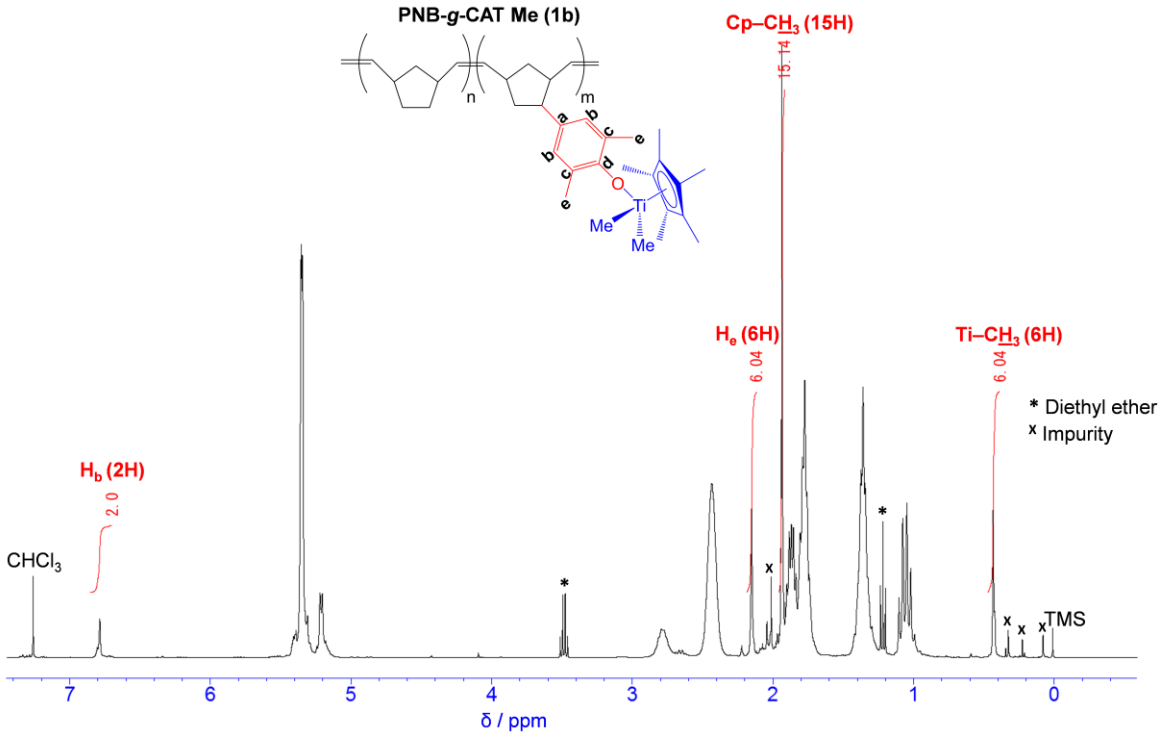

Fig. 12. ^{1}H NMR spectrum of PNB-*g*-CAT Me (**1b**).

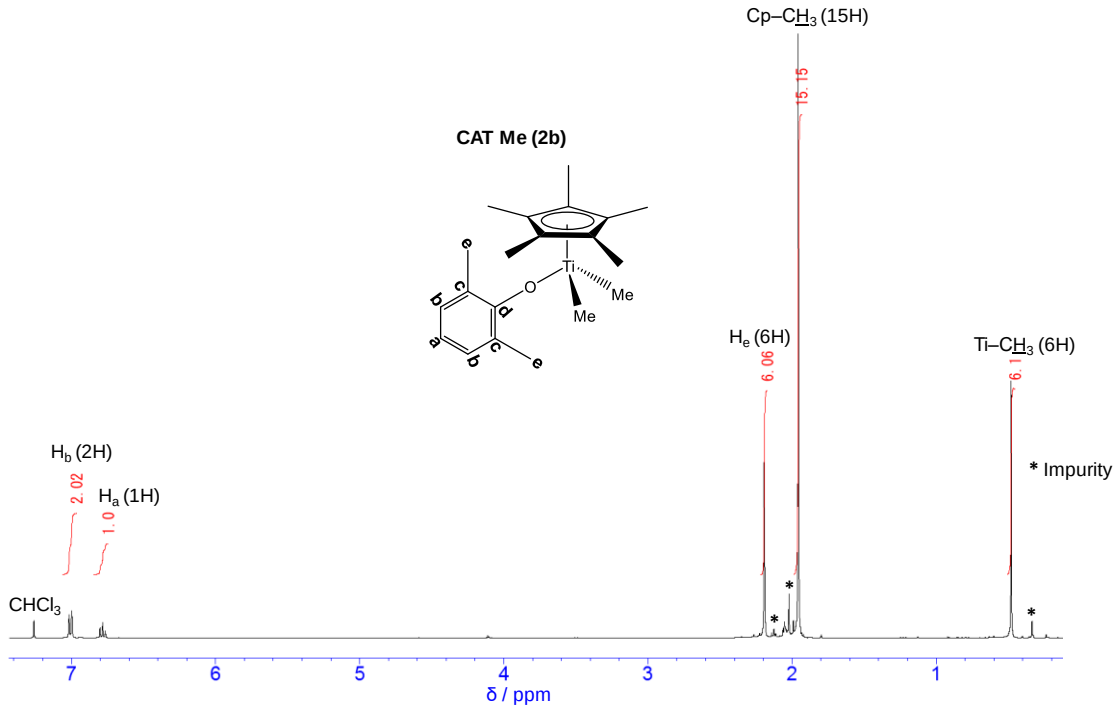

Fig. 13. ^{1}H NMR spectrum of CAT Me (**2b**).

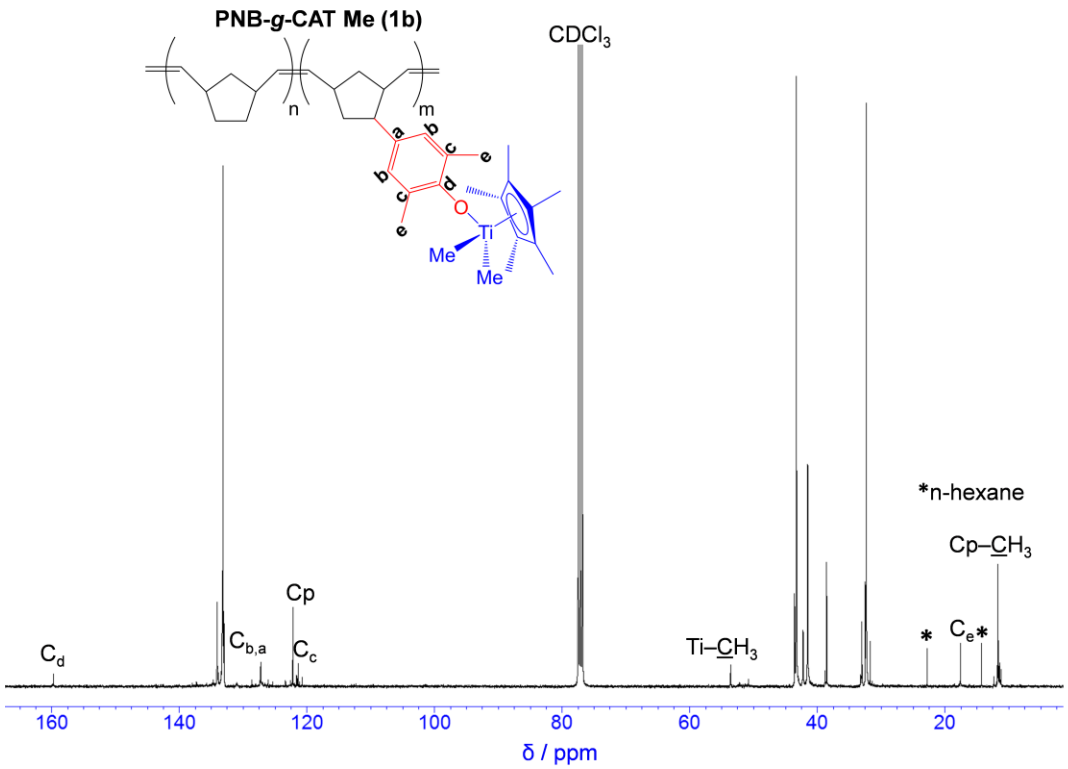

Fig. 14. ^{13}C NMR spectrum of PNB-*g*-CAT Me (**1b**).

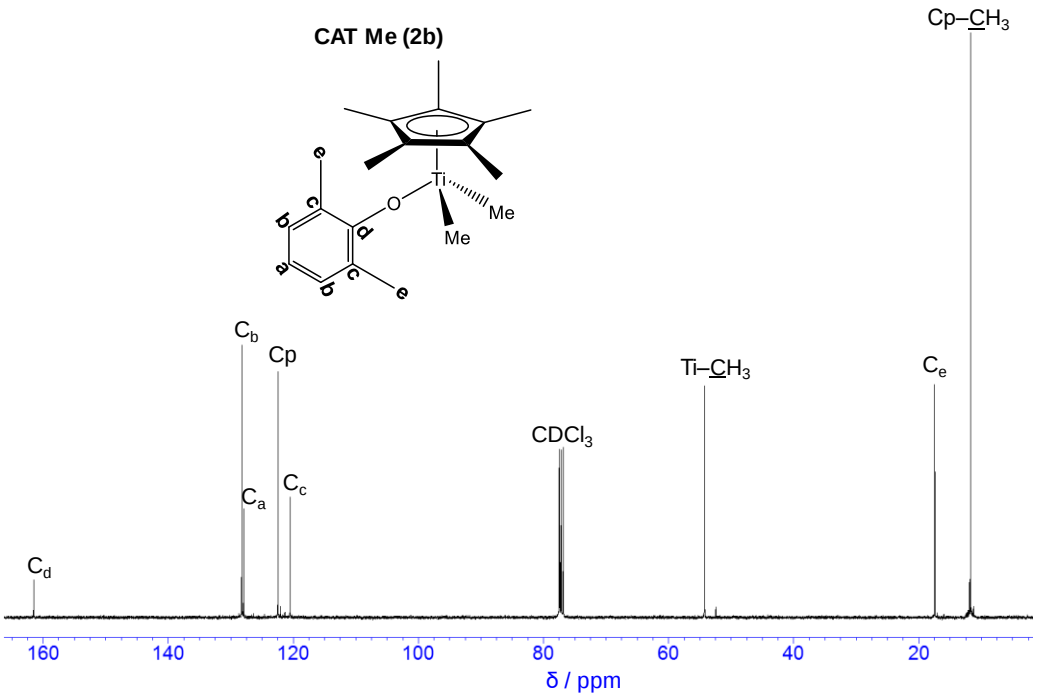

Fig. 15. ^{13}C NMR spectrum of CAT Me (**2b**).

2.3.3. Ethylene homopolymerization

The performance of the PNB-supported catalysts (**1a,b**) was evaluated in the polymerization of ethylene. First, the polymerization was conducted using MMAO as an activator. The results are summarized in Table 4, in which the results for the corresponding molecular analogues (**2a,b**) are included for comparison.

At 30 °C, CAT Cl (**2a**) exhibited a high activity (run 10), comparable to the previously reported activity using methyl aluminoxane (MAO) as an activator [40]. The activity decreased at 50 °C (run 11) due to the deactivation of the catalyst at an elevated temperature [44]. PNB-*g*-CAT Cl (**1a**) showed a reasonable activity (run 12), while the grafting reduced the original activity of CAT Cl (**2a**) by 4–5 times (run 10 vs. 12). The activity of PNB-*g*-CAT Cl (**1a**) further decreased at 50 °C (run 12 vs. 13), which suggested that the deactivation at an elevated temperature was hardly prevented by employing a polymer support as a macro-ligand. The activity of CAT Me (**2b**) was slightly lower than that of CAT Cl (**2a**) under an identical condition (run 10 vs. 15), and it was strongly dependent on the Al/Ti ratio (runs 14-17), reaching the maximum activity at the Al/Ti ratio of 3000. The activity of PNB-*g*-CAT Me (**1b**) was much closer to that of CAT Me (**2b**) (run 15 vs. 20) and 2.5 times higher than that of PNB-*g*-CAT Cl (**1a**) (run 12 vs. 20). Both of the supported and molecular catalysts did not provide measurable activities at 0 °C (runs 18,22).

Compared with the corresponding molecular analogues, the activity levels of the supported catalysts were very different between PNB-*g*-CAT Cl (**1a**) and PNB-*g*-CAT Me (**1b**). In general, immobilization on solid supports causes several consequences in the olefin polymerization performance of molecular catalysts. For instance, a support stabilizes molecular catalysts and dissipates the heat of polymerization so as to suppress

undesired deactivation [26,27]. Additional steric hindrance from a support also interferes the complexation and/or the reaction of reagents at the active sites, which can lead to a higher molecular mass of polymer when the active sites are less accessible for free alkylaluminum [54,55], a lower activity when less accessible for an activator [24], and *vice versa*. In Table 4, the activity of PNB-*g*-CAT Cl (**1a**) was much lower than CAT Cl (**2a**), while the extent of the deactivation at 50 °C was similar between the two catalysts (runs 10-13). Hence, the lower activity of PNB-*g*-CAT Cl (**1a**) was plausibly ascribed by the steric hindrance for MMAO to effectively alkylate and/or ionize the metal centres. The inefficiency in the activation was more or less relieved for PNB-*g*-CAT Me (**1b**) as it gave comparable activities to CAT Me (**2b**). It was believed that the bulkiness of the polymer support struggled more with the alkylation than with the ionization when MMAO was employed as an activator.

Table 4

Ethylene homopolymerization using MMAO as an activator[a]

Run	Catalyst (μmol)	Al/Ti (mol/mol)	*T* (°C)	Activity (kg-PE/mol-Ti·h)	M_w[b] × 10^{-5}	M_w/M_n[b]
10	**2a** (5.0)	6000	30	9200 ± 170	2.2	6.1
11	**2a** (5.0)	6000	50	6000	n.d.[c]	n.d.[c]
12	**1a** (5.0)	6000	30	2110 ± 13	4.2	16.3
13	**1a** (5.0)	6000	50	1370 ± 52	n.d.[c]	n.d.[c]
14	**2b** (5.0)	12000	30	5760 ± 220	1.8	7.2
15	**2b** (5.0)	6000	30	6900 ± 230	4.6	6.8
16	**2b** (5.0)	3000	30	8100 ± 180	n.d.[c]	n.d.[c]
17	**2b** (5.0)	1500	30	5250	n.d.[c]	n.d.[c]
18	**2b** (5.0)	6000	0	Trace	n.d.[c]	n.d.[c]
19	**1b** (5.0)	12000	30	5000 ± 15	6.6	9.1
20	**1b** (5.0)	6000	30	4940 ± 110	5.6	11
21	**1b** (5.0)	3000	30	3000	n.d.[c]	n.d.[c]
22	**1b** (5.0)	6000	0	Trace	n.d.[c]	n.d.[c]

[a] Polymerization conditions: Ethylene pressure = 0.6 MPa, toluene = 300 mL, *t* =10 min.

[b] Determined by high-temperature GPC.

[c] Not determined.

Irrespective of the type of the catalysts, the ethylene polymerization using MMAO resulted in the production of PE with a M_w/M_n value much greater than 2. This fact indicated inevitable formation of multiple active sites in the course of the polymerization. Similarly broad distributions were reported in previous literature [44], which was partly associated with free alkylaluminum contained in MAO [56]. In Table 4, the activity was found to be correlated with the molecular weight distribution

of the produced PE samples: A lower activity accompanied a larger fraction of low molecular weight polymers, thus broadening the molecular weight distribution. Potential isomerization of active sites by the action of the activator system or under-activation of the catalysts (insufficient contact with MMAO) [57,58] would explain the obtained correlation. The supported catalysts afforded higher M_w values when compared to the corresponding molecular analogues under identical conditions (Table 4 and Fig. 16). As explained above, the suppression of the chain transfer reaction is the most plausible reason. It is noted that the increment in the M_w value for the supported catalysts resulted in an extra broadening of the distribution by expanding the deviation between low and high molecular weight fractions (became clearly bimodal in Fig. 16).

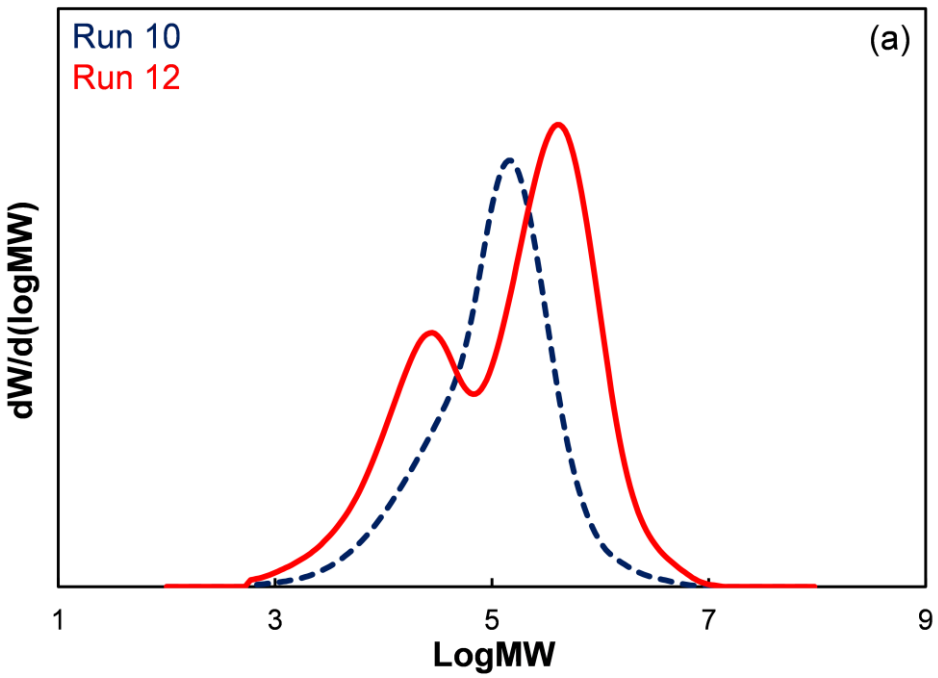

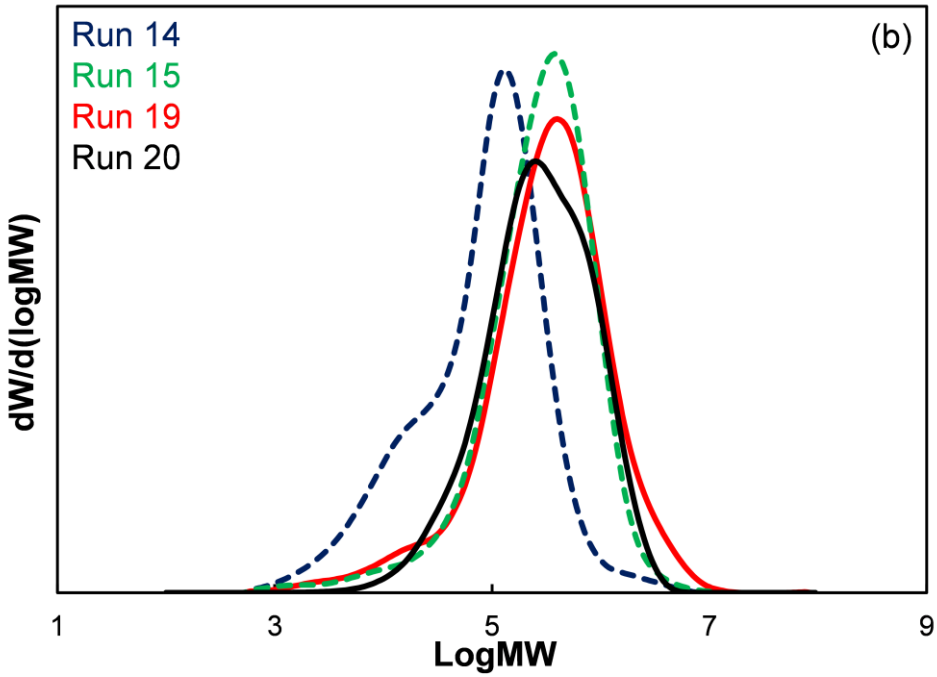

Fig. 16. Molecular weight distributions of PE samples prepared using MMAO as an activator under identical conditions: a) **1a** vs. **2a**, and b) **1b** vs. **2b**. The solid and dashed lines correspond to PE samples obtained using the polymer-supported and molecular catalysts, respectively.

According to the observed inefficiency of the activation using MMAO, ethylene polymerization was performed using a less bulky TIBA/$Ph_3CB(C_6F_5)_4$ activator system [54]. Table 5 summarizes the results of the polymerization, where a catalyst amount corresponding to 5.0 μmol of Ti was injected. The activity of the molecular catalysts was not sensitive to the employed activators (runs 10,15 vs. 23,27), in consistent with a previous report [44]. Contrary, it was found that the utilization of TIBA/$Ph_3CB(C_6F_5)_4$ dramatically improved the activities of both of the PNB-supported catalysts (**1a,b**), which were comparable or even higher than those of their molecular analogues under identical conditions (*e.g.* run 23 vs. 24, 27 vs. 29). Especially, PNB-*g*-CAT Cl (**1a**)

significantly recovered its activity using TIBA/$Ph_3CB(C_6F_5)_4$. This is consistent with the earlier discussion that the activation of PNB-*g*-CAT Cl (**1a**) using MMAO was sterically hindered. In Table 4, the activation using MMAO never led to observable activities at 0 °C, while the activity levels were kept almost constant between 0 and 30 °C when TIBA/$Ph_3CB(C_6F_5)_4$ was employed instead. Obviously, the activation using MMAO necessitates a higher energetic barrier to be surpassed.

In attempts to maximize the productivity and further narrower the molecular weight distribution in the ethylene polymerization, the injection amount of PNB-*g*-CAT Cl (**1a**) or CAT Cl (**2a**) was halved (2.5 μmol of Ti). The results are summarized in Table 6. It was found that the activity of both PNB-*g*-CAT Cl (**1a**) and CAT Cl (**2a**) improved by the introduction of the new conditions (runs 23,24 vs. 33,37). The best activity of PNB-*g*-CAT Cl (**1a**) was achieved at the Al/Ti ratio of 1000 (run 38), which exceeded that of CAT Cl (**2a**) under the identical condition (run 34 vs. 38). To the best of my knowledge, the activity level of 28600 kg-PE/mol-metal·h has been hardly reached by any of the polymer-supported catalysts for ethylene polymerization.

Table 5

Ethylene homopolymerization using TIBA/$Ph_3CB(C_6F_5)_4$ as an activator[a]

Run	Catalyst (μmol)	Al/Ti (mol/mol)	T (°C)	Activity (kg-PE/mol-Ti·h)	M_w[b] × 10^{-5}	M_w/M_n[b]	T_m[c] (°C)	X_c[c] (%)
23	**2a** (5.0)	500	30	8900 ± 240	2.4	3.3	134.0	73
24	**1a** (5.0)	500	30	11200 ± 400	3.2	3.1	136.0	78
25	**1a** (5.0)	250	30	8500 ± 140	n.d.[d]	n.d.[d]	n.d.[d]	n.d.[d]
26	**1a** (5.0)	125	30	7100	n.d.[d]	n.d.[d]	n.d.[d]	n.d.[d]
27	**2b** (5.0)	500	30	8600 ± 400	3.3	4.8[e]	134.0	73
28	**2b** (5.0)	500	0	9000 ± 120	n.d.[d]	n.d.[d]	137.0	79
29	**1b** (5.0)	500	30	15300 ± 45	3.1	2.7	136.0	74
30	**1b** (5.0)	125	30	16100 ± 780	4.1	2.3	137.0	75
31	**1b** (5.0)	500	0	14000	n.d.[d]	n.d.[d]	138.0	75

[a] Polymerization conditions: Ethylene pressure = 0.6 MPa, toluene = 300 mL, Ti/$Ph_3CB(C_6F_5)_4$ = 1 mol/mol, t =10 min.

[b] Determined by high-temperature GPC.

[c] Determined by DSC.

[d] Not determined.

[e] A shoulder was observed at the high molecular weight side.

Table 6

Ethylene homopolymerization using TIBA/$Ph_3CB(C_6F_5)_4$ as an activator at a lower catalyst amount[a]

Run	Catalyst (μmol)	Al/Ti (mol/mol)	T (°C)	Activity (kg-PE/mol-Ti·h)	M_w[b] × 10^{-5}	M_w/M_n[b]	T_m[c] (°C)	X_c[c] (%)
32	**2a** (2.5)	1000	30	15900 ± 490	2.3	3.6	134.0	74
33	**2a** (2.5)	500	30	10900 ± 150	n.d.[d]	n.d.[d]	136.0	75
34	**2a** (2.5)	1000	0	16400 ± 390	5.7	2.5	137.0	78
35	**2a** (2.5)	500	0	20250 ± 340	7.4	2.7	138.0	80
36	**1a** (2.5)	1000	30	17300 ± 650	4.0	3.7	137.5	76
37	**1a** (2.5)	500	30	17900 ± 125	n.d.[d]	n.d.[d]	136.5	75
38	**1a** (2.5)	1000	0	28600 ± 114	4.9	2.3	137.2	77
39	**1a** (2.5)	500	0	23000 ± 600	5.5	2.2	137.5	76

[a] Polymerization conditions: Ethylene pressure = 0.6 MPa, T = 0 °C, toluene = 300 mL, Ti/$Ph_3CB(C_6F_5)_4$ = 1 mol/mol, t =10 min. The catalyst amount was halved from that in Table 4.

[b] Determined by high-temperature GPC.

[c] Determined by DSC.

[d] Not determined.

Regarding the activity improvements by grafting (*e.g.* 65% for run 38 vs. 34, 75% for run 37 vs. 33), a potential explanation would be the stabilization of molecular catalysts by grafting, as has been often reported for solid supports [54]. However, this idea was not likely since the soluble polymer support hardly suppressed the deactivation at an elevated temperature (runs 11,13). Therefore, potential synergism needs to be assumed among multiple active centres confined in a nano-sized random coil. Considering the fact that 32 Ti centres in the case of **1a** are confined in a polymer chain of a random coil state, whose hydrodynamic volume is 2.0 x 10^4 nm^3, the local Ti concentration can be estimated as 2.6 μmol/mL. This concentration is over 10^2 times greater than that of the molecular catalyst (**2a**) dissolved in 300 mL of toluene (8.3 x 10^{-3} μmol/mL for 2.5 μmol of Ti added in the polymerization). The average distance between two neighboring Ti centres is estimated as 11 nm for **1a**, with respect to 72 nm for the molecular catalyst (**2a**). However, it should be noted that the estimated distance between two neighboring Ti centres is just a thermal average, and it can be shorter or greater, depending on each instantaneous conformation of the polymer chain. Though several explanations could be assumed for explaining the synergism, a direct interaction is unlikely as the cationic active centres must repulse from each other. There have been a few mechanisms proposed for explaining the origin of synergistic or cooperative catalysis in the case of binuclear catalysts [30,59], in which the two active centres do not have direct interaction, similar to the present case. The most likely explanation for the present results is that "a local high concentration of active centres might increase the local concentration of reagents that can interact with them (*e.g.* ethylene) around a random coil." A mechanistic elucidation must necessitate a detailed kinetic study, typically using a stopped-flow technique [60-63].

In relation to the significant activity enhancement, the molecular weight distributions obtained using the TIBA/$Ph_3CB(C_6F_5)_4$ activator system (Tables 5 and 6) became unimodal (Figs. 17a–c) and much narrower compared to those reported in Table 4. This result indicated that the TIBA/$Ph_3CB(C_6F_5)_4$ activator system was more advantageous in retaining the single-site nature of aryloxide-containing half-titanocene catalysts. The PNB-supported catalysts tended to produce PE with a narrower molecular weight distribution as compared to those produced by their molecular analogues under the identical conditions (*e.g.* run 27 vs. 29, 35 vs. 39), which in turn suggested a role of the PNB support to enhance the single-site nature of the catalysts. The M_w/M_n values became nearly 2 for runs 30, 38 and 39. It is worth noting that the presence of the support clearly enlarged the molecular weight of PE at 30 °C (Figs. 16a,b and 17a,c), while such an enlargement was not observed at 0 °C (Fig. 17b). This temperature response was clearly different from that of the molecular analogues (the molecular weight increased at a lower temperature as usual), and would add up another unique aspect of the soluble polymer-supported catalysts in responding the surrounding environment. Lastly, the observed T_m and X_c values (Tables 5 and 6, Fig. 18) of the PE samples dictated the formation of exclusively linear high-density PE for all the cases, which is reasonable for the aryloxide-containing half-titanocene catalysts [40].

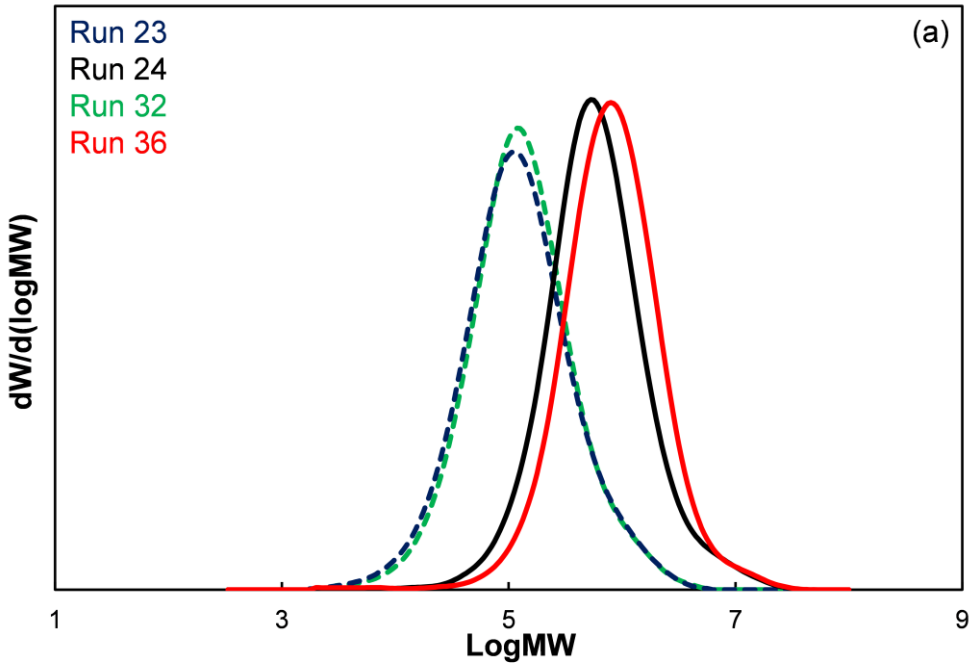
Run 23
Run 24
Run 32
Run 36
(a)
dW/d(logMW)
1
3
5
7
9
LogMW

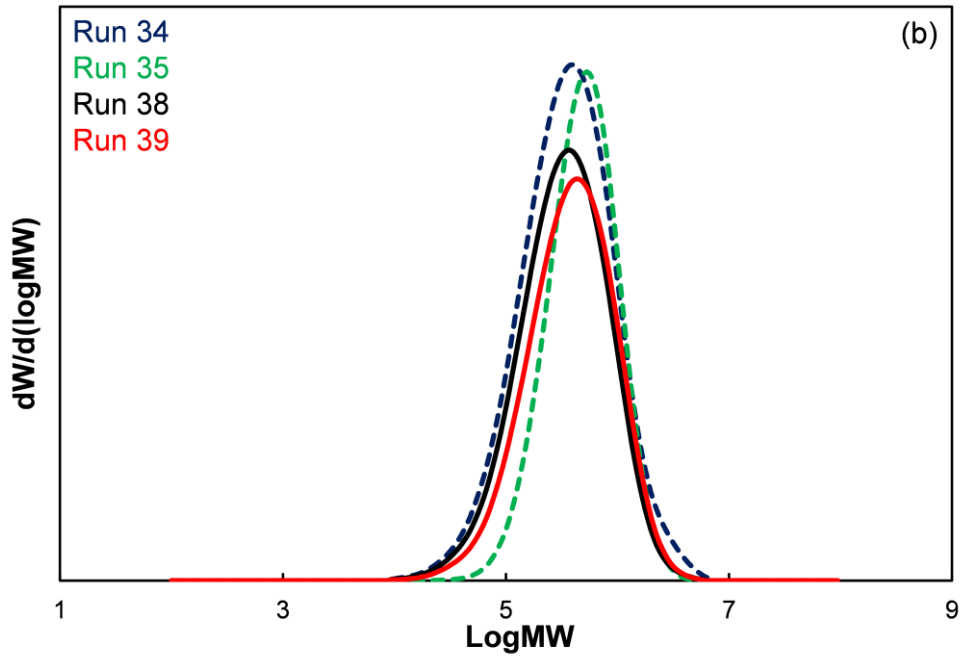
Run 34
Run 35
Run 38
Run 39
(b)
dW/d(logMW)
1
3
5
7
9
LogMW

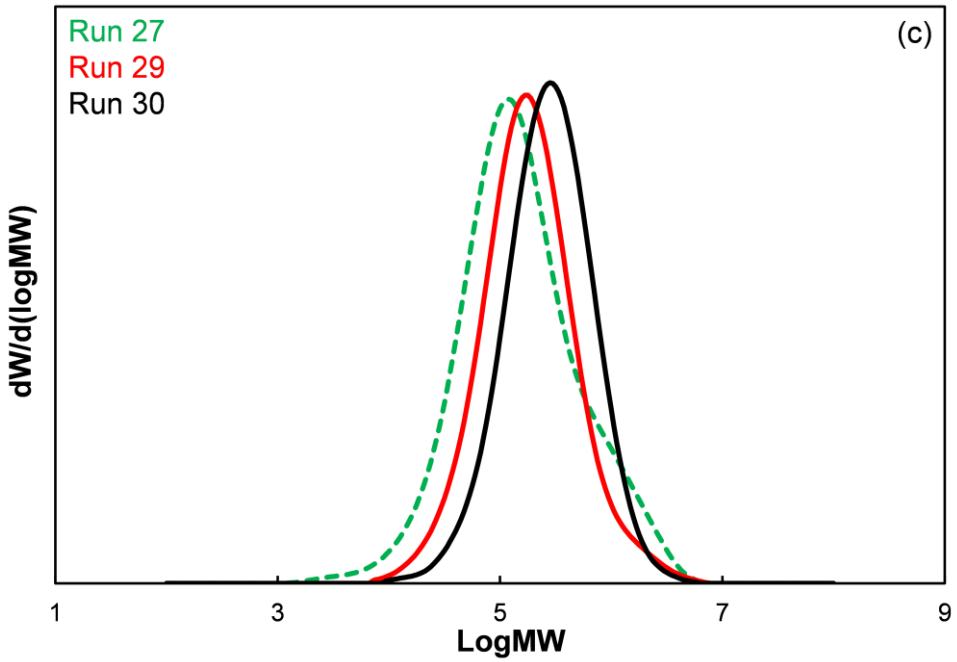

Fig. 17. Molecular weight distributions of PE samples prepared using TIBA/$Ph_3CB(C_6F_5)_4$ as an activator under identical conditions: a) **1a** vs. **2a** (30 °C), b) **1a** vs. **2a** (0 °C), c) **1b** vs. **2b** (30 °C). The solid and dashed lines correspond to PE samples obtained using the polymer-supported and molecular catalysts, respectively.

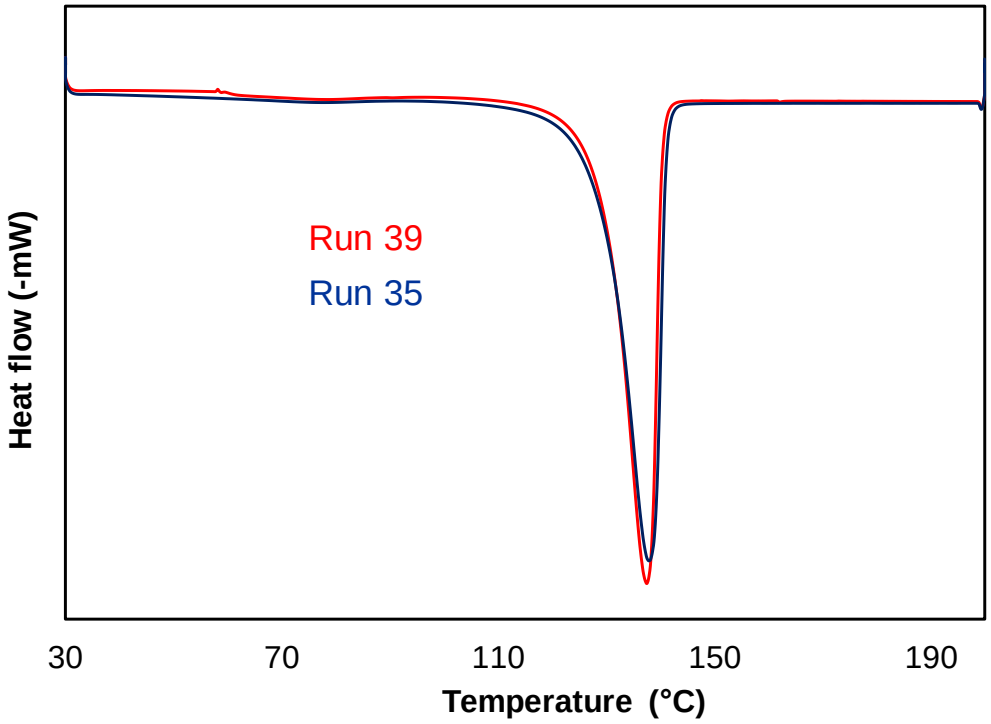

Fig. 18. DSC thermogram of PE samples obtained using the PNB-*g*-CAT Cl (**1a**) and its molecular analogue CAT Cl (**2a**).

2.3.4. Ethylene/1-octene copolymerization

Aryloxide-containing half-titanocene complexes are effective catalysts for the copolymerization of ethylene with linear α-olefins, cyclic olefins, styrene and a variety of sterically encumbered olefins, while substituents on the aryloxide ligand as well as modification on cyclopentadienyl ring strongly influences the comonomer incorporation and molecular weight of produced polymers [41,64-66]. In order to evaluate the performance of a PNB-supported catalyst (**1a**), ethylene/1-octene copolymerization was conducted at 30 °C, using TIBA/$Ph_3CB(C_6F_5)_4$ as an activator system. The results are summarized in Table 7, in which the results for the molecular analogue (**2a**) are also included for comparison.

Table 7

Ethylene/1-octene copolymerization using TIBA/$Ph_3CB(C_6F_5)_4$ as an activator[a]

Run	Catalyst (μmol)	Ethylene pressure (MPa)	1-octene (mol/L)	Activity (kg-PE/mol-Ti·h)	1-octene content[b] (mol%)
40	**2a** (5.0)	0.4	0.32	9900 ± 490	17.7
41	**1a** (5.0)	0.4	0.32	4000 ± 120	14.8
42	**1a** (5.0)	0.2	0.32	1800 ± 40	26.0
43	**1a** (5.0)	0.6	0.32	8160 ± 240	10.8
44	**1a** (5.0)	0.6	0.53	8300 ± 60	15.8
45	**1a** (5.0)	0.6	0.74	9500 ± 120	24.7
46	**1a** (5.0)	0.6	1.06	12600 ± 470	36.4

[a] Polymerization conditions: Toluene+1-octene = 300 mL, TIBA = 2.5 mmol, Ti/$Ph_3CB(C_6F_5)_4$ = 1 mol/mol, T = 30 °C, t =10 min.

[b] Calculated from ^{13}C NMR based on dyad distributions.

It was found that the PNB-*g*-CAT Cl (**1a**) showed reasonable activity in ethylene/1-octene copolymerization (run 41). However, synergistic comonomer incorporation improvement was not observed in ethylene/1-octene copolymerization with PNB-*g*-CAT Cl (**1a**). The observed activity as well as comonomer incorporation amount of PNB-*g*-CAT Cl (**1a**) was lower than those of the molecular analogue (**2a**), probably due to the additional steric interference caused by the PNB random coil, which lowered that rate of monomer insertion. The lack of synergy in ethylene/1-octene copolymerization can be further attributed to the poorer solubility of PNB chains in 1-octene with respect to toluene. Therefore, in the polymerization medium, the multiple active centres confined in a random coil could not improve the 1-octene

concentration around them, as it was proposed in the case of ethylene homopolymerization. Nevertheless, the activity of PNB-*g*-CAT Cl (1**a**) in the copolymerization increased with an increase of ethylene pressure (run 41 vs. 43), while the 1-octene content in the resultant copolymers increased on lowering the ethylene pressure (run 41 vs. 42) or with an increase of 1-octene concentration in the feed (runs 43 to 46). Fig. 19 represents the ^{13}C NMR spectra of poly(ethylene-co-1-octene) samples synthesized by PNB-*g*-CAT Cl (1**a**) and its molecular analogue CAT C (**2a**). Table 8 summarizes the assignments of peaks in the ^{13}C NMR spectrum of poly(ethylene-co-1-octene) [67].

It was found that the PNB-*g*-CAT Cl **(1a)** showed remarkable incorporation of 1-octene in ethylene/1-octene copolymerization without scarifying the activity (runs 43 to 46). The monomer sequence distributions in the resultant poly(ethylene-co-1-octene) samples prepared by PNB-*g*-CAT Cl (**1a**) and CAT Cl (**2a**) are summarized in Table 9. The copolymers obtained by PNB-*g*-CAT Cl (**1a**) and CAT Cl (**2a**) contained similar amounts of EOE and EEO + OEE sequences, while CAT Cl (**2a**) produced copolymer with higher amounts of OEO and EOO + OOE sequences (Table 9). In the case of the copolymers obtained by PNB-*g*-CAT Cl (**1a**), the EEE triad decreased with the increase of 1-octene concentration, which was accompanied by the increase in the OOO triad. The products of the monomer reactivity ratios represented as "r_E x r_O", which reflects the chemical compositions of the copolymers, are reported in Table 9. For all the poly(ethylene-co-1-octene) samples prepared by PNB-g-CAT Cl (**1a**), the obtained values of r_E x r_O were close to one suggesting a random distribution of monomers in the copolymer samples [68]. These results are consistent with those obtained for the group 4 transition metal catalysts [41,68].

Contrary, in the case of poly(ethylene-co-1-octene) synthesized by CAT Cl (**2a**), the value of r_E x r_O was relatively higher, indicating a greater degree of intra-chain heterogeneity of chemical composition as compared to the poly(ethylene-co-1-octene) synthesized by PNB-g-CAT Cl (**1a**) under the identical condition (run 40 vs. 41).

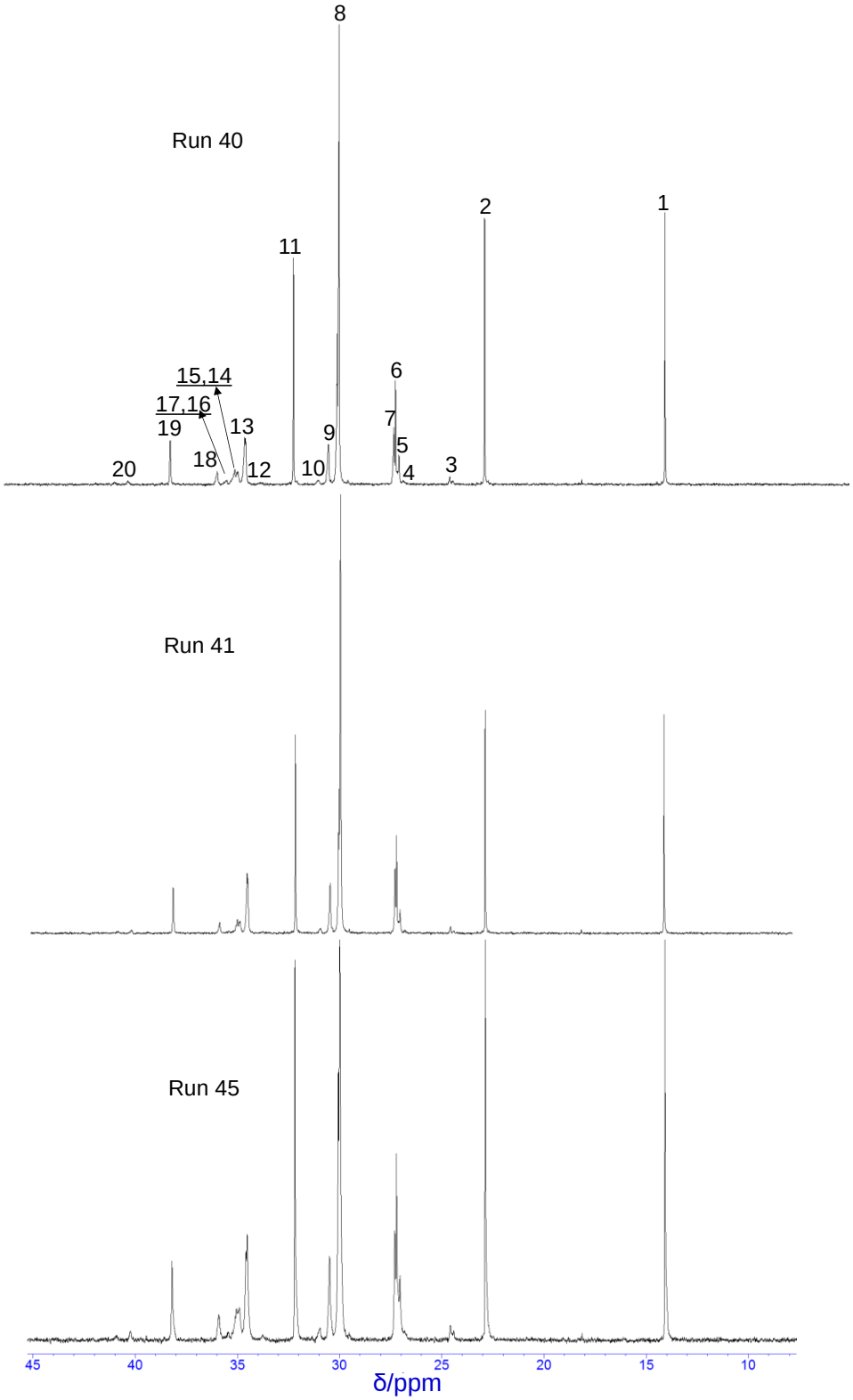

Fig. 19. ^{13}C NMR spectra of poly(ethylene-co-1-octene) samples synthesized by PNB-*g*-CAT Cl (**1a**) and its molecular analogue CAT Cl (**2a**).

Table 8

Assignment of carbons in ^{13}C NMR spectrum of poly(ethylene-co-1-octene) samples

Peak number	Type of carbon	Sequence[a]
1	CH_3	EO*E
		OO*E
		OO*O
2	CH_2 (2)	EO*E
		OO*E
		OO*O
3	CH_2 (ββ)	OE*O
4	CH_2 (5)	OO*O
5	CH_2 (5)	OO*E
6	CH_2 (5)	EO*E
7	CH_2 (βδ)	OE*EO
8	CH_2 (δδ)	EE*E
	CH_2 (4)	EO*E
	CH_2 (4)	OO*E
	CH_2 (4)	OO*O
9	CH_2 (γδ)	OE*EE
10	CH_2 (γγ)	OE*EO
11	CH_2 (3)	EO*E
		OO*E
		OO*O
12	CH	OO*O
13	CH_2 (αδ)	EO*EE
	CH_2 (6)	EO*E
14	CH_2 (αγ)	EO*EO
15	CH_2 (αδ)	OO*EE
	CH_2 (6)	OO*E
16	CH_2 (αγ)	OO*EO
17	CH_2 (6)	OO*OE
18	CH	EOO*E
19	CH	EO*E
20	CH_2 (αα)	EO*OE

[a] The asterisk is applied on a monomer unit containing the assigned carbon.

Table 9

Monomer sequence distributions in the poly(ethylene-co-1-octene) samples[a]

Run[a]	1-octene[b]	Triad distribution[b] (mol%)						Dyad distribution[c] (mol%)			r_E x r_O[d]
	(mol%)	EEE	EEO + OEE	EOE	OEO	EOO + OOE	OOO	EE	EO + OE	OO	
40	17.7	62.4	12.7	12.4	4.7	7.2	0.6	68.8	27	4.2	1.6
41	14.6	67.4	11.7	12.5	3.5	4.9	0	73.3	24.3	2.4	1.2
42	26.0	48.4	14.9	16.7	8.0	8.8	3.2	55.8	36.5	7.7	1.3
44	15.8	64.9	13.1	13	3.7	4.8	0.5	71.4	25.6	3.0	1.3
45	24.7	49.3	15.6	17.8	7.0	7.5	2.8	57.1	36.3	6.6	1.1
46	36.4	33.1	14.6	23.0	10.5	11.1	7.7	40.4	46.4	13.2	1.0

[a] Samples were obtained from Table 7.

[b] Calculated based on ^{13}C NMR.

[c] [EE] = [EEE] + 1/2{[EEO] + [OEE]}, [OO] = [OOO] + 1/2{[EOO] + [OOE]}, [EO] + [OE] = [OEO] + [EOE] + 1/2{[EEO+ OEE] + [OOE + EOO]}, [E] = [EE] + 1/2{[EO] + [OE]}, [O] = [OO] + 1/2{[EO] + [OE]}.

[d] r_E x r_O = 4{[EE][OO]}/{[EO]+[OE]}^{2} (from reference 41).

2.4. Conclusions

In an attempt to conceptually bridge the two extreme ends of catalysts (molecular and solid catalysts), a new type of bridging catalysts for olefin polymerization was proposed, which integrates multiple Ti centres in a nano-sized random coil of soluble polymer chains. A series of monodisperse polynorbornene (PNB) bearing different contents of aryloxide ligands were synthesized by means of Grubbs ring-opening metathesis polymerization. To these, two kinds of half-titanocene precursors (Cp*$TiCl_3$ and Cp*$TiMe_3$) were effectively grafted, affording structurally well-defined and soluble supported catalysts with the random coil size defined by the molecular weight and the active site density defined by the aryloxide content. Extensive investigation of the ethylene polymerization performance of these supported catalysts in full comparison with the molecular analogues uncovered several important catalytic aspects:

i) The activation of the supported catalysts using modified methylaluminoxane was sterically hindered especially in terms of alkylation, which could be completely alleviated by the utilization of a less hindered tri-*iso*-butylaluminum/$Ph_3CB(C_6F_5)_4$ activator system.

ii) The activity of the supported catalysts was found to be greater in ethylene homopolymerization using tri-*iso*-butylaluminum/$Ph_3CB(C_6F_5)_4$ activator system than those of the molecular analogues, for which a synergism among multiple active centres confined in a random coil was presumed.

iii) The polymer-supported catalysts were superior to the molecular analogues in producing polyethylene with a higher molecular weight and narrower polydispersity when activated by tri-*iso*-butylaluminum/$Ph_3CB(C_6F_5)_4$.

iv) The polymer-supported catalyst showed remarkable incorporation of 1-octene

monomer in ethylene/1-octene copolymerization to result copolymers having random distribution of 1-octene units.

While all the above findings were interesting, the most important is that I have successfully proposed a potential advantage of “concentrated” active sites compared with isolated sites. It is also important that the present success was enabled as a consequence of a well-defined nature of the supported catalysts, which is promising to exploit cooperative catalysis in a well-defined manner.

References

[1] B. Cornils, W.A. Herrmann, in: B. Cornils (Ed.), W.A. Herrmann (Ed.), Applied Homogeneous Catalysis with Organometallic Compounds, Vol. 1, Wiley–VCH, Weinheim, 2002, Chapter 1, pp. 1–16.

[2] W.A. Herrmann, B. Cornils, Angew. Chem. Int. Ed. 36 (1997) 1048–1067.

[3] A.M. Echavarren, D.J. Cárdenas, in: A. de Meijere (Ed.), F. Diederich (Ed.), Metal-Catalyzed Cross-Coupling Reactions, Wiley–VCH, Weinheim, 2004, Chapter 1, pp. 1–40.

[4] N. Miyaura, A. Suzuki, Chem. Rev. 95 (1995), 2457–2483.

[5] T.M. Trnka, R.H. Grubbs, Acc. Chem. Res. 34 (2001) 18–29.

[6] G.J. Britovsek, V.C. Gibson, D.F. Wass, Angew. Chem. Int. Ed. 38 (1999) 428–447.

[7] T. Hayashi, Acc. Chem. Res. 33 (2000) 354–362.

[8] W. Kaminsky, A. Laban, Appl. Catal. A: Gen. 222 (2001) 47–61.

[9] L.C. Wilkins, R.L. Melen, Coord. Chem. Rev. 324 (2016) 123–139.

[10] M.M. Stalzer, M. Delferro, T.J. Marks, Catal. Lett. 145 (2015) 3–14.

[11] J.M. Thomas, W.J. Thomas, Principle and Practice of Heterogeneous Catalysis, Wiley–VCH, Weinheim, 2014, Chapter 8, pp. 629–645.

[12] J. Hagen, Industrial Catalysis: A Practical Approach, Wiley–VCH, Weinheim, 2006, Chapter 8, pp. 281–294.

[13] J. Weitkamp, ChemCatChem 4 (2012) 292–306.

[14] S. Matsumoto, Catal. Today 90 (2004) 183–190.

[15] K. Soga, T. Shiono, Prog. Polym. Sci. 22 (1997) 1503–1546.

[16] G.W. Huber, S. Iborra, A. Corma, Chem. Rev. 106 (2006) 4044–4098.

[17] B.K. Min, C.M. Friend, Chem. Rev. 107 (2007) 2709–2724.

[18] T. Taniike, T. Funako, M. Terano, J. Catal. 311 (2014) 33–40.

[19] http://www.ishhc17.org., 12/10/2017.

[20] E. Albizzati, U. Giannini, G. Collina, L. Noristi, L. Resconi, in: E.P. Moore Jr. (Ed.), Polypropylene Handbook, Hanser, New York, 1996, Chapter 2, pp. 11–55.

[21] T.J. Pullukat, R.E. Hoff, Cat. Rev. Sci. Eng. 41 (1999) 389–428.

[22] G.W. Coates, Chem. Rev. 100 (2000) 1223–1252.

[23] M.C. Baier, M.A. Zuideveld, S. Mecking, Angew. Chem. Int. Ed. 53 (2014) 9722–9744.

[24] M. Jezequel, V. Dufaud, M.J. Ruiz-Garcia, F. Carrillo-Hermosilla, U. Neugebauer, G.P. Niccolai, F. Lefebvre, F. Bayard, J. Corker, S. Fiddy, J. Evans, J.P. Broyer, J. Malinge, J.M. Basset, J. Am. Chem. Soc. 123 (2001) 3520–3540.

[25] C. Copéret, J.M. Basset, Adv. Synth. Catal. 349 (2007) 78–92.

[26] G.G. Hlatky, Chem. Rev. 100 (2000) 1347–1376.

[27] J.R. Severn, J.C. Chadwick, R. Duchateau, N. Friederichs, Chem. Rev. 105 (2005) 4073–4147.

[28] B. Heurtefeu, C. Bouilhac, É. Cloutet, D. Taton, A. Deffieux, H. Cramail, Prog. Polym. Sci. 36 (2011) 89–126.

[29] S. Hotta, K. Asuka, S. Kitade, K. Takahashi, I. Kouzai, T. Tayano, US Patent 20150010747A1 (2015), to Japan Polypropylene Corporation.

[30] M. Delferro, T.J. Marks, Chem. Rev. 111 (2011) 2450–2485.

[31] L. Li, M.V. Metz, H. Li, M.-C. Chen, T.J. Marks, L. Liable-Sands, A.L. Rheingold, J. Am. Chem. Soc. 124 (2002) 12725–12741.

[32] S. Liu, A. Motta, A.R. Mouat, M. Delferro, T.J. Marks, J. Am. Chem. Soc. 136 (2014) 10460–10469.

[33] A. Leitgeb, J. Wappel, C. Slugovc, Polymer 51 (2010) 2927–2946.

[34] C.W. Bielawski, R.H. Grubbs, Prog. Polym. Sci. 32 (2007) 1–29.

[35] W.J. Sommer, M. Weck, Adv. Synth. Catal. 348 (2006) 2101–2113.

[36] M. Holbach, M. Weck, J. Org. Chem. 71 (2006) 1825–1836.

[37] K. Nomura, H. Ogura, Y. Imanishi, J. Mol. Catal. A: Chem. 185 (2002) 311–316.

[38] K. Nomura, Y. Kuromatsu, J. Mol. Catal. A: Chem. 245 (2006) 152–160.

[39] K. Nomura, K. Tanaka, S. Fujita, Organometallics 31 (2012) 5074–5080.

[40] B. Kitiyanan, K. Nomura, Organometallics 26 (2007) 3461–3465.

[41] K. Nomura, J. Liu, S. Padmanabhan, B. Kitiyanan, J. Mol. Catal. A: Chem. 267 (2007) 1–29.

[42] G. Floros, N. Saragas, P. Paraskevopoulou, N. Psaroudakis, S. Koinis, M. Pitsikalis, N. Hadjichristidis, K. Mertis, Polymers 4 (2012) 1657–1673.

[43] B. Düz, C.K. Elbistan, A. Ece, F. Sevin, Appl. Organomet. Chem. 23 (2009) 359–364.

[44] K. Nomura, N. Naga, M. Miki, K. Yanagi, Macromolecules 31 (1998) 7588–7597.

[45] P. Schwab, R.H. Grubbs, J.W. Ziller, J. Am. Chem. Soc. 118 (1996) 100–110.

[46] B. Xue, K. Ogata, A. Toyota, Polym. Degrad. Stab. 93 (2008) 347–352.

[47] W.L. Truett, D.R. Johnson, I.M. Robinson, B.A. Montague, J. Am. Chem. Soc. 82 (1960) 2337–2340.

[48] R.M. Silverstein, F.X. Webster, D.J. Kiemle, Spectrometric Identification of Organic Compounds, John Wiley & Sons Inc., Hoboken, 2005, Chapter 2, pp. 72–92.

[49] T.L. Choi, R.H. Grubbs, Angew. Chem. 115 (2003) 1785–1788.

[50] B. Kitiyanan, K. Nomura, Stud. Surf. Sci. Catal. 161 (2006) 213–218.

[51] G. Strobl, The Physics of Polymers, Springer-Verlag, Berlin, 1996, Chapter 2, pp. 43–49.

[52] N.P. Evlampieva, M.L. Gringol'ts, I.I. Zaitseva, O.V. Okatova, T.S. Dmitrieva, P.P. Khlyabich, E.I. Ryumtsev, Russ. J. Appl. Chem. 81 (2008) 2014–2020.

[53] T.F.A. Haselwander, W. Heitz, S.A. Krugel, J.H. Wendorff, Macromolecules 30 (1997) 5345–5351.

[54] M.W. McKittrick, C.W. Jones, J. Catal. 227 (2004) 186–201.

[55] A. Amgoune, M. Krumova, S. Mecking, Macromolecules 41 (2008) 8388–8396.

[56] V. Busico, R. Cipullo, F. Cutillo, N. Friederichs, S. Ronca, B. Wang, J. Am. Chem. Soc. 125 (2003) 12402–12403.

[57] J.N. Pédeutour, K. Radhakrishnan, H. Cramail, A. Deffieux, Macromol. Rapid Commun. 22 (2001) 1095–1123.

[58] M. Bochmann, J. Organomet. Chem. 689 (2004) 3982–3998.

[59] M.R. Salata, T.J. Marks, Macromolecules 42 (2009), 1920-1933.

[60] T. Keii, M. Terano, K. Kimura, K. Ishii, Macromol. Rapid Commun. 8 (1987) 583–587.

[61] B. Liu, H. Matsuoka, M. Terano, Macromol. Rapid Commun. 22 (2001) 1–24.

[62] V. Busico, R. Cipullo, V. Esposito, Macromol. Rapid Commun. 20 (1999) 116–121.

[63] A. Thakur, S. Poonpong, M. Terano, T. Taniike, Macromol. React. Eng. 8 (2014) 766–770.

[64] K. Nomura, T. Komatsu, Y. Imanishi, Macromolecules 33 (2000) 8122–8124.

[65] K. Nomura, M. Tsubota, M. Fujiki, Macromolecules 36 (2003) 3797–3799.

[66] K. Nomura, Dalton Trans. 41 (2009) 8811–8823.

[67] K. Kimura, S. Yuasa, Y. Maru, Polymer 25 (1984) 441–446.

[67] J. Suhm, M.J. Schneider, R. Mulhaupt, J. Polym. Sci. A, 35 (1997) 735–740.

Chapter 3

Origin of Cooperative Catalysis Embodied by Aryloxide-Containing Half-Titanocene Catalysts Confined in a Single Polynorbornene Chain

ABSTRACT:

A series of monodisperse and soluble polynorbornene (PNB) supported aryloxide-containing half-titanocene catalysts with different active site densities were synthesized. The bottom-up strategy applied for the synthesis of PNB-supported catalysts allowed the precise control of the number of grafted Ti centres per random coil of PNB chains over a wide range. The PNB-supported catalysts were extensively characterized by ^{1}H, ^{13}C NMR and UV-Vis spectroscopy. In ethylene polymerization at a lower temperature, the activity enhancement of these PNB-supported catalysts as compared to their molecular analogue as well as along the active site density revealed the existence of a synergy or cooperation among multiple active centres confined in a nano-sized random coil of PNB chains. On the other hand, at a higher temperature, the effect of active site isolation was found to be crucial for achieving the highest activity of a PNB-supported catalyst.

3.1. Introduction

In catalysis “cooperative effect” is a term, used to describe an improvement in catalytic performance by synergy or cooperation of two or more proximate active centres during a chemical transformation [1]. Cooperative catalysis is a unique feature of many metalloenzymes, such as ureases, in which two or proximate metal centers cooperate to activate both electrophilic and nucleophilic reactants, leading to superior activity and selectivity [2-4]. In the field of abiotic homogeneous catalysis, syntheses of nature inspired multimetallic complexes, which can undergo cooperative catalysis has gained great attentions [5-10]. In recent studies, cooperation of Lewis base and acid centers in a single catalytic system has been exploited for a variety of reactions, which include, Corey-Chaykovsky epoxidations, asymmetric Strecker reactions, Diels-Alder reactions, metallosalen catalyzed asymmetric ring opening polymerization of epoxides and enantioselective cycloaddition reactions between ketene enolates and various electrophiles [5-10]. Improved activity and selectivity of the multinuclear cooperative catalysts with respect to the mononuclear catalysts arise due to proximity of multiple active centers, which can selectively improve the local concentration of reagents by conformationally favourable covalent or noncovalent interactions [11,12]. Such utilization of cooperative catalysis in molecular catalysts motivated the development of binuclear or multinuclear (trinuclear, tetranuclear etc.) molecular catalysts in the field of olefin polymerization [12]. The importance of cooperative catalysis in the field of catalytic olefin polymerization is straight forward in a sense that if the co-presence of proximate metal centres can improve selectivity for distinctive enchainment pathways, then there is a possibility to obtain higher catalytic activity as well as unique polymer microstructures in terms of molecular weight, branching and

comonomer incorporation amount in a way to directly influence polymer properties and their end-use applications. Thus, in the past two decades there have been serious efforts devoted towards the exploitation of cooperative catalysis for function integrations in homogeneous olefin polymerization catalysis [12]. For this, different strategies were developed to fix two or more metal centres in proximity using different ligands. Representative examples are early transition metal based binuclear/trinuclear metallocene and half-metallocene catalysts [13-15], late transition metal based binuclear phenoxyiminato and α-diimine catalysts [16,17], late transition metal based tetranuclear α-diimine catalysts and etc. [18]. With these multinuclear catalysts, generally higher catalytic activity and improved polymer molecular weight were observed compared to their mononuclear analogues. It was suggested that some trapping of monomers could be possible due to the high local metal concentrations in these multinuclear catalysts [12]. Also, electronic, steric, and ion-pairing effects present in these catalysts might play a role in achieving higher activities as compared to their mononuclear analogues [12]. Great success in this area was achieved by the pioneering research of Marks *et al.*, in which, a series of constrained geometry based homo and hetero binuclear molecular catalysts were synthesized, and their synergistic combination with a binuclear cocatalyst was explored [12,19-22]. This combination helped to bring the two metal centres to a closest possible distance. In these catalysts, function integrations have been achieved by the cooperation between two sterically open proximate metal centres *via* secondary agostic (noncovalent) interaction, which significantly influenced the monomer enchainment and the chain transfer kinetics. Unique catalytic consequences due to the said cooperativity were apparently observed by higher catalytic activity, enhanced branching, higher α-olefin incorporation, and molecular weight increment as

compared to their mononuclear analogues [12,19-22]. Systematic study on the structure-performance relationship of a variety of binuclear catalysts with the aid of DFT calculations suggested the importance of ligand architecture, ligand electronic characteristics and metal−metal distance in cooperative catalysis [22]. Surely, the advantage of a binuclear catalyst is attributed to the design precession at the molecular level *i.e.*, a proper placement of two metal centres at an optimum distance for maximum cooperation to embody catalytic multifunctionality in a single complex. But the synthetic limitations make it difficult to design ligand framework, which can integrate multiple number of nuclei, to incorporate more functions in a single molecule. Thus, exploitation of cooperative catalysis in multinuclear catalysts having well-defined structural features is an important direction to design new multifunctional catalysts in the field of olefin polymerization.

In Chapter 2, I successfully provided a new bridging catalyst system for the integration of functions in a well-defined way by confining multiple active centres in a random coil of a single polynorbornene (PNB) chain. It was established that PNB having uniform chain length as well as a controlled density of ancillary donor ligands at side chain can be efficiently synthesized by Grubbs ring-opening metathesis polymerization (ROMP). Furthermore, these well-defined polymers were used as a soluble support for half-titanocene molecular catalysts. Such a supported catalyst equips well-defined characteristics in terms of active site design analogous to the molecular catalyst as well as a controlled active site density in a random coil of a single polymer chain, whose size can be defined by the Flory radius. Extensive investigation in ethylene polymerization, revealed an enhanced activity of these soluble polymer-supported catalysts as compared to their molecular analogues. Based on the

improved local concentration of Ti in these polymer-supported catalysts with respect to their molecular analogues, a synergy or cooperation among multiple active centres confined in a random coil of PNB chains was assumed as the reason for the observed activity improvements. In the present chapter, I aim to explore the origin of the said synergy or cooperation among neighbouring active sites confined in a nano-sized random coil in order to embody the concept of function accumulation in the new catalyst system.

In the present chapter, a series of PNB-supported half-titanocene catalysts [23,24] with different active site densities were prepared and employed in ethylene polymerization to study a potential cooperation among confined active centres in a well-defined way.

3.2. Experimental

3.2.1. Materials

All commercially available reagents were of a research grade and used without further purification unless specified. Bicyclo[2.2.1]hepta-2,5-diene (norbornadiene), 4-bromo-2,6-dimethyphenol, bis(triphenylphosphine)palladium(II) dichloride ($Pd(PPh_3)_2Cl_2$), bicyclo[2.2.1]hept-2-ene (norbornene), 2,6-dimethylphenol, pentamethylcyclopentadienyltitanium (IV) trichloride (Cp^*TiCl_3) and trityl tetrakis(pentafluorophenyl)borate ($Ph_3CB(C_6F_5)_4$) were purchased from Tokyo Chemical Industry. Ammonium formate (NH_4HCO_2), the Grubbs 1st generation catalyst, and ethyl vinyl ether were purchased from Sigma-Aldrich. Triethylamine was purchased from Kanto Chemical. *N*,*N*-Dimethylformamide (DMF, Wako Pure Chemical Industries) was dried over molecular sieves 4A with N_2 bubbling.

Tri-*iso*-butylTIBA (TIBA) was donated by Tosoh Finechem. Ethylene of a polymerization grade was donated by Sumitomo Chemical and used as delivered. For the synthesis of PNB supports and catalysts, dichloromethane (CH_2Cl_2) and toluene (Sigma-Aldrich and Wako Pure Chemical Industries) of an anhydrous grade were used. They were further dehydrated over molecular sieves 3A and 4A with N_2 bubbling, respectively. Diethyl ether of an anhydrous grade was purchased from Tokyo Chemical Industry and degassed before use. Toluene (Kanto Chemical) for polymerization was used after being passed through a column of molecular sieves 4A and bubbled with N_2. Deuterated chloroform ($CDCl_3$, Kanto Chemical) was stored in a teflon sealed schlenk containing molecular sieves 3A and degassed before use.

3.2.2. Measurements

All ^1H and ^{13}C $\{^1H\}$ NMR spectra of the PNB supports and PNB-supported catalysts were recorded on a 400 MHz Bruker Advance spectrometer in $CDCl_3$ at 25 °C and all chemical shifts were given in ppm. The residual peak of $CHCl_3$ at 7.26 ppm and the peak of $CDCl_3$ at 77.16 ppm were used as references in ^1H and ^{13}C NMR, respectively. The number-average molecular weight (M_n), weight-average molecular weight (M_w) and the polydispersity index (M_w/M_n) of PNB supports were determined by gel permeation chromatography (GPC, Shimadzu SCL-10A) equipped with a RID-10A detector and calibrated with polystyrene standards. Tetrahydrofuran (THF) of a GPC grade (Wako Pure Chemical Industries, stabilizer-free) was used as the eluent with an isocratic flow rate of 1.0 mL/min at 35 °C. UV-Vis spectroscopy (JASCO V670 UV-VIS spectrometer) was utilized to characterize molecular and PNB-supported catalysts in a toluene solution at the concentration of 0.25-0.4 μmol/mL. The melting

temperature (T_m) and crystallinity (X_c) of polyethylene (PE) were acquired on a differential scanning calorimeter (DSC, Mettler Toledo DSC-822) based on the first heating cycle at 10 °C/min up to 180 °C under 200 mL/min of N_2.

3.2.3. Synthesis of 4-bicyclo[2.2.1]hept-5-en-2-yl-2,6-dimethylphenol

The detailed synthetic procedure was given in Chapter 2 (*cf.* section 2.2.3). Briefly, the compound was synthesized by heating a reaction mixture of norbornadiene (46 mmol), 4-bromo-2,6-dimethylphenol (9.0 mmol), triethylamine (28 mmol) and NH_4HCO_2 (37 mmol) in DMF (15 mL), using $Pd(PPh_3)_2Cl_2$ (0.40 mmol) as a catalyst at 80 °C for 16 h under N_2 with constant stirring. The product was isolated by silica column chromatography (1/9 v/v ethylacetate/hexane) in 80% yield. The synthesis and purification of 2-aryloxonorbornene were confirmed by ^1H and ^{13}C NMR spectroscopy (*cf.* Figs. 1a,b, in Chapter 2). The exo-isomer was obtained as the major product (> 95.0%).

3.2.4. Synthesis of PNB supports

In a typical experiment, *e.g.* run 3 in Table 1, 2-aryloxonorbornene (0.68 mmol) and norbornene (12.8 mmol) were dissolved in CH_2Cl_2 (12 mL) in a schlenk tube under N_2. To this, a solution of the Grubbs 1st generation catalyst (8.0 mmol/L) in CH_2Cl_2 (8.0 mL) was added at room temperature. After 3 h, the polymerization was quenched by adding an excess of ethyl vinyl ether. The resultant polymer solution was poured into methanol, collected by filtration, washed with methanol and dried under vacuum for several hours at 30 °C. The polymer was additionally purified by reprecipitation from CH_2Cl_2/diethyl ether, and finally collected as a white solid after vacuum drying for

several hours at 30 °C. The comonomer content in the PNB supports (runs 1 to 5 in Table 1) was varied through the 2-aryloxonorbornene amount from 0.10 to 2.30 mmol to the fixed amount of norbornene (12.8 mmol). The peaks in the ^{1}H and ^{13}C NMR spectra were consistently assigned based on literature [25,26] as follows.

^{1}H NMR (400 MHz, $CDCl_3$, δ): 0.90-1.13 (m, 1H, H_7), 1.20-1.46 (m, 2H, $H_{5,6}$), 1.65-2.01 (m, 3H, $H_{5,6,7}$), 2.20 (s, 6H, H_e), 2.42 (bs, 2H, $H_{1,4}$, *trans*), 2.78 (bs, 2H, $H_{1,4}$, *cis*), 4.42 (s, 1H, OH), 5.12-5.25 (m, 2H, ,$H_{2,3}$, *cis*), 5.26-5.42 (m, 2H, $H_{2,3}$, *trans*), 6.78 (s, 2H, H_b).

^{13}C NMR (100 MHz, $CDCl_3$, δ): 16.2 (C_e); 32.3, 32.5, 33.0, 33.2, 38.6, 38.8, 41.5, 42.2, 43.3, 43.6, 50.5, 50.8, 52.0 (saturated carbons of PNB backbone); 122.6 (C_c), 127.7 (C_b); 130.9, 133.0, 133.2, 133.3, 133.9, 134.1, 134.7 (olefinic carbons of PNB backbone); 137.2 (C_a), 150.2 (C_d).

*3.2.5. Synthesis of PNB-g-CAT Cl (**1a-e**)*

Five different kinds of PNB-supported catalysts were synthesized using the PNB supports (runs 1 to 5) of Table 1. A flame-dried schlenk tube was exchanged with N_2 and charged with a solution of Cp*$TiCl_3$ (1.5-2.7 mmol) in CH_2Cl_2 (20-25 mL). To this, a solution of a PNB support (1/25-1/6 equivalent of the aryloxide ligand with respect to Cp*$TiCl_3$) in CH_2Cl_2 (20-35 mL) was added dropwise under N_2 with continuous stirring at room temperature. The ratio of Cp*$TiCl_3$ to aryloxide ligands became 25 in the case of the lowest aryloxide containing PNB-supported catalyst preparation, since the minimum concentration of Cp*$TiCl_3$ in the reaction solution was fixed at 8 mg/mL. The solution was slowly warmed to the boiling temperature of the solvent and then refluxed for 36-42 h. Thereafter, the product was precipitated out by

adding diethyl ether, and unreacted Cp*$TiCl_3$ was washed out. The catalysts were obtained in 75-80% yield as pale to intense red solids after repetitive washing with diethyl ether and vacuum drying for several hours.

*3.2.6. Synthesis of Cp*Ti(O-2,6-$Me_2C_6H_3$)Cl_2 (**CAT Cl, 2**)*

The complex was synthesized according to the reference [23]. The structure was confirmed by ^{1}H and ^{13}C NMR spectroscopy (*cf*. Figs. 9,11 in Chapter 2).

^{1}H NMR (400 MHz, $CDCl_3$, δ): 2.22 (s, 15H, Cp–C$\underline{H}_3$), 2.28 (s, 6H, H_e), 6.83 (t, J = 7.6 Hz, 1H, H_a), 6.95 (d, J = 7.6 Hz, 2H, H_b).

^{13}C NMR (100 MHz, $CDCl_3$, δ): 13.2 (Cp–$\underline{C}H_3$), 17.4 (C_e), 123.0 (C_c), 128.5 (C_b), 128.9 (C_a), 132.7 (Cp), 162.2 (C_d).

3.2.7. Ethylene polymerization

Ethylene polymerization was performed in a 1 L autoclave equipped with a mechanical stirrer rotating at 350 rpm. In a typical experiment, *e.g.* runs 6 in Table 3, toluene (300 mL) and TIBA (Al = 2.5 mmol) were introduced into the reactor and the solution was saturated with ethylene (0.6 MPa, absolute pressure) at 0 °C for 30 min. Thereafter, a toluene solution (0.5 mL) of the catalyst (Ti = 2.5 μmol) was injected into the reactor, followed by the injection of a solution (0.5 mL) of $Ph_3CB(C_6F_5)_4$ (2.5 μmol) to initiate the polymerization. The polymerization was conducted for 10 min with a continuous supply of ethylene at 0.6 MPa. The resultant polymer solution was poured into acidic ethanol, repeatedly washed with deionized water, collected by filtration and dried under vacuum for several hours at 60 °C.

3.3. Results and discussion

3.3.1. Synthesis and characterization of PNB supports

Table 1 summarizes the characteristics of the PNB supports to be used in the catalyst synthesis.

Table 1

PNB supports employed for the catalyst synthesis[a]

Run	Comonomer in feed[b] (mol%)	Isolated yield (%)	*trans*[c] (%)	Comonomer content[c] (mol%)	M_n[d] $\times 10^{-4}$	M_w/M_n[d]	Pendant group /chain[e]
1	0.7	97	84	0.5	5.5	1.17	3
2	2.2	94	84	2.0	5.3	1.20	11
3	5.0	95	84	4.8	7.0	1.18	36
4	11	92	82	10	7.7	1.16	82
5	17	93	79	14	6.9	1.14	103

[a] Polymerization conditions: Norbornene = 12.8 mmol, catalyst = 64.0 μmol, CH_2Cl_2 = 20 mL, T = 25 °C, t = 3.0 h.

[b] [2-aryloxonorbornene/(norbornene + 2-aryloxonorbornene)] × 100.

[c] Derived from ^{1}H NMR.

[d] Determined by GPC.

[e] Calculated from the M_n value and the comonomer content.

In Table 1, at a fixed norbornene/catalyst ratio of 200 mol/mol, random copolymerization was conducted at room temperature with increasing the 2-aryloxonorbornene fraction (0.7 to 17 mol%) in the feed (runs 1 to 5). The successful PNB support synthesis was confirmed by both ^{1}H and ^{13}C NMR

spectroscopy (*cf*. Figs 2,3 in Chapter 2). For each PNB support synthesis, over 90% of the yield and nearly quantitative comonomer incorporation were observed. The PNB supports exhibited M_w/M_n values close to one. These facts assured the well-defined nature of the synthesized PNB supports. The narrow molecular weight distribution allowed a reasonable estimation of the number of pendant groups per chain for each PNB support from their respective M_n and comonomer content, which was found to vary in the range of 3–106.

*3.3.2. Synthesis and characterization of PNB-supported catalysts (**1a-e**)*

In order to synthesize PNB-supported catalysts with different active site densities for cooperative catalysis, the grafting reaction of Cp*$TiCl_3$ to PNB supports (runs 1 to 5 in Table 1) containing different contents of aryloxide ligands was explored. Fig. 2 represents the ^{1}H NMR spectra of the PNB-supported catalysts (**1a-e**). The ^{1}H NMR spectra of the corresponding PNB supports are also shown for comparison (Fig. 1). In Fig. 2, the grafting of Cp*$TiCl_3$ to the PNB supports was confirmed with a shift in the peak position of methyl protons of the Cp ring from 2.39 to 2.20 ppm. A similar peak shift was also observed in the case of the molecular analogue (**2**). The, grafting percentage of Cp*$TiCl_3$ was derived based on Eq. (1),

$$Graft\ yield\ (\%) = \frac{\frac{1}{15} I_{Cp-CH_3}}{\frac{1}{2} I_{H_b}} \times 100 \qquad \text{Eq. (1).}$$

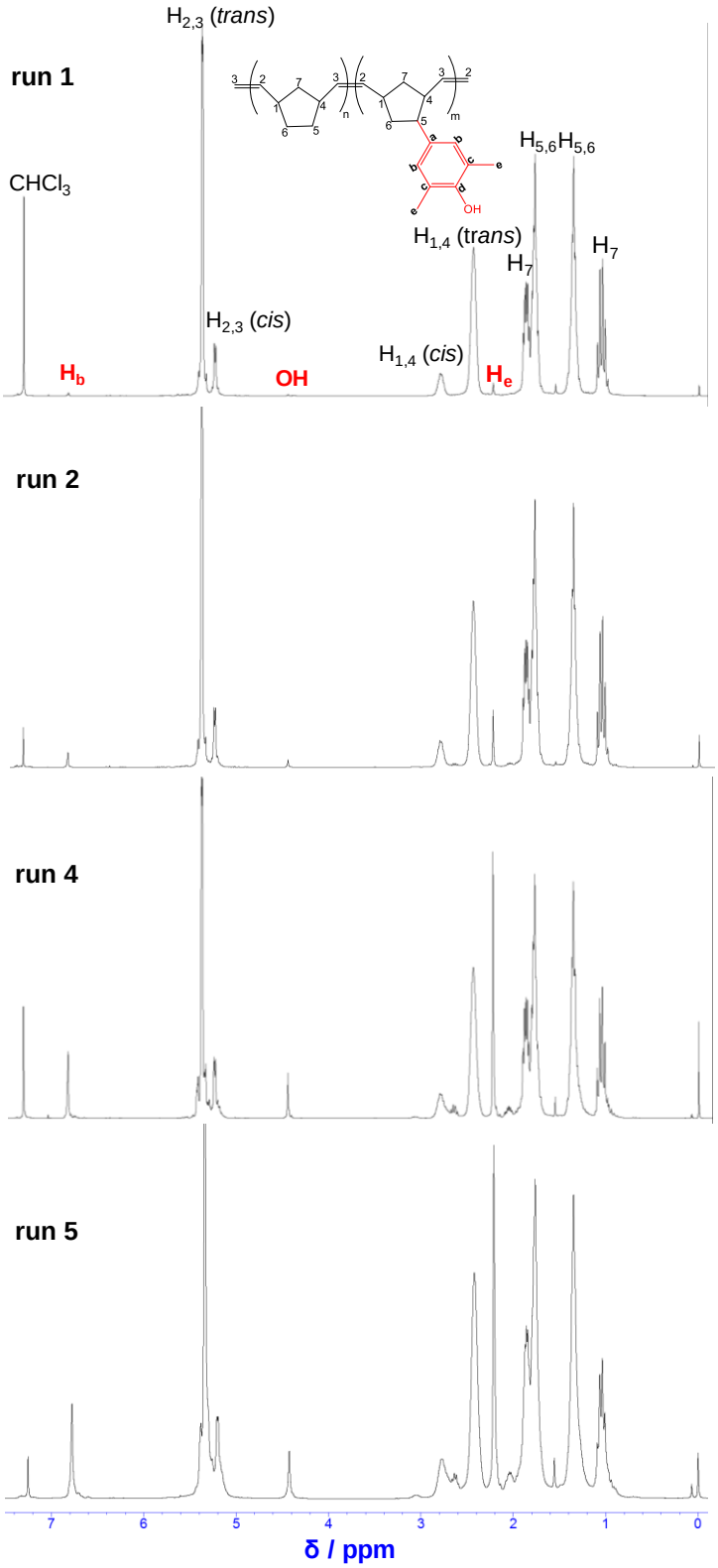

Fig. 1. ^{1}H NMR spectra of PNB supports (Table 1) with different 2-aryloxonorbornene contents.

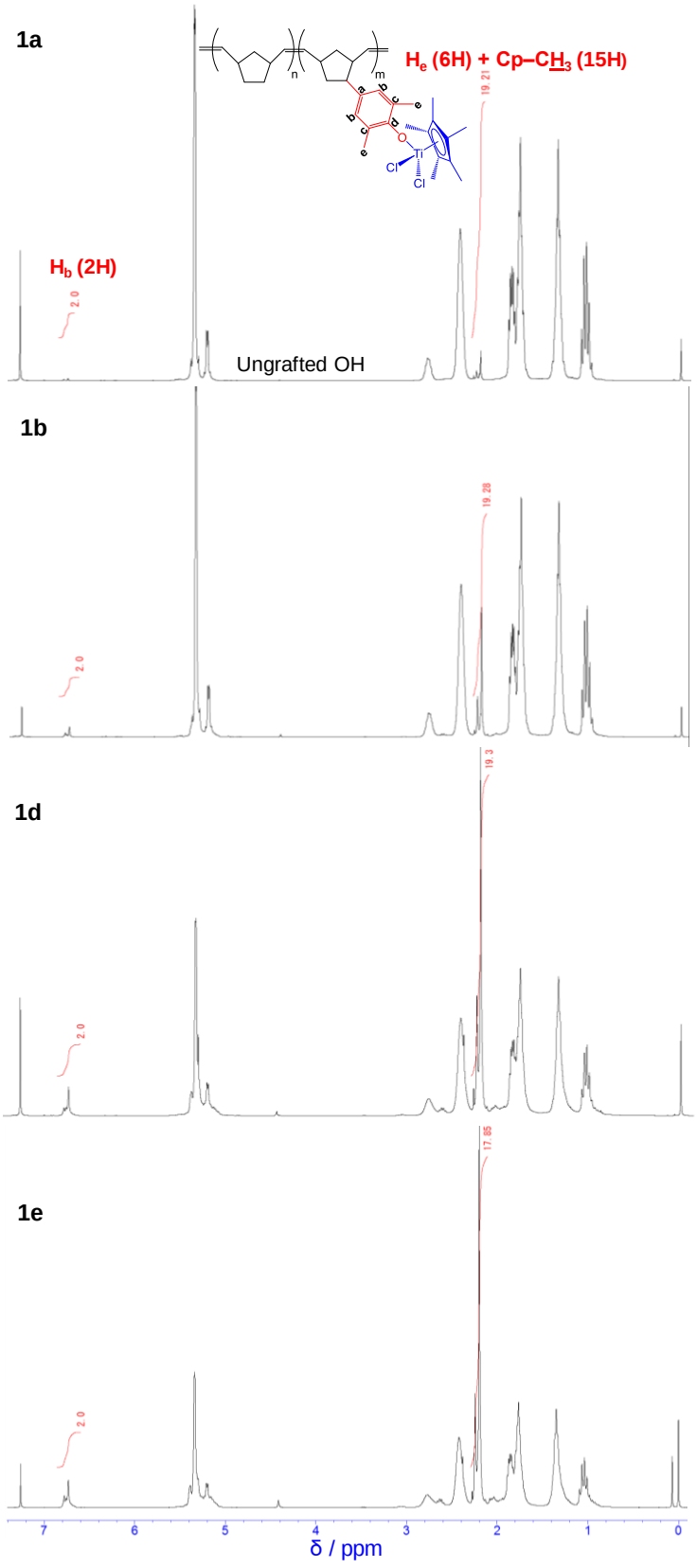

Fig. 2. ^{1}H NMR spectra of PNB-supported catalysts (**1a-e**).

Successful catalyst synthesis was further confirmed by ^{13}C NMR as shown in Fig. 3 (^{13}C NMR of **1d**). For instance, the peak position of the carbon (C_d) that is bonded to the oxygen of the aryloxo group was found to be shifted from 150.2 to 160.7 ppm. The other important peaks were also shifted by the grafting, and these shifts were consistent with those observed for the molecular analogue (**2**). However, in the ^{13}C NMR spectrum of **1e,** a minor peak (assigned as Cp'─$\underline{C}H_3$) was observed at 13.6 ppm (Fig. 4). Since the position of the new peak was located between the peak position of the five methyl carbons of Cp ring of the original PNB-supported catalyst (at 13.1 ppm) and Cp*$TiCl_3$ (at 14.6 ppm), there should be an obvious formation of secondary Ti species for **1e** (*e.g.* bis(aryloxy)cyclopentadienyltitanium (IV) chloride). Formation of a similar Ti species was also reported previously in the case of polystyrene supported half-titanocene catalysts [27]. The fraction of the secondary Ti centres was estimated as *ca*. 6 mol% based on NMR peak integrations (Fig. 4), which meant that the majority of the Ti centres (*ca.* 94 mol%) still had the same structure as those of **1a-d**.

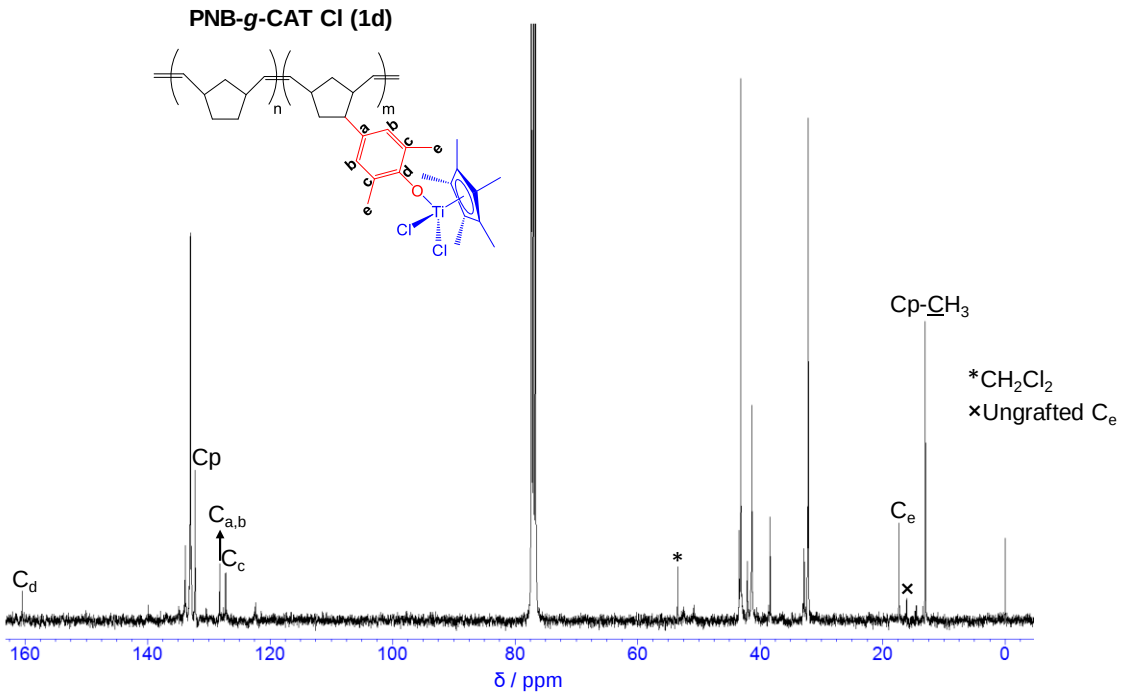

Fig. 3. ^{13}C NMR spectrum of PNB-*g*-CAT Cl (**1d**).

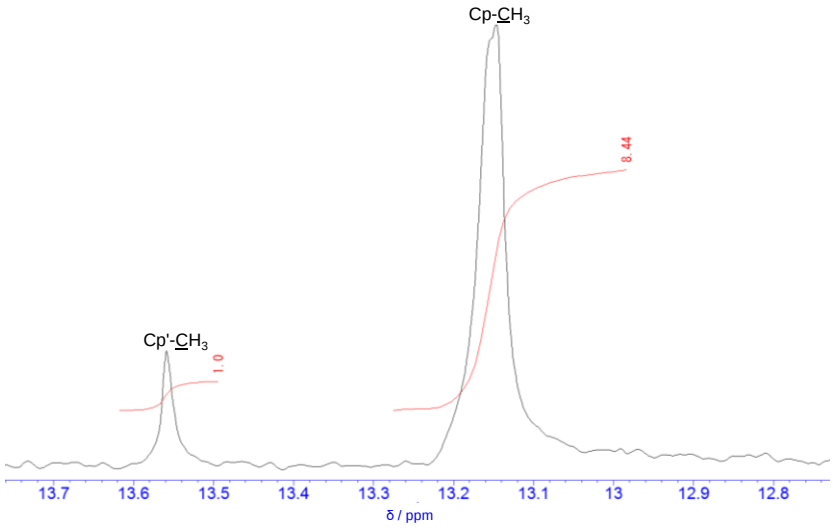

Fig. 4. Part of the ^{13}C NMR spectrum of PNB-*g*-CAT Cl (**1e**).

For all the five PNB-supported catalysts (**1a-e**), the calculated grafting percentage of Cp*$TiCl_3$, and thus estimated number of Ti centres per PNB chain are listed in Table

2. It was found that the grafting percentage of Cp^*TiCl_3 remained constant for **1a-d**, which was approximately 88%, while a significant decrease in the graft yield to 79% was observed for **1e**.

Table 2

Summary of PNB-supported catalyst synthesis[a]

Catalyst	Graft yield[a] (%)	Ti centres per chain[b]
PNB-*g*-CAT Cl (**1a**)	88.0	2
PNB-*g*-CAT Cl (**1b**)	88.5	9-10
PNB-*g*-CAT Cl (**1c**)	88.3	31-32
PNB-*g*-CAT Cl (**1d**)	88.6	72-73
PNB-*g*-CAT Cl (**1e**)	79.0	82

[a] Calculated based on Eq. 1.

[b] Calculated from the graft yield and the of number of pendant groups per chain of the corresponding PNB support.

UV-Vis spectroscopy is a powerful tool to understand the electronic properties of metallocene catalysts through the detection of typical electronic transitions such as ligand-to-metal charge-transfer transitions (LMCT) [28,29]. LMCT occurs between the frontier molecular orbitals, in which the HOMO is localized at ligands (*e.g.* Cp*) and the LUMO is localized at the metal atom. The spectra of Cp^*TiCl_3 and CAT Cl (**2**) diluted in toluene are represented in Fig. 5a. For Cp^*TiCl_3 an absorption band due to the LMCT of Cp* to Ti was observed with the maximum of absorbance (λ_{max}) located at 452 nm. By replacing an electron withdrawing chloride ligand by the electron donating aryloxide ligand (*i.e.*, CAT Cl (**2**)), the electron density on the metal centre

increases, which in turn enlarges the HOMO-LUMO gap and thus higher energy is required for the corresponding charge transfer transition [29]. As a result, the LMCT peak was shifted to the higher energy side (hypsochromic shift) with the λ_{max} value at 416 nm. Similar hypsochromic shifts were usually observed, when the electron density on the metal centre increased [29,30]. In the case of CAT Cl (**2**), another absorption peak in the UV range was observed with a λ_{max} value at 333 nm. This second peak was due to the π–π* transition of the benzene ring of the 2-aryloxide ligand. Similar peak was also reported for aryloxide containing chromocene (III) [31]. Fig. 5b represents the absorption spectra of a PNB support (run 3 in Table 1) and homo PNB dissolved in toluene at a concentration of 2.0 mg/mL. Both the polymers did not have significant absorptions in the visible region, whereas only the PNB support showed the absorption in the UV region due to the π–π* transition of the benzene ring of the 2-aryloxide pendant groups, with the λ_{max} value at 332 nm (Fig. 5b).

The absorption spectra of three PNB-supported catalysts (**1a**,**c,d**) dissolved in toluene are represented in Figs. 5c (**1a**) and 5d (**1c**,**d**). In Figs. 5c and 5d, the observed values of λ_{max} of LMCT absorptions were in the range of 418-422 nm, close to the corresponding λ_{max} value for CAT Cl (**2**). Moreover, in the case of **1c**,**d**, another peak due to the absorption corresponding to the π–π* transition of the benzene ring of the 2-aryloxide ligand was observed (Fig. 5d) in the UV range, in which the λ_{max} values lied in the range of 339-354 nm. Contrary, the same peak was not observed in the case of **1a** (Fig. 5c), plausibly due to the very low concentration of aryloxide ligands distributed in a large amount of polymer. Thus, the similar absorption patterns in the case of CAT Cl (**2**) and PNB-supported catalysts, suggested that the electronic environment around the Ti centres were similar with each other. Moreover, electronic environment was not

affected by the active site density of the PNB-supported catalysts.

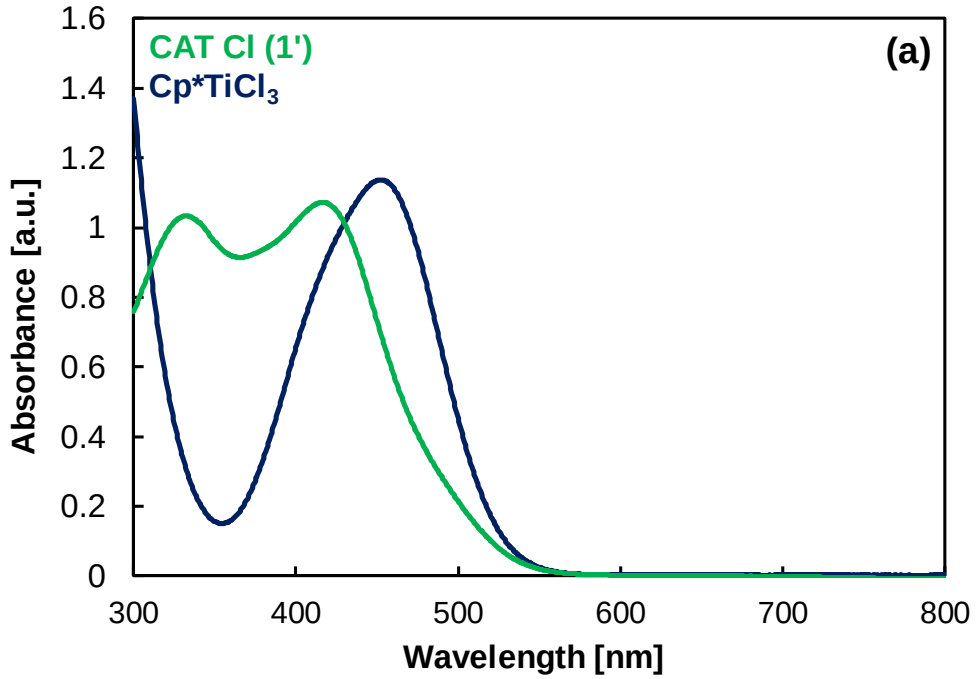

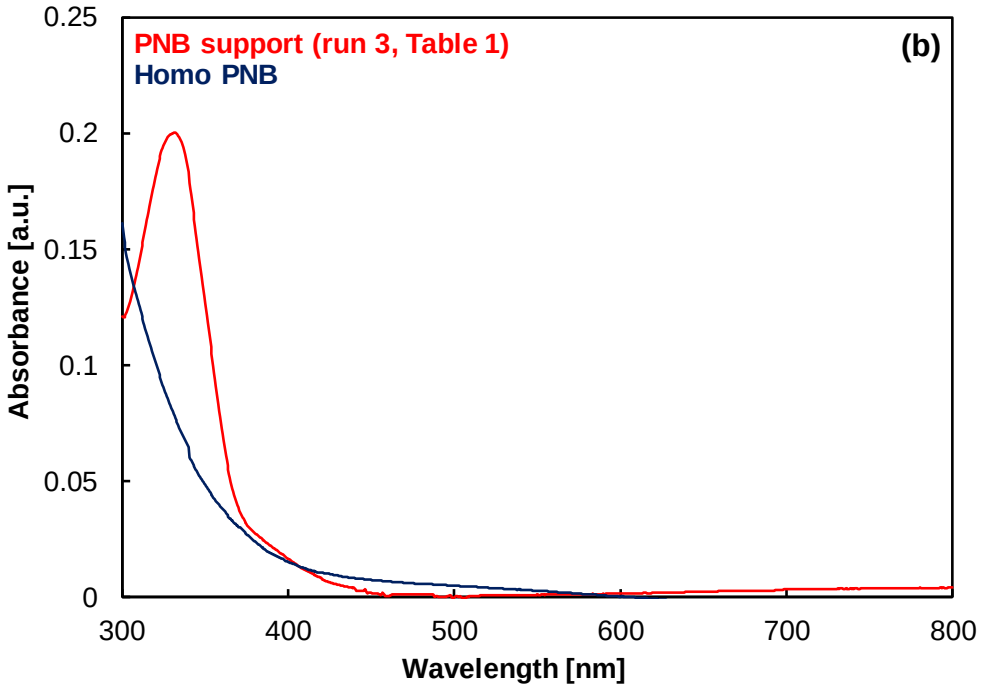

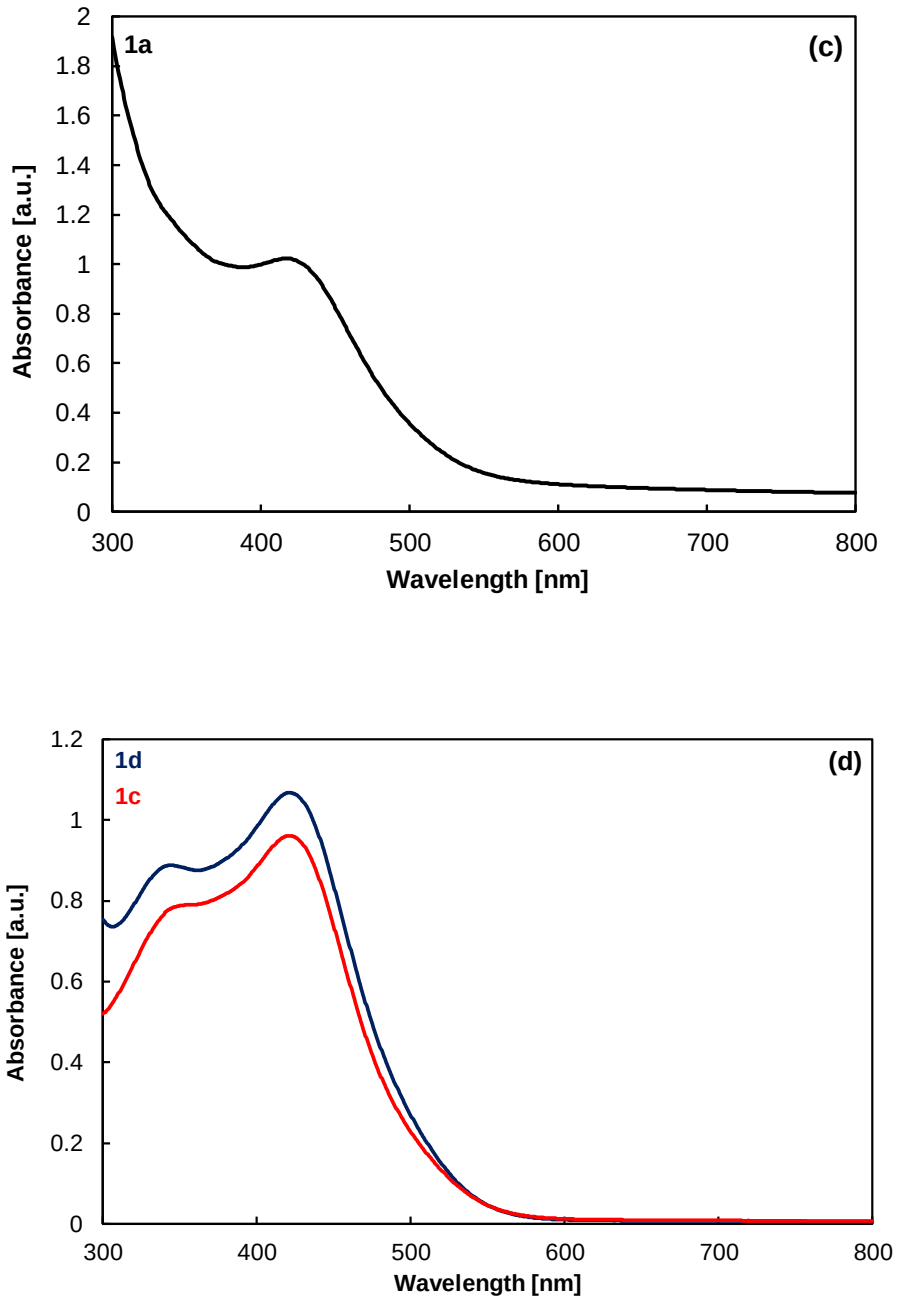

Fig. 5. UV-Vis spectra of: a) Precursor (Cp^*TiCl_3) and molecular catalyst (CAT Cl, **2**), b) a PNB support (run 3 in Table 1) and homo PNB, c) PNB-*g*-CAT Cl (**1a**) and d) PNB-*g*-CAT Cl (**1c**,**d**).

3.3.3. Ethylene polymerization

In chapter 2, it was found that **1c (1a** in chapter 2) had a very high activity of 28600 kg-PE/mol-Ti·h at 0 °C and Al/Ti ratio of 1000. The activity of the molecular catalyst (**2**) under the identical condition was 16400 kg-PE/mol-Ti·h. Based on the activity improvement (65%) by grafting, a potential synergy or cooperation among multiple active centres confined in a nano-sized random coil of PNB chains was assumed. To validate the hypothesis, ethylene polymerization was conducted with PNB-supported catalysts (**1a**-**e**) having different active site densities at 0 °C. The results are summarized in Table 3, and plotted in Fig. 6. In Table 3, the polymerization results of the molecular analogue (**2**) are also included for comparison.

Table 3

Ethylene polymerization at 0 °C[a]

Run	Catalyst	Ti centres per chain[b]	Activity (kg-PE/mol-Ti·h)	M_w[c] × 10^{-5}	M_w/M_n[c]	T_m[d] (°C)	X_c[d] (%)
6	**2**	n.a.[e]	16400 ± 390	5.7	2.5	137.0	78
7	**1a**	2	22100 ± 50	n.d.[f]	n.d.[f]	138.0	80
8	**1b**	9	22800 ± 100	n.d.[f]	n.d.[f]	n.d.[f]	n.d.[f]
9	**1c**	31	28600 ± 110	4.9	2.3	137.2	77
10	**1d**	72	29800 ± 200	n.d.[f]	n.d.[f]	137.5	81
11	**1e**	82	24600 ± 200	n.d.[f]	n.d.[f]	n.d.[f]	n.d.[f]

[a] Polymerization conditions: Ethylene pressure = 0.6 MPa, toluene = 300 mL, catalyst = 2.5 μmol, TIBA = 2.5 mmol, Ti/$Ph_3CB(C_6F_5)_4$ = 1 mol/mol, T = 0 °C, t =10 min.

[b] Calculated from the graft yield and the of number of pendant groups per chain of the corresponding PNB support.

[c] Determined by high-temperature GPC.

[d] Determined by DSC.

[e] Not applicable

[f] Not determined.

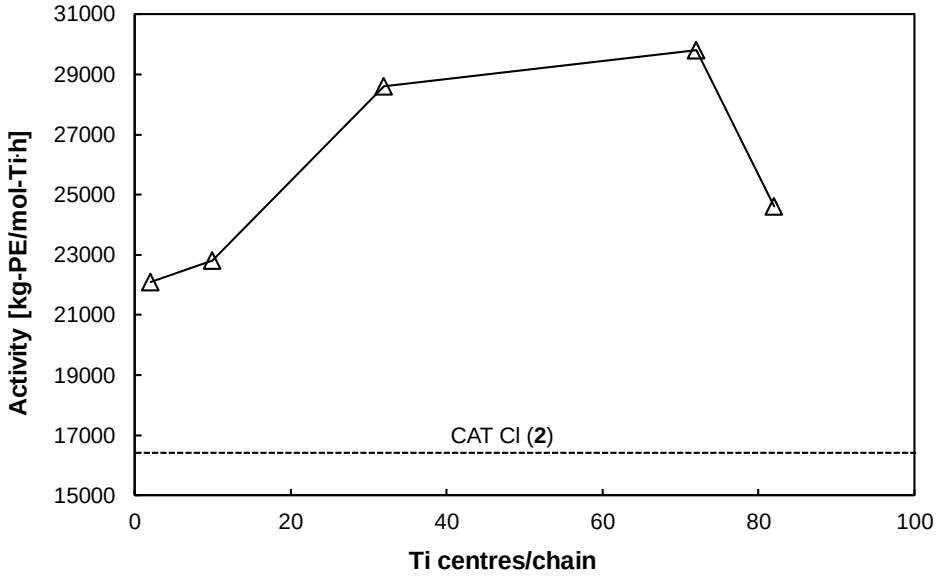

Fig. 6. Effect of the active site density on the ethylene polymerization activity of PNB-*g*-CAT Cl (**1a-e**).

It was found that at 0 °C, the activity of **1a** and **1b** bearing 2 and 9 Ti centres per PNB chain decreased to 22100 and 22800 kg-PE/mol-Ti·h (runs 7,8) from the activity level of 28600 kg-PE/mol-Ti·h of **1c** (run 9). The observed activity of **1a** and **1b** at 0 °C was closer to that of the "isolated" molecular analogue (**2**) (*e.g.* run 6 vs. 7). Contrary, **1d** bearing 72 Ti centres per chain showed the activity further higher than that of **1c** (run 9 vs. 10). Thus, the improvement of the catalyst activity along with the active site density suggested the existence of a synergy or cooperation among the multiple active centres confined in a random coil of PNB chains. Such a synergism in increasing the

local density of active sites has been rarely reported in literatures [32]. In the case of **1e** bearing 82 Ti centres per chain, the activity was found to be lower than those of **1c** and **1d**. The potential reasons for this activity drop are as follows: (i) Formation of secondary Ti centres (*e.g.* bis(aryloxy)cyclopentadienyltitanium (IV) chloride) as observed in ^{13}C NMR might cause some extent of intramolecular cross linkage to make a random coil less open and flexible. In such a scenario, the complexation and/or the reaction of reagents at the active sites are sterically hindered. (ii) A very high local concentration of Ti centres might increase the activation energy for the ionization of the catalyst in a steric and/or electrostatic reason. However, it should be noted that the activity of **1e** was still far superior to that of the "isolated" molecular analogue (**2**) and even higher than those of the PNB-supported catalysts with lower active site densities (**1a**,**b**).

Next, ethylene polymerization was carried out at 30 °C with PNB-supported catalysts having different active site densities (**1a**,**b**,**c**). It was found that at 30 °C and at the Al/Ti ratio of 1000, the molecular catalyst (**2**) and the PNB-supported catalyst (**1c)** showed comparable activities, although the latter produced PE with a much higher M_w value (run 12 vs. 17). In contrast to the results at 0 °C, where the activity was enhanced with the increased active site density, in run 14, at the Al/Ti ratio of 1000, the activity of **1a** was nearly double of the activity showed by CAT Cl (**2**) and **1c** under the identical conditions (run 14 vs. 12,17). The activity of **1b** at the Al/Ti ratio of 1000, was found to be intermediate between **1a** and **1c**. Whereas, at the Al/Ti ratio of 500, **1c** showed greatly improved activity (75% for run 18 vs. 13). Also, the activity of **1a** was higher than that of **1c** at the Al/Ti ratio of 500 (run 15 vs. 18).

Table 4

Ethylene polymerization at 30 °C[a]

Run	Catalyst	Ti centres per chain[b]	Al/Ti (mol/mol)	Activity (kg-PE/mol-Ti·h)	M_w[c] × 10^{-5}	M_w/M_n[c]
12	**2**	n.a.[d]	1000	15900 ± 490	2.3	3.6
13	**2**	n.a.[d]	500	10900 ± 150	n.d.[e]	n.d.[e]
14	**1a**	2	1000	29800 ± 200	n.d.[e]	n.d.[e]
15	**1a**	2	500	21800 ± 250	n.d.[e]	n.d.[e]
16	**1b**	9	1000	20000	n.d.[e]	n.d.[e]
17	**1c**	31	1000	17300 ± 650	4.0	3.7
18	**1c**	31	500	17900 ± 120	n.d.[e]	n.d.[e]

[a] Polymerization conditions: Ethylene pressure = 0.6 MPa, toluene = 300 mL, catalyst = 2.5 μmol, TIBA = 1.25 or 2.5 mmol, Ti/$Ph_3CB(C_6F_5)_4$ = 1 mol/mol, T = 30 °C, t =10 min.

[b] Calculated from the graft yield and the of number of pendant groups per chain of the corresponding PNB support.

[c] Determined by high-temperature GPC.

[d] Not applicable

[e] Not determined.

The observed activity trend in Table 4 can be explained by considering the factor of site isolation during polymerization. It is well-known that molecular catalysts are prone to deactivate by a bimolecular pathway and a support can help to prevent the said deactivation by site isolation [33]. However, additional steric hindrance from a support interferes the complexation and/or the reaction of reagents at the active site and in general the steric hindrance dominates the effect of site isolation. Therefore, the

activity enhancement has been rarely observed for supported catalysts [34]. Contrary, in the case of PNB-supported catalysts, it was found that the steric hindrance from the support can be relieved using a less bulky TIBA/$Ph_3CB(C_6F_5)_4$ activator system (*c.f.* section 2.3.3 in Chapter 2). Hence, the effect of site isolation should persist in the case of the PNB-supported catalysts. Out of all the four catalysts in Table 3, **1a** could provide the maximum site isolation and thus it provided the highest activity, since it had only two Ti centres per PNB chain. This conclusion was consistent with the decreased activity of the three PNB-supported catalysts in the order **1a** > **1b** > **1c**. Moreover, the results of Table 4 also clarified that in the case of **1a**, the observed higher activity at 30 °C as compared to 0 °C was due to the absence of active site deactivation by the bimolecular pathway and the observed temperature effect for **1a** was consistent with the Arrhenius behaviour (k=Aexp(-ΔE_a/RT)), *i.e.*, activity should increase exponentially with temperature in the absence of catalyst deactivation. These discussions make it clear that the activity of the PNB-supported catalysts depends on the interplay between synergy among multiple active centres confined in a nano-sized random and the active site stabilization by site isolation. At a lower temperature of 0 °C, there was negligible active site deactivation and therefore, the synergy effect dominated to increase the activity with the increase of active site density. All of these results are interesting and indeed reveal the tunable catalytic performance of the PNB-supported catalysts by precise tuning of their active site density.

Olefin polymerization well follows linear Langmuir-Hinshelwood Kinetics as represented by Scheme 1.

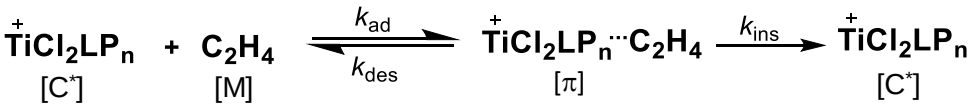

Scheme 1. Langmuir-Hinshelwood mechanism of olefin polymerization reaction.

The polymerization activity (R_p) is given by Eq. (2),

$R_p = k_p[C^*][M] = k_{ins}K_{ad}[C^*][M]$ Eq. (2).

where k_p, $[C^*]$ and [M] correspond to the propagation rate constant of polymerization, working active site concentration and global monomer concentration, respectively. Also, K_{ad} (k_{ad}/k_{des}) and k_{ins} correspond to the equilibrium constant of monomer adsorption and the rate constant of monomer insertion, respectively. Since, [M] is same for all the catalysts, therefore a higher activity of PNB-*g*-CAT Cl (**1c** or **1d**) at 0 °C must be originated from either a higher value of k_p and $[C^*]$ or both for these two catalysts as compared to **1a**,**b** or CAT Cl (**2**).

In order to understand the origin of the synergistic activity enhancement of the PNB-supported catalysts, the effect of TIBA amount and ethylene pressure on the polymerization activity was studied and the results are summarized in Table 5,6 and Fig. 7,8. To study the effect of TIBA amount, two PNB-supported catalysts (**1a**,**d)** and their molecular analogue (**2)** were employed. Polymerizations were conducted by varying the TIBA amount in the range of 0.35–2.5 mmol and at a temperature of 0 °C.

Table 5

Effect of TIBA amount on polymerization activity[a]

Run	Catalyst	TIBA (mmol)	Al/Ti (mol/mol)	Yield (g)	Activity (kg-PE/mol-Ti·h)
19	**2**	0.35	140	9.3	22300 ± 360
20	**2**	0.65	260	8.3	19900
21	**2**	1.25	500	8.8	21100
22	**2**	2.50	1000	6.8	16400 ± 390
23	**1a**	0.35	140	6.2	14900
24	**1a**	0.65	260	7.3	17500 ± 200
25	**1a**	1.25	500	8.0	19200 ± 240
26	**1a**	2.50	1000	9.2	22100 ± 50
27	**1d**	0.35	140	8.4	20100 ± 700
28	**1d**	0.65	260	9.9	23800 ± 900
29	**1d**	1.25	500	12	28800
30	**1d**	2.50	1000	12.4	29800 ± 200

[a] Polymerization conditions: Ethylene pressure = 0.6 MPa, toluene = 300 mL, catalyst = 2.5 μmol, Ti/$Ph_3CB(C_6F_5)_4$ = 1 mol/mol, *T* = 0 °C, *t* =10 min.

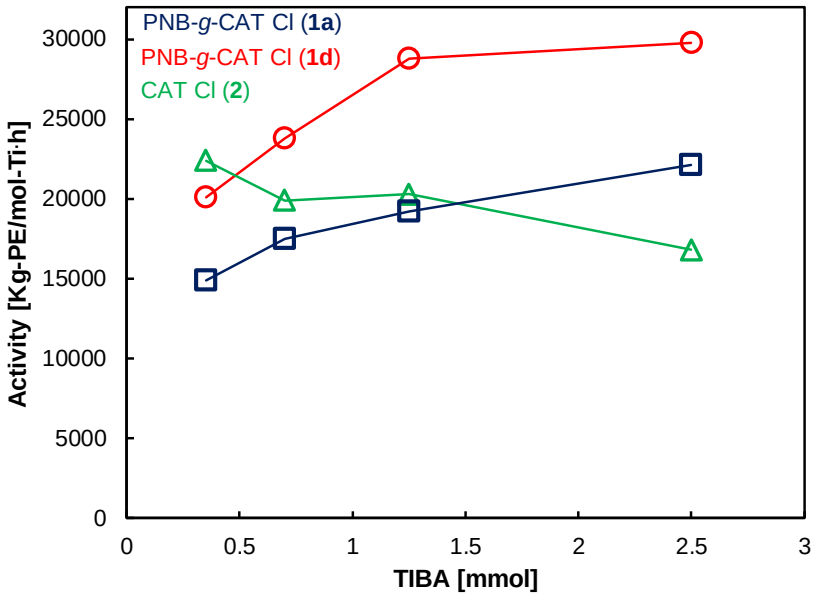

Fig. 7. Effect of the TIBA amount on the polymerization activity of PNB-*g*-CAT Cl (**1a**,**d**) and CAT Cl (**2**).

It was found that the activity of the molecular catalyst (**2**) was highest at a TIBA amount of 0.35 mmol, while the activity decreased with the increase of TIBA amount (Fig. 7). These results suggest that the molecular catalyst is more accessible to reagents and therefore its activation is easier at a lower TIBA amount. However, due to the easier accessibility, the molecular catalyst (**2**) should also have a greater propensity for deactivation and therefore the activity decreased at a higher TIBA amount. In contrast, the activity of the PNB-supported catalysts (**1a**,**d**) increased with the TIBA amount. This is because the active centres are sterically hindered and therefore they require higher amount of TIBA for sufficient activation. Also, support can prevent potential deactivation of the active sites, due to which the activity of the PNB-supported catalysts was stable at a higher TIBA amount. These results further suggest that hindered activation and suppression of deactivation is similar for **1a** and **1d,** so [C^*] must be similar for these two catalysts under all conditions. Therefore, the reason of synergistic activity enhancement of the PNB-supported catalysts (**1c** or **1d**) is not due to a higher value of [C^*], *i.e.*, active site density should not contribute to a higher value of [C^*].

To study the effect of ethylene pressure on the polymerization activity, two PNB-supported catalyst (**1a**,**d**) and their molecular analogue (**2**) were employed. Polymerizations were conducted by varying the ethylene pressure in the range of 0.12-0.6 MPa at a temperature of 0 °C. It was found that the activity of the PNB-supported catalysts (**1a**,**d**) increased linearly with the ethylene pressure (Fig. 8),

i.e., the activity showed a nearly first order dependence on the ethylene pressure. Whereas, the activity of the molecular analogue (**2**) did not increase linearly with the ethylene pressure. The activity of molecular catalyst (**2**) saturated at a much lower ethylene pressure, suggesting the potential deactivation of the catalyst by heat of polymerization at a higher pressure. Grafting of the molecular catalyst (**2**) to the PNB support stabilizes the active sites, for example, by preventing from dimerization, undesired reduction and by heat dissipation.

Table 6

Effect of ethylene pressure on polymerization activity[a]

Run	Catalyst	Ethylene pressure (MPa)	Yield (g)	Activity (kg-PE/mol-Ti·h)
31	**2**	0.12	4.1	9800
32	**2**	0.2	4.9	11700 ± 100
33	**2**	0.3	5.6	13400
34	**2**	0.4	6.4	15400
35	**2**	0.6	6.8	16400 ± 390
36	**1a**	0.12	2.6	6200
37	**1a**	0.2	4.0	9600
38	**1a**	0.3	5.6	13400 ± 210
39	**1a**	0.4	6.7	16100
40	**1a**	0.6	9.2	22100 ± 50
41	**1d**	0.12	2.8	6700
42	**1d**	0.2	4.6	11000
43	**1d**	0.3	6.3	15100 ± 100
44	**1d**	0.4	7.5	18000
45	**1d**	0.6	12.3	29500

[a] Polymerization conditions: Toluene = 300 mL, catalyst = 2.5 μmol, TIBA = 2.5 mmol,

Ti/$Ph_3CB(C_6F_5)_4$ = 1 mol/mol, T = 0 °C, t =10 min.

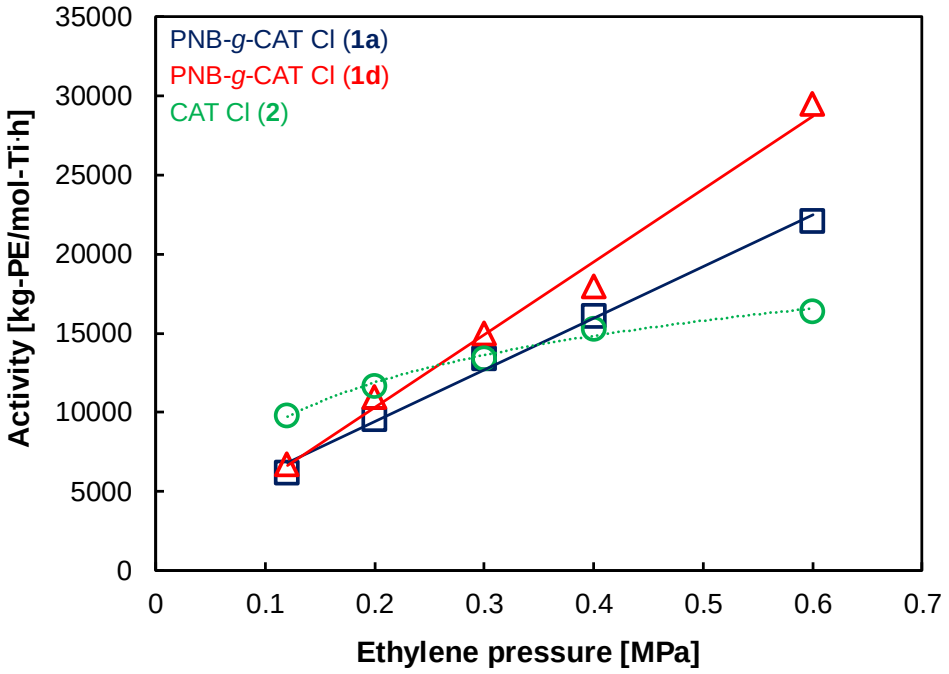

Fig. 8. Effect of the ethylene pressure on the polymerization activity of PNB-*g*-CAT Cl (**1a**,**d**) and CAT Cl (**2**).

In Fig. 8, the slope of a straight line is given by the product of k_p and [C*] (R_p = k_p[C*][M]). Since, [C*] can be assumed to be similar for **1a** and **1d**, the ratio of k_p between the two PNB-supported catalysts can be determined by the ratio of the slopes of the two straight lines in Fig. 8, which was found to be $k_{p,\mathbf{1d}}/k_{p,\mathbf{1a}}$ = 1.4 ($[C^*]_{\mathbf{1a}} \approx [C^*]_{\mathbf{1d}}$). Thus it can be concluded that active site density contributes to a higher value of k_p, which resulted in the higher activity of **1c** or **1d** as compared to **1a**,**b**.

The k_p of polymerization can be correlated to the entropy ($\Delta^{\ddagger}S$) and the enthalpy ($\Delta^{\ddagger}H$) of activation by the Eyring equation (Transition state theory), which has the form $k_p = (\kappa k_B T/h)\exp(\Delta^{\ddagger}S/R)\exp(-\Delta^{\ddagger}H/RT)$. Thus, k_p is higher if enthalpic penalty ($\Delta^{\ddagger}H$)

or entropic loss ($\Delta^{\ddagger}S$) during activation is lower. $\Delta^{\ddagger}H$ can be lowered by stabilizing the transition state, which depends on the active site structure. However, similar ^{1}H, ^{13}C NMR and UV-Vis spectra as well as similar molecular weight of produced PE suggest that all the PNB-supported catalysts and their molecular analogue (**2**) have an identical active site structure. Thus, $\Delta^{\ddagger}H$ must be similar for the PNB-supported catalysts and their molecular analogue. This in turn suggests that the improvement of k_p by the active site density must be due to a lower entropic loss during polymerization for **1c** or **1d** as compared to **1a**,**b** or CAT Cl. In general, in the molecular activation by solid catalysts, the catalyst-substrate complex is formed in two steps (Scheme 2): (i) Surface adsorption and diffusion of reactants, and (ii) Complexation. Whereas in the case of molecular catalysts, the reactants are directly adsorbed on the active sites to form catalyst-substrate complex. Therefore, the overall entropic loss in activation is lower in the case of solid catalysts as compared to molecular catalysts. Similar to the solid catalysts, a mechanism can be proposed for the PNB-supported catalysts with higher active site density. In the case of PNB-supported catalysts with higher active site density, "a high local concentration of active sites might improve the rate of monomer adsorption and lower the entropic loss during monomer catalyst complexation'' as represented by Scheme 2.

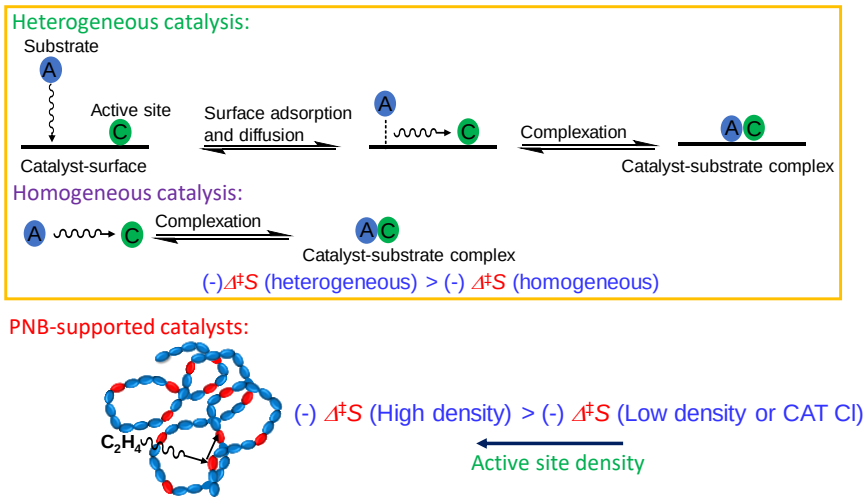

Scheme 2. Proposed mechanism of cooperative catalysis by PNB-supported catalysts.

3.4. Conclusions

In an attempt to study cooperative catalysis based on well-defined structural features, in this chapter, a series of PNB-supported aryloxide ligand containing half-titanocene catalysts, bearing different number of active centres confined in a nano-sized random coil of PNB chains were synthesized. It was established that with the present strategy of catalyst preparation, the number of Ti centres per PNB chain can be precisely controlled over a wide range. Detailed characterization and extensive investigation of the ethylene polymerization performance of these PNB-supported catalysts in comparison with the molecular analogue enabled to understand several important aspects regarding the catalyst performance.

i) The PNB-supported catalysts uncovered two important mechanisms: Site isolation and cooperation. Site isolation is advantageous at a higher temperature and cooperation at a lower temperature.

ii) Because of site isolation and cooperation, the activity of the PNB-supported

catalysts is higher than that of the molecular analogue.

iii) Decrease of entropic loss during monomer-catalyst complexation is believed to be the origin of cooperation among neighbouring active sites in PNB-supported catalysts.

Based on the above findings, I have successfully introduced a new catalyst system in which multiple active centres can be precisely integrated in a nano-sized random coil of PNB chains to obtain tunable catalytic performance of the PNB-supported catalysts. The advantage of the confinement strategy of the new catalyst system enabled to explore cooperative catalysis among multiple active centres in a well-defined way. This research is expected to provide a new direction for the exploitation of multimetallic cooperative catalysis in the field of catalytic olefin polymerization.

References

[1] K. Endo, M. Ogawa, T. Shibata, Angew. Chem. Int. Ed. 49 (2010) 2410–2413.

[2] L.R. Gahan, S.J. Smith, A. Neves, G. Schenk, Eur. J. Inorg. Chem. 19 (2009) 2745–2758.

[3] N. Mitic, S.J. Smith, A. Neves, L.W. Guddat, L.R. Gahan, G. Schenk, Chem. Rev. 106 (2006) 3338–3363.

[4] J.P. Collman, R. Boulatov, C.J. Sunderland, L. Fu, Chem. Rev. 104 (2004) 561–588.

[5] T. Sone, A. Yamaguchi, S. Matsunaga, M. Shibasaki, J. Am. Chem. Soc. 130 (2008) 10078–10079.

[6] N. Kato, T. Mita, M. Kanai, B. Therrien, M. Kawano, K. Yamaguchi, H. Danjo, Y. Sei, A. Sato, S. Furusho, M. Shibasaki, J. Am. Chem. Soc. 128 (2006) 6768–6769.

[7] K. Yamatsugu, L. Yin, S. Kamijo, Y. Kimura, M. Kanai, M. Shibasaki, Angew. Chem. Int. Ed. 48 (2009) 1070–1076.

[8] D.H. Paull, C.J. Abraham, M.T. Scerba, E.A. Danforth , T. Lectka, Acc. Chem. Res. 41 (2008) 655–663.

[9] R.G. Konsler, J. Karl, E.N. Jacobsen, J. Am. Chem. Soc. 120 (1998) 10780–10781.

[10] W. Hirahata, R.M. Thomas, E.B. Lobkovsky, G.W. Coates, J. Am. Chem. Soc. 130 (2008) 17658–17659.

[11] R.M. Haak, S.J. Wezenberg, A.W. Kleij, Chem. Commun. 46 (2010) 2713–2723.

[12] M. Delferro, T.J. Marks, Chem. Rev. 111 (2011) 2450–2485.

[13] K. Soga, H.T. Ban, T. Uozumi, J. Mol. Catal. A: Chem. 128 (1998) 273−278.

[14] M.H. Lee, S.K. Kim, Y. Do, Organometallics 24 (2005) 3618−3620.

[15] Q. Yan, K. Tsutsumi, K. Nomura, RSC Adv. 7 (2017) 41345–41358.

[16] M.R. Salata, T.J. Marks, Macromolecules 42 (2009) 1920−1933.

[17] X. Mi, Z. Ma, L. Wang, Y. Ke, Y. Hu, Macromol. Chem. Phys. 204 (2003) 868−876.

[18] R.M. Enus, S.F. Mapolie, G.S. Smith, J. Organomet. Chem. 693 (2008) 2279−2286.

[19] L. Li, M.V. Metz, H. Li, M.-C. Chen, T.J. Marks, L. Liable-Sands, A.L. Rheingold, J. Am. Chem. Soc. 124 (2002) 12725–12741.

[20] S. Liu, A. Motta, A.R. Mouat, M. Delferro, T.J. Marks, J. Am. Chem. Soc. 136 (2014) 10460–10469.

[21] J. Wang, H. Li, N. Guo, L. Li, C.L. Stern, T.J. Marks, Organometallics 23 (2004) 5112−5114.

[22] J.P. McInnis, M. Delferro, T.J. Marks, Acc. Chem. Res. 47 (2014) 2545−2557.

[23] K. Nomura, N. Naga, M. Miki, K. Yanagi, Macromolecules 31 (1998) 7588–7597.

[24] K. Nomura, J. Liu, S. Padmanabhan, B. Kitiyanan, J. Mol. Catal. A: Chem. 267 (2007) 1–29.

[25] G. Floros, N. Saragas, P. Paraskevopoulou, N. Psaroudakis, S. Koinis, M. Pitsikalis, N. Hadjichristidis, K. Mertis, Polymers 4 (2012) 1657–1673.

[26] B. Düz, C.K. Elbistan, A. Ece, F. Sevin, Appl. Organomet. Chem. 23 (2009) 359–364.

[27] R.M. Kasi, E.B. Coughlin, Macromolecules 36 (2003) 6300–6304.

[28] H.H, Jaffe, M. Orchin, Theory and Applications of Ultraviolet Spectroscopy, John Wiley and Sons, New York, 1962, pp 508–513.

[29] N.I. Makela, H.R. Knuuttila, M. Linnolahti, T.A. Pakkanen, M.A. Leskela, Macromolecules 35 (2002) 3395–3401.

[30] K. Goto, T. Taniike, M. Terano, Macromol. Chem. Phys. 214 (2013) 1011−1018.

[31] M. Sun, Y. Mu, Y. Liu, Q. Wu, L. Ye, Organometallics 30 (2011) 669–675.

[32] B. Kitiyanan, K. Nomura, Stud. Surf. Sci. Catal. 161 (2006) 213–218.

[33] J.R. Severn, J.C. Chadwick, R. Duchateau, N. Friederichs, Chem. Rev. 105 (2005) 4073–4147.

[34] A. Amgoune, M. Krumova, S. Mecking, Macromolecules 41 (2008) 8388–8396.

Chapter 4

General Summary and Conclusions

In this thesis, in Chapter 2, a novel catalyst system in olefin polymerization, which attempts to conceptually bridge the two extreme ends of catalysts, *i.e.* molecular catalysts with well-defined but less functional features and solid catalysts with multifunctional but ill-defined features, has been disclosed. The catalyst design involved a bottom-up strategy, started from the synthesis of well-defined functional polynorbornene (PNB) by precise ring opening metathesis polymerization (ROMP) between norbornene and its derivative containing an aryloxide pendant group using the Grubbs first generation catalyst. Detailed characterization of the functional PNB showed the successful synthesis of nearly monodisperse polymers with controlled density of aryloxide ligands at their side chain. It was proved that the pendant groups in the PNB could be precisely tuned over a wide range at nearly identical polymer chain length. Dynamic light scattering technique revealed a nano-sized random coil conformation of PNB chains in a dilute solution. These well-defined PNB were subsequently employed as a soluble support for grafting half-titanocene complexes (Cp^*TiMe_3 and Cp^*TiCl_3) to afford structurally well-defined supported catalysts, confirmed by ^{1}H and ^{13}C NMR spectroscopy. Ethylene polymerization by the soluble PNB-supported catalysts using a bulky activator system namely modified methylaluminoxane revealed the negative influence of steric interference from the polymer support on catalyst activity, and its positive influence on improving molecular weight of produced polyethylene. On the contrary, extensive ethylene polymerization using a less bulky tri-*iso*-butylaluminum/$Ph_3CB(C_6F_5)_4$ activator system revealed unique catalytic features of these soluble polymer-supported catalysts, represented by a cooperative or synergistic activity enhancement among multiple active centres confined in a nano-sized random coil of polymer chains. Moreover, the supported catalysts

were found to be superior to the molecular analogues in producing polyethylene with a higher molecular weight and narrower polydispersity when activated by tri-*iso*-butylaluminum/$Ph_3CB(C_6F_5)_4$. From the study presented in Chapter 2, it can be concluded that the well-defined nature of the novel polymer-supported catalysts is powerful in studying interactions between active centres and supports as well as among active centres themselves in catalysis. The beauty of the present catalyst design lies in the integration of multiple active centres within a single polymer chain in a well-defined manner, which is expected as promising in exploring cooperative catalysis.

In order to explore the origin of cooperative catalysis embodied by aryloxide-containing half-titanocene catalysts confined in a single PNB chain, in Chapter 3, a series of PNB-supported catalysts with different active site densities were successfully synthesized. The precise Grubbs catalyzed ROMP technique for PNB support synthesis in combination with efficient grafting reaction of a half-titanocene precursor (Cp^*TiCl_3) allowed the precise control of the number of grafted Ti centres per PNB chain over a wide range. Detailed characterization of the PNB-supported catalysts by ^1H, ^{13}C NMR and UV-Vis spectroscopy revealed that the structure of the Ti centres in all the PNB-supported catalysts is identical to that of their molecular analogue. Extensive investigation of the ethylene polymerization performance of these PNB-supported catalysts in comparison to their molecular analogue clarified two unique catalytic aspects. Firstly, it was found that at a lower temperature, when there was negligible deactivation of the catalysts, the activity of the PNB-supported catalysts increased with the increase of the number of active centres per PNB chain. The activity of the PNB-supported catalysts with the lowest active site density (2 Ti centres per PNB chain) was closer to that of the isolated molecular analogue. These results

confirmed the role of cooperative catalysis among multiple active centres confined in a nano-sized random coil of PNB chains in improving the activity of the PNB-supported catalysts. Such an improvement of catalytic activity by increasing the local density of active sites has been rarely reported in the field of catalytic olefin polymerization. Secondly, it was found that at a higher temperature, the highest activity in ethylene polymerization was achieved by employing a PNB-supported catalyst with the lowest active site density. In the absence of synergistic or cooperative effect, the enhanced activity of the PNB-supported catalyst with the lowest active site density indicated the stabilization of the active sites by site isolation. These results further emphasize that the PNB-supported catalysts are advantageous over the molecular analogue in terms tunable catalytic performance by precise tuning of their active site density. This is an important conclusion for these novel polymer-supported catalysts, suggesting that they are potential candidates as new multifunctional catalysts with well-defined structures in the field of catalytic olefin polymerization.

I believe that the research work carried out in this thesis has clearly delivered the advantages of grafting of a molecular catalyst to a soluble polymer support based on the clearest molecular design. Further, the new catalytic concept of confining multiple active centres of an aryloxide containing half-titanocene catalyst in a nano-sized random coil of polymer chains for cooperative catalysis can be extended to many other molecular catalysts to explore new catalytic functions in a well-defined way. This research is thus expected to provide a new direction for the exploitation of multimetallic cooperative catalysis in the field of catalytic olefin polymerization.

List of Publications and Other Achievements

Ashutosh Thakur

A) Publications

1. "New Quenching Method for Improving Large-Scale Stopped Flow Technique"
   A. Thakur, S. Poongpong, M. Terano, T. Taniike, Macromolecular Reaction Engineering, **2014**, 8, 766-770.
2. "Synthesis of Aryloxide-Containing Half-Titanocene Catalysts Grafted to Soluble Polynorbornene Chains and Their Application in Ethylene Polymerization: Integration of Multiple Active Centres in a Random Coil"
   A. Thakur, R. Baba, P. Chammingkwan, M. Terano, T. Taniike, Journal of Catalysis, **2018**, 357, 69-79.
3. "Influence of Functional Groups on Ethylene Polymerization Performance of Silsesquioxane-Supported Phillips-Type Catalyst"
   R. Baba, A. Thakur, P. Chammingkwan, M. Terano, T. Taniike, Dalton Transactions, **2017**, 46, 12158-12166.
4. "Design of Pd@Graphene Oxide Framework Nanocatalyst with Improved Activity and Recyclability in Suzuki-Miyaura Cross-Coupling Reaction"
   T.P.N. Tran, A. Thakur, D.X. Trinh, A.T.N. Dao, T. Taniike, Applied Catalysis A: General, **2017**, 549, 60-67.

B) Domestic Conferences

1. **Oral Presentation**: Grubbs Catalysed ROMP to Synthesize Aryloxide Ligands Containing Polynorbornene: Well-Defined Polymer to Support Half-Metallocene Catalysts; A. Thakur, M. Terano, T. Taniike, **The 45th Petrochemical Symposium of Japan Petroleum Institute,** Nagoya, Japan, November 2015.
2. **Oral Presentation**: Synthesis of Side-Chain Functionalized Polynorbornene Supported Half-Metallocene Catalysts and Their Application in Ethylene Polymerization; A. Thakur, M. Terano, T. Taniike, **The 46th Petrochemical Symposium of Japan Petroleum Institute,** Kyoto, Japan, November 2016.
3. **Oral Presentation**: Development of Single Polynorbornene Chain Supported Half-Metallocene Catalysts to Embody Catalytic Multifunctionality in Ethylene Polymerization; A. Thakur, R. Baba, M. Terano, T. Taniike, **66th Symposium on**

Macromolecules, Ehime, Japan, September 2017.

4. **Oral Presentation**: Effect of Active-site Density on Ethylene Polymerization by a Series of Side Chain Functionalised Polynorbornene Supported Half-Metallocene Catalysts; A. Thakur, M. Terano, T. Taniike, **The 47th Petrochemical Symposium of Japan Petroleum Institute**, Tottori, Japan, November 2017.

C) International Conferences

1. **Poster Presentation**: Application of Cryo-Probe NMR in Ultra-Short Time Propylene Polymerization, A. Thakur, M. Terano, T. Taniike, **International Symposium on Advanced Materials**, JAIST, Japan, March 2015.
2. **Poster Presentation**: Ultra-Short Time Propylene Polymerization for Characterization of Primary Structure of Polymer by High-Temperature Cryo-Probe NMR, A. Thakur, M. Terano, T. Taniike, **IUPAC 11th International Conference on Advanced Polymers via Macromolecular Engineering**, Yokohama, Japan, October 2015.
3. **Oral and Poster Presentation**: Identification of Regio-Defects in Polypropylene Formed in Quasi-Living Stopped-Flow Polymerization Process, A. Thakur, M. Terano, T. Taniike, **World Polyolefin Congress,** Tokyo, Japan, November 2015.
4. **Poster Presentation**: Single Polymer Chain Supported Well-defined and Multifunctional Catalyst Design for High Precession Olefin Polymerization, A. Thakur, M. Terano, T. Taniike, **253rd ACS National Meeting on Advanced Materials, Technologies, Systems & Processes**, San Francisco, California, USA, April 2017.
5. **Oral Presentation**: Integration of Multiple Active Centres in a Random Coil of Single Polynorbornene Chain to Embody Catalytic Multifunctionality in Ethylene Polymerization, A. Thakur, M. Terano, T. Taniike, **Asian Polyolefin Workshop 2017**, Tianjin, China, October 2017.

D) Award

1. **Outstanding poster presentation**, World Polyolefin Congress, Tokyo, Japan, November 2015.

2. **Excellent Poster Award**, JAIST World Conference 2018, Nomi, Japan, February 2018.